STRUCTURE AND MOTION CHARACTERISTICS OF

TROPICAL CUMULONIMBUS CLOUDS

by

Walter Fernandez

Atmospheric Physics Group
Department of Physics
Imperial College of Science and Technology

A thesis submitted for the Degree of Doctor of Philosophy
in the University of London

1980

STRUCTURE AND MOTION CHARACTERISTICS OF TROPICAL CUMULONIMBUS CLOUDS

Walter Fernandez

ABSTRACT

A classification of storms in squall lines, thunderstorm clusters, and isolated thunderstorms was made using radar data collected during the second phase of the Venezuelan International Meteorological and Hydrological Experiments (VIMHEX-1972). The near-environmental conditions in advance of these types of storms are examined, as is the modification of the environment during the passage of such storms over a site. The squall lines occurring over West Africa and the eastern tropical Atlantic are then studied in a similar manner using data collected in two international experiments: Operation Pre-GATE ASECNA (OPGA) and the GARP Atlantic Tropical Experiment (GATE). Conceptual models of the airflow inside these storms are constructed and some aspects of storm movement are considered. The observational evidence for mesoscale downdraughts in tropical squall line systems is described and the possible mechanisms for the formation of such downdraughts are discussed.

Raymond's (1975) wave-CISK model is applied to several tropical convective storms observed in Venezuela, the Eastern Atlantic and West Africa to predict their propagation velocity. Similar calculations are carried out with Moncrieff and Miller's (1976) analytical model for tropical cumulonimbus and squall lines. A comparison of the models' predictions with the observed values is made. In some cases the models give good predictions, but not in others. In general, Raymond's model underestimates the propagation speed of the storms, while the Moncrieff-Miller model overestimates it. The models are then considered in conditions of constant wind shear. Despite the obvious differences between the models it is found that, for Richardson number small ($R < 1$) and very large, they give comparable predictions for the storm velocity. It appears that a very good approximation for the wave-CISK model over the entire R range is to put the storm speed proportional to the shear, plus a constant.

Finally, some characteristics of hurricane rainbands are described and a review of the concepts on the origin of such rainbands is made.

CONTENTS

CHAPTER 1

INTRODUCTION

1.1 General nature of cumulonimbus clouds

Cumulonimbus clouds are among the most majestic sights of atmospheric phenomena. The usual occurrence of lightning and thunder within or from this type of cloud lends to its popular name of thunderstorm cloud. They might occur as an isolated "hot tower" or as a group of clouds or squall lines. According to the Glossary of Meteorology (Huschke, 1970) a squall line is defined as any non-frontal line or narrow band of active thunderstorms (with or without squalls). However, there is often as much contrast in meteorological variables across a strong non-frontal line as there is across a front, and for this reason the distinction is somehow semantic (Lilly, 1979). Cumulonimbus clouds are also associated with the tropical cyclone, one of the most destructive forces of nature.

The formative processes of cumulonimbus start as a result of convection from the ground or instability in the free atmosphere, or both effects acting at the same time. The synoptic situation plays an important role in the cumulonimbus organization and may provide a triggering mechanism for the release of the instability. The visual cloud is, nevertheless, the result of many physical processes acting together, which involve the interaction of a very large size range of cloud particles and an even larger range of interacting motion scales.

Cumulonimbus clouds are very frequent over the tropical areas and they become less frequent with increasing latitude, being rare over the polar regions. However, the most intense and destructive storms occur in some mid-latitude regions (such as the mid-west of the United States)

where strong storms are observed accompanied by large hailstones and tornadoes. In most of the tropical regions the number of thunderstorm days is larger than 100 per year, and in some parts may be as much as 200 per year. The main regions are Central and South America, Africa and the southeast part of Asia.

The tropical regions are the main source of heat energy which drives the atmospheric circulations. It was shown by Riehl and Malkus (1957) that the oceanic regions in which the trade winds are observed provide an appreciable amount of the energy in the form of latent and sensible heat. The trade winds transport water vapour towards the equatorial zone where it is lifted and condensed in deep convective systems, producing sensible heat and potential energy, which are then transported to higher latitudes by the upper winds. Riehl and Malkus (1958) showed that only a small fraction of the area comprising a 10 degree latitude belt near the equator, needs to be occupied by cumulonimbus clouds to maintain the heat balance of the equatorial trough zone and provide the energy transport toward higher latitudes. They estimated that at any given time a total number of approximately 1500 to 5000 cumulonimbi embedded in about 30 synoptic disturbances are sufficient for heat balance requirements. Gray (1970, 1978) has emphasized the importance of cumulonimbus clouds for vertical momentum transport and the production of kinetic energy for export to higher latitudes.

In addition to their important role in relation to the general circulation, cumulonimbus clouds (and cumulus convection in general) interact with the synoptic systems in which they are embedded. An example of this type of interaction is observed in the formation of a tropical cyclone, in which the CISK mechanism proposed by Charney and

Eliassen (1964) plays an important role. In the CISK mechanism the cumulus convection and the tropical disturbance are considered to support each other: convection providing the heat energy to drive the disturbance and the disturbance producing the low-level moisture convergence into the convective elements. This type of interaction, under proper atmospheric conditions, may produce an intensification of the disturbance into a hurricane. On the other hand, deep convection may sometimes dissipate the synoptic system with which it is associated. Zipser (1969), using data from the Line Islands Experiment, showed that highly unsaturated downdraughts produced first on the convective scale and the mesoscale, may become organized over the entire extent of the system. Cumulus development is then suppressed in the downdraught air and this may produce a rapid decay of the weather system.

1.2 The scales of deep convection in the tropics

In the tropics deep convection exhibits different levels of organization, each with a different characteristic space scale (see, for example, GARP-JOC, 1970). These levels of organization are more clearly observed over the oceans than over the land. The individual cumulonimbus tower has a characteristic dimension of about 1 to 10 km (the scale of convective cells). These cumulonimbi may be organized in mesoscale lines or rings with dimensions of about 10 to 100 km (the mesoconvective scale). When a number of these mesoconvective systems occur in close proximity, their outflows at high levels merge forming a common cirrus shield with dimensions of about 100 to 1000 km (the scale of cloud clusters). After the convection ceases, such cirrus shields may persist for a day or even more. The cloud clusters are associated with lower-tropospheric waves with characteristic scales of the order of 2000 to 10,000 km (the long-wave scale). In some regions the clusters are

located in the troughs of such waves, and east of the troughs in other regions. The cloud clusters are also observed along the inter-tropical convergence zone (ITCZ) and their changes are associated with the interactions between the ITCZ and large-scale troposphere wave-like disturbances. Another example of cumulonimbus organization (on the scale of cloud clusters) is observed in the hurricane. As pointed out by Ludlam (1976) the tropical cyclone provides perhaps the nearest approach to a field of cumulonimbus.

The lifetime of the convective systems varies with the scale. The characteristic time for individual cumulonimbus towers is of the order of an hour. The meso-convective scale systems have their own characteristic time, which may be as much as one to five days, depending on the type of organization. The large-scale waves in which the cloud clusters are embedded have very long lifetimes. Their vertical structure differs with season and geographical region, although their phase speed appears to be uniform (8-9 m s^{-1}) and independent of the horizontal wavelength.

The hierarchy of levels of organization described above is more clearly discernible over the oceans. Over land the convective activity tends to be more dispersed and sometimes takes the form of mesoscale systems, evenly distributed, which have been referred to as "popcorn cumulonimbi". However, over some land regions such as West Africa, massive long-lasting squall lines develop and travel long distances.

1.3 Significance, objectives and scope of the thesis

In the tropics most of the precipitation is of convective origin and is concentrated in a relatively small number of cumulonimbi. These so-called "hot towers" occupy only a small fraction, even in active

disturbances. Therefore to understand the dynamics of synoptic scale systems in the tropics, it is necessary to understand the nature of the interaction between the cumulonimbus scale motions and the synoptic scale disturbances in which they are embedded. However, this involves an understanding of the dynamics and thermodynamics of the cumulonimbus clouds. An understanding of tropical convection requires, in turn, the investigation of fundamental questions, such as: what determines the size, the type of organization and the life-cycle of the convective systems ? How does an individual element influence its neighbours? How much compensating vertical motion takes place in the immediate vicinity of these elements? What role do downdraughts play in their maintenance? What are their transport characteristics of momentum, heat and water vapour? How do they modify the environment? What are the environmental conditions associated with different types of organization? On the other hand, one of the best examples of cumulonimbus organization arise in the formation of hurricane rainbands. At present there is not a satisfactory explanation for their generation near the hurricane eye and their outward progression. The organization of cumulonimbus in rainbands must be intimately related to the structure and working of the hurricane as a whole. Little is known about the structure and dynamics of these rainbands or of the embedded cumulonimbi. Are there some similarities with squall lines occurring over land or over the oceans?

One of the most important properties of severe storms is their motion relative to the earth's surface. If the storm speed is small then severe weather can be experienced locally for several hours, whereas if it is large the storm can move to places far from that of its origin. The characteristics of storm motion are thus of great importance in applied fields such as hydrometeorology and agrometeorology. On the other hand, in recent years some theories of storm motion have

been developed (Moncrieff and Green, 1972; Moncrieff and Miller, 1976; Raymond, 1975, 1976). At the present time there exists a strong need to evaluate the predictions from such theories using observations of tropical convective systems (Lilly, 1979), and this will be an important aspect to dealt with in this thesis.

The objectives of this work are:

a) To study the environmental conditions associated with some types of tropical cumulonimbus organization.

b) To determine the way in which these tropical convective systems modify the environment and the way in which they move.

c) To study the dynamical structure of tropical squall lines, constructing conceptual models using observational data.

d) To examine the mechanisms for the formation of mesoscale downdraughts in tropical squall line systems.

e) To evaluate some theories of storm motion proposed in the literature using observations of tropical convective systems.

f) To study the characteristics of hurricane rainbands as well as theories of rainband formation.

In order to accomplish such objectives, several case studies were selected from three international experiments: the Venezuelan International and Hydrological Experiments (second phase, VIMHEX-1972), Operation Pre-GATE ASECNA (OPGA, 1973) and the GARP Atlantic Tropical Experiment (GATE, 1974). In addition, radar films of eight tropical cyclones and other meteorological data obtained from several countries (Australia, Hong Kong, Japan and the United States) were examined.

In order to study possible differences or similarities in the environmental conditions associated with different types of convective

systems, a storm classification was made using observations from VIMHEX-1972. In presenting such a classification, the characteristics and structure of the Venezuelan storms are examined. The squall lines occurring over West Africa and the eastern tropical Atlantic are then studied in a similar manner and a comparison with the Venezuelan storms is made. This is followed by a discussion of the observational evidence for mesoscale downdraughts in tropical squall line systems and the possible mechanisms for the formation of such downdraughts. Then, with the observational data available from the experiments mentioned above, an evaluation of theories of storm motion is made. Finally, the characteristics of spiral rainbands in hurricanes, as well as theories of hurricane rainband formation, are examined.

CHAPTER 2

ENVIRONMENTAL CONDITIONS AND STRUCTURE OF SOME TYPES OF CONVECTIVE MESOSYSTEMS OBSERVED OVER VENEZUELA*

2.1 Introduction

The conditions favourable for the occurrence of severe convective phenomena in mid-latitudes have been described by Newton (1963), Ludlam (1963), Carlson and Ludlam (1968), and Miller (1967). The significant features are conditional and convective instability, availability of abundant moisture in lower levels, bands of strong winds in lower and upper levels, turning of the wind with height, and some mechanism which can trigger the release of instability; thus the main characteristics of the storm's environment may, in principle, be determined from conventional rawinsonde observations. However, good representative rawinsonde data are not available in most of the cases. In some mid-latitude regions, such as the mid-west of the United States, special rawinsonde observations have been available for many years and several studies on the environmental conditions associated with severe storms have been made. In the tropics, on the contrary, it is only recently that experiments such as BOMEX (Barbados Oceanographical and Meteorological Experiment), VIMHEX (Venezuelan International Meteorological and Hydrological Experiments), and GATE (GARP Atlantic Tropical Experiment), have provided the data necessary for studying the environmental conditions associated with convective storms. With such data some studies of the modification

---

* A slightly modified version of this chapter has been accepted for publication in the Archiv für Meteorologie, Geophysik und Bioklimatologie, Serie A.

of the environment during the passage of squall lines have been made, but even in those carried out with squall lines, some important aspects such as the wind shear in the storm's near environment have not been described in detail.

The wind shear plays an important role in the organization of the updraught-downdraught structure in severe convective storms, and, as a consequence, in their evolution. This aspect has been incorporated in conceptual models of mid-latitude storms (Newton and Newton, 1959; Browning and Ludlam, 1962; Browning, 1964) and its importance has also been examined in two-dimensional numerical studies (Takeda, 1971; Hane, 1973) and three-dimensional numerical studies (e.g. Pastushkov, 1975; Wilhelmson, 1974; Miller and Pearce, 1974; Moncrieff and Miller, 1976; Thorpe and Miller, 1978; Schlesinger, 1978, Klemp and Wilhelmson, 1978).

Ludlam (1963) pointed out the possibility that the available potential energy is most effectively converted into kinetic energy when the degree of wind shear is matched to the degree of instability, so that the most efficient storms might be characterized by a kind of Richardson number, R (expressed, for example, as a ratio between convective available potential energy which could be generated by buoyancy forces, and the available kinetic energy produced by the shear). Green and Pearce (1962), Moncrieff and Green (1972), Moncrieff and Miller (1976) and Moncrieff (1978) have elaborated such ideas and have developed two-dimensional and quasi-three-dimensional nonlinear analytic theories of cumulonimbus convection. From the theory two regimes of convection are obtained, one occurring at values of $R \leq 1$ in which inflow at low levels and outflow at upper levels at the front and relative to the system are required (typical, *but not exclusively*, of mid-latitudes) and the other occurring at values of $R > 3$ in which inflow at all levels at the front

and relative to the system is required (typical, *but not exclusively*, of tropical regions). Here we will be dealing with the second type of convection regime. We will study the near-environmental conditions associated with different types of convective storms observed over Venezuela. We will describe in detail the inflow conditions, as well as the modification of the environment during the passage of the storms. Finally, some aspects of storm motion will be examined.

2.2 Case studies

We will be dealing with convective storms observed during the second phase of VIMHEX (VIMHEX-1972). The design of the experiment, which was carried out from June to September, 1972, was simple. A modified 10 cm M-33 radar with a 2^{o} beam was installed at Carrizal, Venezuela (9^{o} 22.8'N, 66^{o} 55.0'W) and was operated to a range of 90 km. Radiosondes were launched as frequently as necessary (every 65 to 100 minutes). The type of sonde was the VIZ-1290 of the United States National Weather Service. A raingauge network within a distance of 60 km from Carrizal was also available to study the distribution of precipitation. The rawinsonde data, as well as radar echo statistics and rainfall information, have been compiled by Betts and Miller (1975) and Betts and Stevens (1974), respectively.

Several papers have appeared in the literature in relation to the Venezuelan convective mesosystems. Cruz (1973) studied some radar echo characteristics of the storms observed during the first phase of VIMHEX (VIMHEX-1969). Betts (1976a, 1976b) has used the VIMHEX-1972 data to study the structure and thermodynamic transformations of the subcloud layer, as well as to develop a model for this layer. Betts et al. (1976) made a comparison of the results predicted by the theory of Moncrieff and Miller (1976) with observations of some squall lines. Fernandez and Thorpe (1979) made an evaluation of theories of storm

motion, in which part of the data used was from VIMHEX-1972. Miller and Betts (1977) applied a density current model to classify the storms' travel speeds, peak surface gusts and the accelerated flow at low levels behind the storms, and to relate these to the low-level flow ahead of the storms. The climatological aspects of precipitation and its dependence on the synoptic situations have been examined by Riehl (1973), Riehl et al. (1973), Riehl and Lueckefedt (1976), and Riehl (1977a, 1977b). For our purposes we have classified the storms into three groups, as follows:

a) Group of echoes with line structure normal to the direction of motion. We will refer to these systems as squall lines (SL).

b) Group of echoes which merged but are not of squall line type, or group of echoes which did not merge. We will refer to these systems as thunderstorm clusters (TC).

c) Isolated echoes, but not necessarily a single cell. We will refer to these systems as isolated thunderstorms (IT).

The above classification is descriptive and, in principle, does not necessarily imply that each type of storm has the same dynamical character. Our interest here, however, is to examine possible differences or similarities in the environmental conditions associated with these types of storms, in the way in which the storms modify the environment, and also in the storm's movement.

Of the 159 distinct echoes observed during the second phase of VIMHEX there are 23 SL, 45 TC and 76 IT, the other 15 being special cases. Although the number of storms is large, it is difficult to find rawinsonde observations representative of specific storm types. The reason for this is that at the time of sounding, storms of different

types may coexist. Therefore we have examined carefully all the echo tracks, together with the rawinsonde data, in order to find some situations representative of each storm type. We have been able to select seventeen situations (6 SL, 6 TC and 5 IT) in which, except for a few SL cases, only storms of one specific type were present. With the soundings taken before the passage of the 17 storms, we will examine the environmental thermodynamic and windfield characteristics associated with the different storm types. Not all the cases, however, present soundings representative of the environmental structure after the passage of the storms. Only three cases of TC and three of IT have soundings that are representative of the atmospheric conditions at the rear of the systems. We will use such cases to examine the modification of the environment by the different types of storms.

In the experiment, each storm was identified by a number. The group of SL selected for this study includes storms 27, 35, 47, 53, 60 and 64; the group of TC includes storms 33, 43, 46, 51, 135 and 89; and the group of IT includes storms 9, 14, 31, 55 and 58. The corresponding sounding numbers are given in Table 2.5. In the next sections we will use mean values for each set of storms rather than the individual values for each storm, but the standard deviations (σ), corresponding to such mean values, will be indicated.

2.3 Environmental thermodynamic and windfield characteristics

2.3.1 Radar echo characteristics

Table 2.1 shows some radar echo information for the different storm types. The values of maximum echo area, echo lifetime and maximum echo height are, in general, greater in the case of SL than in the cases of TC and IT. The values of storm speed are similar for the three storm

Table 2.1 Mean values of radar echo data of travelling convective storms observed over Venezuela. Numbers in parentheses are the respective standard deviations.

Storm type	Max. echo area km^2	Echo life-time hrs	Max. echo height km	Storm motion (vector mean) Dir. deg.	Speed $m\ s^{-1}$
SL	2660 (799)	3.5 (0.6)	13.0 (2.6)	84 (14)	13.5 (2.3)
TC	376 (166)	2.7 (0.9)	11.6 (1.9)	102 (17)	12.6 (3.0)
IT	264 (128)	2.5 (0.8)	10.4 (1.6)	102 (21)	11.2 (3.1)

Table 2.2 Mean values of thermodynamic variables of the near-environment of convective storms observed over Venezuela. Numbers in parentheses are the respective standard deviations.

Storm type	CAPE $J\ kg^{-1}$	ΔT at 500 mb ^{o}C	$\overline{q}$ Subcloud layer $g\ kg^{-1}$	LCL a.g.l. m
SL	1010 (350)	+ 3.1 (0.6)	15.0 (0.6)	1275 (205)
TC	1005 (600)	+ 2.6 (1.3)	14.5 (1.0)	1300 (228)
IT	980 (301)	+ 2.3 (1.0)	14.0 (0.8)	1325 (332)

types.

2.3.2 Thermodynamic variables

Table 2.2 shows some thermodynamic characteristics of the storms' near-environment. The thermal instability may be deduced from the values of the thermal buoyancy at 500 mb (temperature difference between parcel and environment at 500 mb) and the convective available potential energy (CAPE), defined as

$$\text{CAPE} = \int_{o}^{H} g\, \delta\phi_p \, dz \qquad \text{——(2.1)}$$

where H is the height of cloud top, and $\delta\phi_p$ is the log potential temperature difference between parcel and undisturbed flow. If a pseudo-saturated ascent is assumed, then CAPE is proportional to the positive area on a tephigram. The values of CAPE shown in Table 2.2 were determined, following Betts et al. (1976), by measuring the energy released by pseudo-saturated ascent at the mean equivalent potential temperature (θ_e) of the 980-900 mb layer.

The mean values of CAPE and $\Delta T_{500\ mb}$ are similar for the three storm types. In general, however, the thermal instability is slightly greater in the case of SL and slightly smaller in the case of IT, with intermediate values in the case of TC. However, it can be seen from Table 2.2 that the range of variability of CAPE and $\Delta T_{500\ mb}$ is greater in the case of TC than in the cases of SL and IT. The highest value of thermal instability (CAPE ~1850 J kg^{-1} and $\Delta T_{500\ mb} = 4.7^{o}$C) corresponds to storm 46, which is a TC. Storm 51, also a TC, presents the smallest value of thermal instability (CAPE ~200 J kg^{-1} and $\Delta T_{500\ mb} = 1.2^{o}$C). Nevertheless the maximum echo height of storm 51 is quite appreciable (about 13 km). This shows that a large value of thermal instability is not a necessary condition for the development of convec-

tive storms. In those cases where CAPE is small and storms are nevertheless observed, strong convergence at lower levels might be the mechanism required to overcome the stability of the upper layers. In fact, this is the general case in hurricane situations where CAPE is small and nevertheless strong convection occurs.

The mean values of specific humidity are similar for the different types of storms, being slightly larger in the case of SL. The last column of Table 2.2 gives values for the lifting condensation level (LCL). The values of this quantity for the different types of storms are very similar, being slightly smaller in the case of SL.

2.3.3 Windfield variables

Table 2.3 shows the mean values (and standard deviations) of wind, turning of wind with height and wind shear for the sub-cloud and cloud layers (approximately surface-850 mb and 850-200 mb, respectively). It also shows the speed and height of the mid-level jet (MLJ) and the wind shear between surface and the MLJ.

Sub-cloud layer : The mean wind for this layer is very similar for the three storm types (see Table 2.3). The turning of winds with height (positive values are in a clockwise sense) is quite variable for the different storm types, changing appreciably from storm to storm. The wind may turn as much in a clockwise as in a counterclockwise direction, and for this reason the standard deviations are large.

The wind shear is greater in the case of TC than in the case of SL and IT. This, together with the slightly greater turning of winds with height shown by the TC, is likely to be the reason for the greater asymmetry and three-dimensionality of the TC.

Table 2.3 Mean values of environmental windfield variables for different types of convective storms observed over Venezuela. Numbers in parentheses are the respective standard deviations.

Storm type	Sub-cloud layer: Mean wind $m\,s^{-1}$	Turning deg.	Wind shear $10^{-3}\,s^{-1}$	Cloud layer: Mean wind $m\,s^{-1}$	Turning deg.	Wind shear $10^{-3}\,s^{-1}$	Mid-level jet (MLJ) speed $m\,s^{-1}$	MLJ height km	Wind shear: Surf-MLJ $10^{-3}\,s^{-1}$
SL	5.6 (1.8)	-15 (43)	4.3 (1.5)	6.3 (2.0)	177 (57)	1.5 (0.6)	11.8 (2.5)	2.8 (0.5)	3.6 (0.8)
TC	5.4 (2.4)	-22 (61)	5.8 (1.8)	4.1 (1.4)	193 (26)	2.0 (0.2)	12.5 (1.6)	3.5 (0.8)	3.4 (1.0)
IT	5.5 (1.1)	+ 3 (31)	3.7 (1.6)	6.4 (3.0)	81 (73)	1.4 (0.8)	13.2 (1.3)	4.6 (0.3)	2.3 (0.7)

Table 2.4 Mean values of some stability and windfield variables for Venezuelan and mid-latitude convective storms. Numbers in parentheses are the respective standard deviations.

Variable	Venezuelan storms			Mid-latitude storms	
	SL	TC	IT	MS	SS
ΔT at 500 mb ($^{\circ}C$)	+ 3.1 (0.6)	+ 2.6 (1.3)	+ 2.3 (1.0)	+ 3.9 (1.8)	+ 6.2 (2.2)
Turning of winds in sub-cloud layer (deg.)	- 15 (43)	- 22 (61)	+ 3 (31)	+ 47 (67)	68 (16)
Mean wind speed in sub-cloud layer ($m\,s^{-1}$)	5.6 (1.8)	5.4 (2.4)	5.5 (1.1)	5.0 (1.8)	12.8 (2.7)
Mean wind surface-10 km ($m\,s^{-1}$)	6.6 (1.8)	5.2 (1.3)	6.7 (2.8)	15.2 (5.7)	21.8 (5.4)
Wind shear in cloud layer ($10^{-3}\,s^{-1}$)	1.5 (0.6)	2.0 (0.2)	1.4 (0.8)	2.6 (1.1)	3.5 (0.9)
Storm speed ($m\,s^{-1}$)	13.0 (2.3)	12.0 (3.0)	11.0 (3.1)	11.6 (3.5)	11.4 (2.4)

Cloud layer: In this layer the mean wind is comparable for the SL, TC and IT, being slightly smaller in the case of TC. The turning of winds with height and the magnitude of the wind shear appears, however, to be somewhat greater in the case of TC than in the cases of SL and IT. Again this accounts for the greater asymmetry and three-dimensionality of the TC. The turning of wind with height, except in two cases of IT, is in a clockwise sense. Because of this, the IT show a large standard deviation in such a variable.

The mid-level jet : A characteristic of the wind-field associated with the Venezuelan storms is that it presents a jet at mid-levels (between 800 and 600 mb, about 2 to 5 km a.s.l.) as may be inferred from Figures 2.1 to 2.3. Table 2.3 gives the mean values of the mid-level jet (MLJ) and the wind shear between surface and the MLJ for the different storm types. The value of the MLJ is similar for the SL, TC and IT. There is an appreciable difference, however, in the height at which the MLJ is observed (see Table 2.3). The height of the MLJ is smaller in the case of SL (2.8 km) than in the cases of TC (3.5 km) and IT (4.6 km). The magnitude of the wind shear between surface and the MLJ is similar for the three storm types, being slightly greater in the cases of SL and TC than in the case of IT.

2.3.4 A comparison with mid-latitude storms

In Table 2.4 the mean values of some thermodynamic and windfield variables for the Venezuelan storms are compared with the mean values of nine mid-latitude multicell storms (MS) and five mid-latitude supercell storms (SS). The mean values of the mid-latitude storms were obtained from the data given by Marwitz (1972a, 1972b). The mean

value of $\Delta T_{500\ mb}$ is greater for the mid-latitude multicell and supercell storms than for the tropical convective systems observed over Venezuela. The mean value of the turning of winds with height in the subcloud layer is greater for the mid-latitude storms than for the Venezuelan storms. However, the winds associated with the Venezuelan storms may turn as much in a clockwise sense (veering) as in a counterclockwise sense. This contrasts with the mid-latitude storms studied by Marwitz which, with only one exception, turned in a clockwise sense. The values of the mean wind in the subcloud layer for the mid-latitude multicell and supercell storms are 5.0 and 12.8 m s^{-1}. The value for the mid-latitude multicell storms is comparable with those observed in Venezuela, but the supercell storms have much greater values. In the cloud layer, the mean wind is much greater for the mid-latitude storms than for the Venezuelan storms. Also, the mean values of the wind shear in the cloud layer are greater for the mid-latitude multicell and supercell storms ($2.6 \times 10^{-3} s^{-1}$ and $3.5 \times 10^{-3} s^{-1}$, respectively) than for the Venezuelan storms (about $1.5 \times 10^{-3} s^{-1}$). In the tropics the wind shear measured over the depth of the convective systems is usually small. This is especially marked in tropical areas such as Venezuela, in which a jet at mid-levels is observed, as we pointed out before, and there is a change from easterly shear at low levels to westerly shear at upper levels. As a consequence of this, the wind shear for the cloud layer is relatively small. The storm speed is, however, very similar for the Venezuelan and mid-latitude storms.

From the above discussion, it appears that the greater values of mean wind and wind shear in the subcloud and cloud layers, and the greater values of atmospheric instability, are the main reasons for the greater intensity of the mid-latitude storms, which are usually accompanied by heavy hail and, in some cases, by tornadoes.

2.4 Modification of the environment

In order to study the modification of the environment caused during the passage of the convective mesosystems, we will make use of dry and moist static energies defined, respectively, as

$$s = c_p T + gz \qquad \text{——(2.2)}$$

$$h = s + Lq \qquad \text{——(2.3)}$$

where $c_p T$ is the enthalpy, gz the gravitational potential energy, and Lq the latent heat content, c_p being the specific heat at constant pressure (taken constant as 1.005×10^3 J kg^{-1}), T the temperature, g the gravity acceleration (9.8 m s^{-1}), z the hydrostatic height, L the latent heat of vaporization (taken constant as 2.474×10^6 J kg^{-1}), and q the specific humidity. These quantities have the property of being conserved in dry and moist adiabatic processes, respectively. The moist static energy is unaffected by phase changes, which merely redistribute energy between the enthalpy and the latent heat content. Their use is increasing in parameterization of cumulus convection (e.g., Arakawa and Schubert, 1974) and thus it appears convenient to study the thermodynamic characteristics of the environment in terms of such quantities. A relationship between the moist static energy and the equivalent potential temperature has been pointed out in the literature (Madden and Robitaille, 1970; Betts, 1974).

We will use the relative components of wind along and perpendicular to the direction of motion, rather than the conventional east-west and north-south components, as relative winds are more relevant in studying the dynamics of convective systems. Following Betts et al. (1976) and Mansfield (1977), we will assume here that soundings taken before and after the passage of the convective systems are sufficiently representative of the unmodified inflow and unmodified outflow.

Figures 2.1 to 2.3 show mean profiles of dry static energy, moist static energy, latent heat content and relative winds along and perpendicular to the direction of motion for the three types of convective systems mentioned above. The soundings were averaged over 25 mb intervals, from surface to 150 mb. A discussion of the main points follows.

2.4.1 Dry static energy

In all cases there is a definite decrease of dry static energy at lower levels. This implies a cooling and stabilization of a layer near the ground as a consequence of the convective-scale downdraught and the evaporation of precipitation. In association with this downdraught there exists a competition between two effects: evaporative cooling and adiabatic compressional warming. The observations show that the former effect dominates over the latter. The depth of the layer over which the decrease in dry static energy is observed is variable, but it is smaller in the cases of TC. This decrease in dry static energy at lower levels is greater for the SL (Fig.2.1) and IT (Fig.2.3) than for TC (Fig.2.2). An increase in dry static energy (implying a warming) in a layer located at mid-levels (roughly between 800 and 700 mb) is observed in all cases. These changes in dry static energy may be explained in terms of the two kinds of downdraught, which Zipser (1977) has described as distinct components of the convective system. One of them is a convective-scale saturated downdraught which produces a shallow layer of cool, near-saturated air in the lowest 500 m. The other (described also by Zipser, 1969) is a mesoscale unsaturated downdraught which is responsible for the drier air found over the shallow near-saturated layer mentioned above. Some mechanisms that might produce such unsaturated downdraughts will be examined in Chapter 4.

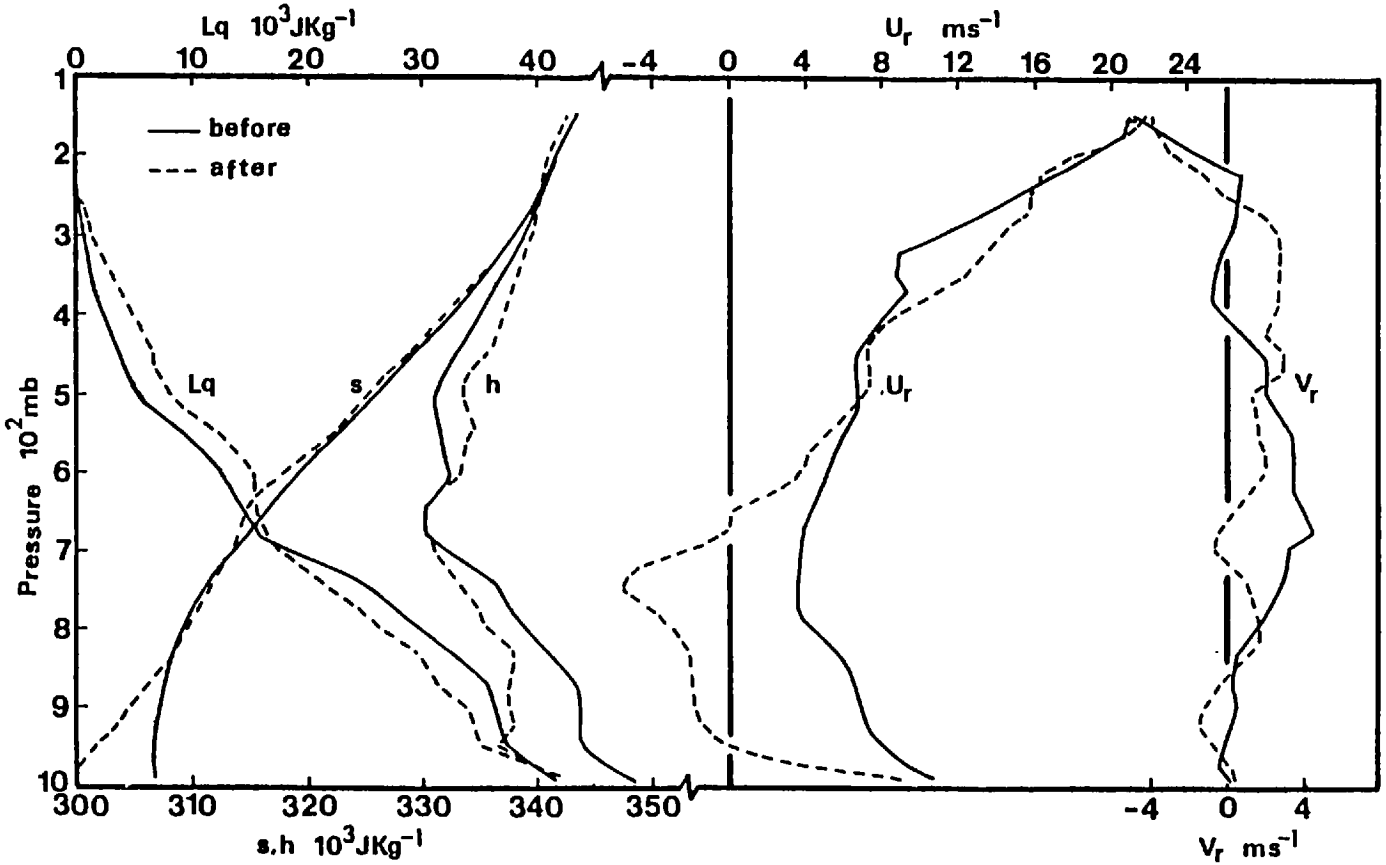

Fig. 2.1 Mean profiles of dry static energy (s), moist static energy (h), latent heat content (Lq), and relative winds along (U_r) and perpendicular (V_r) to the direction of motion before and after the passage of a Venezuelan squall line over the rawinsonde site. Mean motion vector is $81^o/13.5$ m s^{-1}. Composite includes before-after sounding pairs 100-101, 120-121, 176-177, 192-193, 241-242.

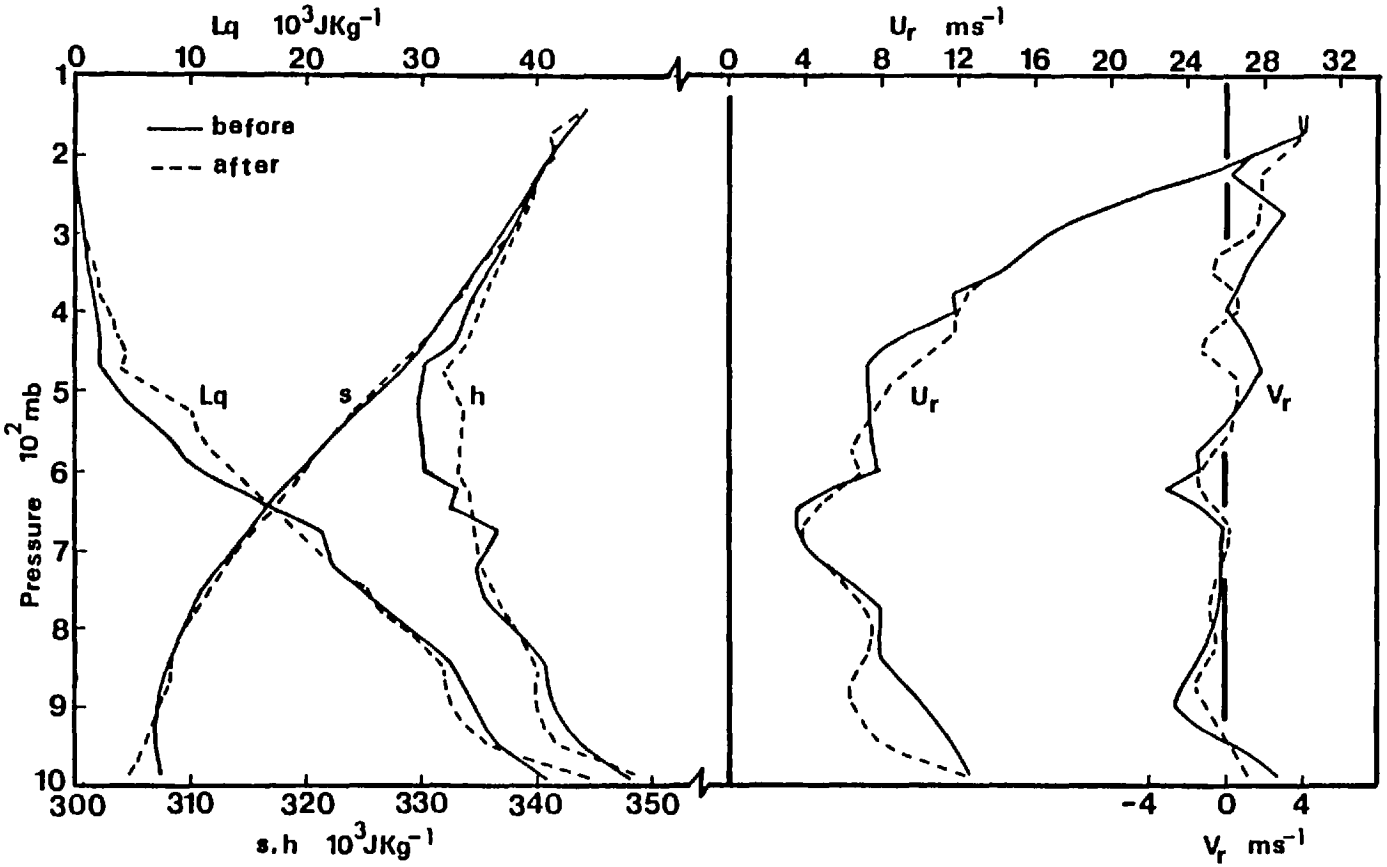

Fig. 2.2 As Fig.1, but for a thunderstorm cluster. Mean vector motion is $108^{o}/14.0$ m s^{-1}. Composite includes before-after sounding pairs 116-117, 157-158, 287-288.

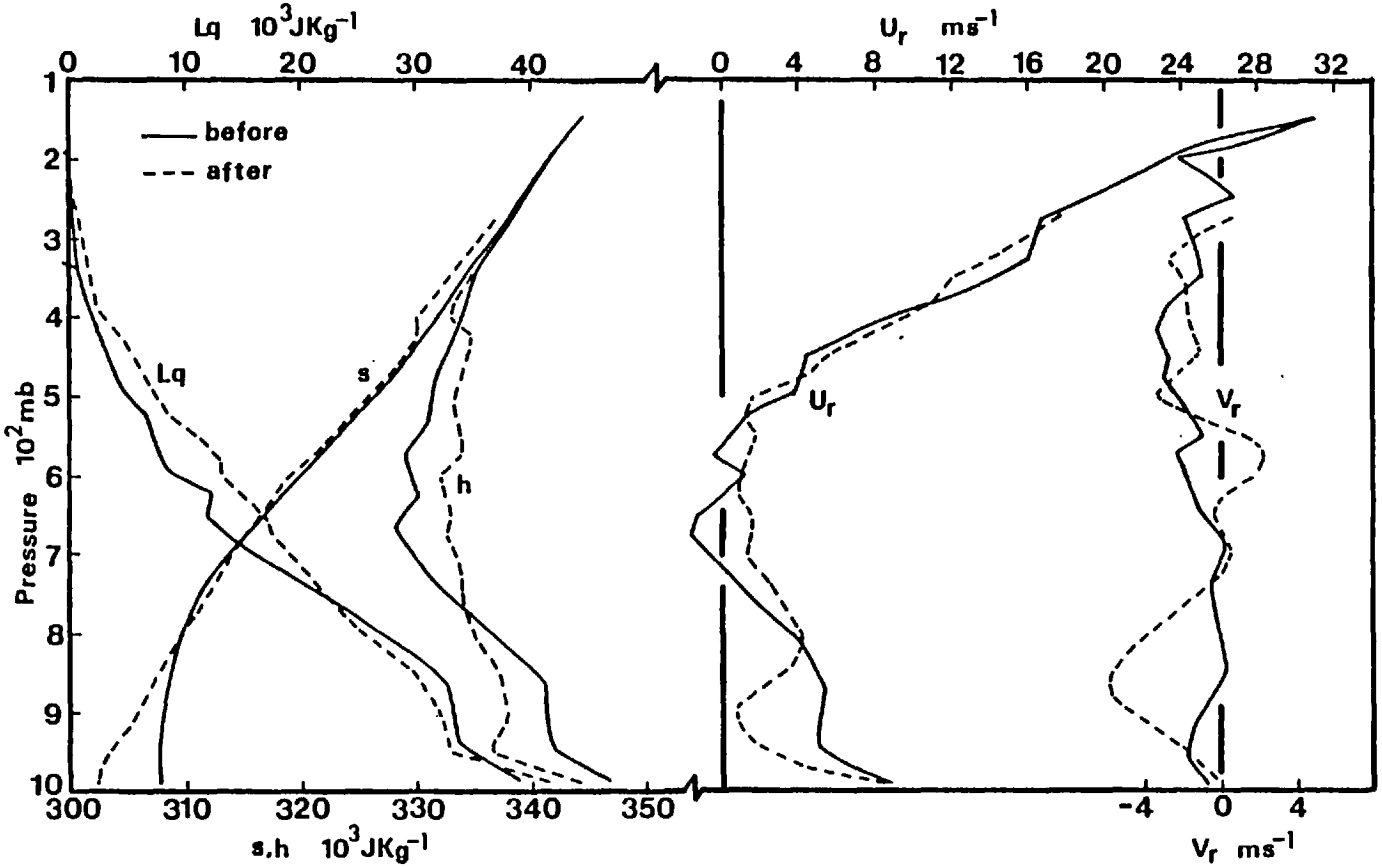

Fig. 2.3 As Fig.1, but for an isolated thunderstorm. Mean motion vector is $114^{o}/11.2$ m s^{-1}. Composite includes before-after sounding pairs 71-72, 203-204, 220-221.

The TC also show an increase in a layer between 700 mb and 600 mb, and above 425 mb. The SL and IT show a decrease in dry static energy in most of the upper levels. This decrease is also shown by the TC, but only at very high levels (above 225 mb). The decrease at upper levels for the SL and TC is about $10^3 J\,kg^{-1}$, corresponding to a cooling of about 1^oK. For the IT this decrease at upper levels is somewhat greater. However, these differences in dry static energy at upper levels are relatively small, and they may not be really significant. On the other hand, the physical processes responsible for such differences are not apparent.

2.4.2 Moist static energy and latent heat content

A fall of moist static energy at low levels and an increase at upper levels is observed for all groups of storms. This indicates that an overturning of the troposphere has taken place; air rich in moist static energy (potentially warm) of low levels is transported to high levels and replaced by air with low values of moist static energy (potentially cold) from mid-levels. The fall in moist static energy at low levels is greater for the SL and IT than for the TC. The increase at upper levels is greater for the IT than for the other storm types.

As the moist static energy is a conservative property in moist adiabatic processes we can use it, assuming mixing is unimportant, in order to determine where the air that enters the system at some level leaves it. Therefore we can deduce the height to which parcels rose or fell in the updraught or downdraught, respectively. Knowing the relative winds, we can then deduce the dynamical structure of the convective mesosystems. These ideas will be used later on in order

to construct conceptual models for the Venezuelan storms.

The profiles of the latent heat content present similar patterns to those of the moist static energy. There is a fall of latent heat content at low levels (except in a layer close to the ground) and an increase at upper levels in all cases. This shows that the down-draught transport of air with lower moist static energy has resulted in a decrease of the latent heat content at low levels. Close to the ground, however, an increase in latent heat content is observed as a consequence of the evaporation of precipitation. The increase in latent heat content at upper levels supports the idea that it consists of air of boundary layer origin. In association with the moist static energy, the fall in latent heat content is greater for the SL and IT than for the TC. The increase at upper levels is greater for the IT than for the other storm types.

2.4.3 Changes in the windfield

The wind profiles taken before the passage of the convective meso-systems show inflow at all levels at the front of the system for all types of storms. An important feature is that the relative winds after the passage of the storms show outflow at the rear of the system at all levels in the case of TC and very small inflow in a narrow layer at middle levels in the case of IT. This supports Moncrieff's and Miller's (1976) analytical model which requires outflow at all levels at the rear of the system. The composite of the squall lines, however, shows inflow at the rear of the systems in the layer between 950-675 mb. As Betts et al. (1976) used only squall lines in their evaluation of the Moncrieff-Miller model, they thought that the model failed in predicting the wind profiles observed at the rear of the system. However, Figures 2.2 and 2.3 show that the model is more realistic than the work carried

out by those authors had suggested.

As we will see in the next chapter, the West African disturbance lines, as well as those occurring over the Eastern tropical Atlantic, show relative inflow at all levels at the front of the system and relative outflow at all levels at the rear of the system.

The inflow observed at the rear of some squall lines may be related to a pressure drop at mid-levels which draws air into the storm from all directions at these levels. This is actually observed in numerical simulations of the Venezuelan squall lines. We have examined the height deviations and windfield at 800 mb and at 32 minutes of a numerical simulation corresponding to storm 47. The numerical results show that at 800 mb there is a pressure drop, which produces convergence of air into the storm. In general, if the relative flow of the converging air is large compared with the relative flow at mid-levels, then inflow at the rear would be observed at such levels.

In general, Figures 2.1 to 2.3 show an increase of easterly momentum at low levels and westerly momentum at upper levels. The increase of easterly momentum at low levels is quite appreciable in the case of SL. The fact that the increase of easterly momentum at low levels is not equal to the increase of westerly momentum at upper levels (see Figs. 2.1 to 2.3) implies a mass imbalance which is very possibly related to the two-dimensionality of the analysis. The changes in the wind component perpendicular to the direction of motion (V_r) emphasize the importance of the three-dimensional structure of the convective systems. The modification of the windfield is greater in the case of SL than in the cases of TC and IT.

As was indicated previously, the type of data given in Figs. 2.1 to 2.3 may be used to construct conceptual models of the dynamical structure of the storms. Fig.2.4 illustrates this for the case of squall lines.

Assuming that the storm is moving towards 270°, air that enters the system at 950 mb with a relative velocity of 90°/8 m s^{-1} becomes part of the updraught and leaves the system at 150 mb with a relative velocity of 100°/22 m s^{-1}. Thus the net turning of the relative winds through the depth of the convective system is small. The downdraught originated from air entering the system at about 800 mb with relative velocity 70°/4.5 m s^{-1}. This air leaves the system at about 975 mb with a relative velocity of 90°/4.6 m s^{-1}. The Venezuelan squall lines also show some relative inflow at the rear of the storm. This inflow air enters the storm at about 800 mb with a relative velocity of 300°/3.5 m s^{-1} and leaves the system at 950 mb with relative velocity 40°/1 m s^{-1}. The downdraught structure is more complicated than the one shown in Fig.2.4 because when the downdraught air arrives at the surface it may spread out in all directions.

The other types of storms (TC and IT) present a similar dynamical structure, except that the depth of the downdraught layer is smaller in the other cases, and also the TC and IT do not show relative inflow at the rear of the storm.

2.4.4 Changes in relation to the size of the storm

As each type of storm includes systems with different radar echo sizes, it might be argued that the modification of the environment during the passage of a convective system is more related to the storm size than to the storm type. However, grouping the storms by size rather than by type did not produce a significant difference between storms with maximum echo area in the 400-1000 km^2 range and those with maximum echo area less than 400 km^2. Storms with maximum echo area in the 2300-3700 km^2 range, which are all squall lines, modify the environment much more strongly than those with maximum echo area less

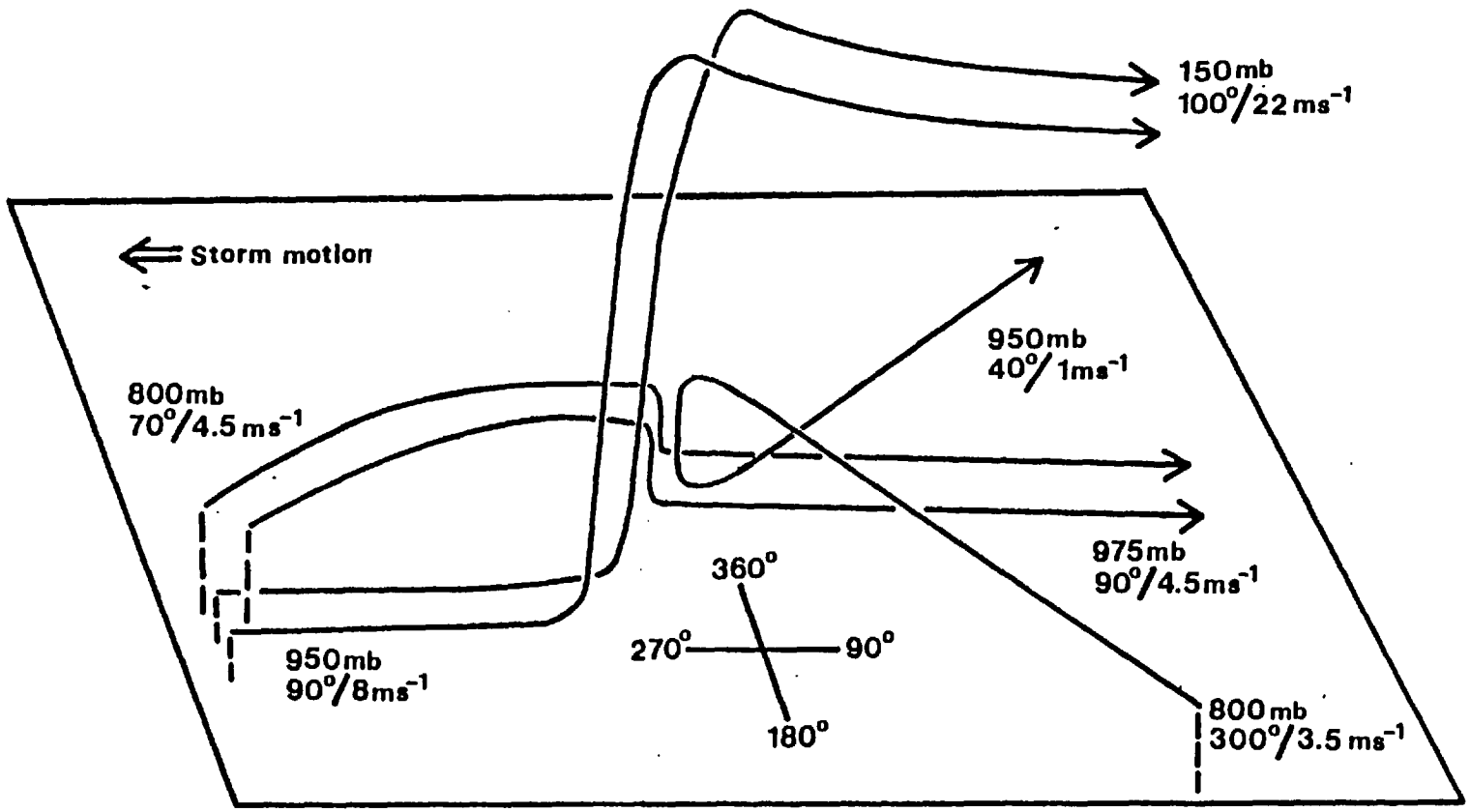

Fig. 2.4 Three-dimensional model of the relative airflow within a Venezuelan squall line. The storm's speed with respect to the ground is 13.5 m s^{-1}.

than 1000 km^2.

2.5 Some aspects of storm movement

It is interesting to compare the velocity of the mid-level jet (MLJ), as well as the mean wind (evaluated, say, over 0-10 km), with the observed storm velocities.

In Table 2.5 values corresponding to the ratios of the observed speed (C_{ob}) to the speed of the mean wind (C_M) and the speed of the MLJ (C_{Max}) are given. This table also shows the differences between the observed storm direction of motion (D_{ob}) and the directions of the mean wind (D_M) and the MLJ (D_{Max}).

In relation to the mean wind, four of the SL moved to the left and the other two to the right. In the cases of TC, three storms moved to the left and three to the right. Three of the IT moved to the left and the other two to the right. Therefore these Venezuelan storms do not show any preference to move to the right or to the left of the mean wind. In a few cases the deviation with respect to the mean wind is substantial (about 40^o), as in storms 27 and 58. In almost all cases, except in the case of storm 9, the storms move at a speed much faster than the speed of the mean wind. The mid-latitude storms, in contrast, move approximately with the speed of the mean wind.

The deviation between the direction of movement of the storms, with respect to the direction of the MLJ, is relatively small for most of the storms. In a few cases, however, as in storms 47, 64, 43 and 31, the deviation with respect to the MLJ is appreciable (about 45^o for storm 47, and about 33^o for storms 64, 43 and 31). From the values of C_{ob}/C_{Max}, an evaluation of the speed of the MLJ as an empirical predictor for the storm speed can be made. It can be seen that the speed of the MLJ is a good predictor for the speed of most of the storms, except

Table 2.5 Comparison of the observed storm velocity with the mean wind and the mid-level jet (MLJ).

Storm	Sounding No.	$\frac{C_{ob}}{C_M}$	$\frac{C_{ob}}{C_{Max}}$	$D_{ob}-D_M$ deg.	$D_{ob}-D_{Max}$ deg.
27/SL	100	1.60	1.19	-43	-14
35/SL	120	2.28	1.04	31	- 8
47/SL	176	1.94	0.91	- 9	-46
53/SL	192	1.62	1.11	8	8
60/SL	226	2.19	1.15	-32	19
64/SL	241	3.04	1.29	-30	-33
Mean	-	2.11	1.12	-12	-12
33/TC	116	3.59	1.21	14	-18
43/TC	157	5.44	1.09	3	32
46/TC	162	1.62	0.75	-20	- 7
51/TC	190	1.41	0.87	18	16
135/TC	264	2.69	1.11	-24	-14
89/TC	287	1.74	0.89	-24	- 2
Mean	-	2.75	0.99	- 5	+ 2
9/IT	71	0.85	0.52	13	16
14/IT	81	1.19	0.89	- 2	- 1
31/IT	106	1.29	0.68	-36	-36
55/IT	203	2.21	0.68	35	10
58/IT	220	6.09	1.04	-40	- 4
Mean	-	2.33	0.76	- 6	- 3

for storms 64, 46, 9, 31 and 55, the last three being IT. We conclude, therefore, that in general the MLJ is a good empirical predictor for the velocity of convective systems occurring in Venezuela. In the next chapter we will see that this is also true for travelling convective storms occurring in other tropical regions, such as West Africa and the Eastern tropical Atlantic. In those cases in which the MLJ is not well marked, the maximum wind in the cloud layer is the appropriate empirical predictor for the storm velocity.

The deviation of the storm with respect to the mean wind or the MLJ may at first glance be attributed to the magnitude of the vertical wind shear and the turning of winds with height. An examination of all the hodographs of the storms considered in this study showed the following points:

a) Storms with weakly sheared hodographs, especially in the cloud layer, show little deviation with respect to the mean wind and the MLJ.

b) If the magnitude of the wind shear in the cloud layer is relatively large ($> 1.5 \times 10^{-3} s^{-1}$) and the turning of winds with height is appreciable, the deviation with respect to the mean wind is large.

A comparison of the hodographs for the Venezuelan storms with some hodographs for mid-latitude storms such as those given by Chisholm and Renick (1972) shows that although the magnitude of the wind shear is much greater for the mid-latitude storms, the turning of winds with height, especially in the cloud layer, presents a more complicated pattern in the case of the Venezuelan storms.

2.6 Conclusions

On the basis of radar data, a classification of storms in squall lines, thunderstorm clusters, and isolated thunderstorms was made. In

examining the environmental conditions associated with the storms, few significant differences were observed. In general, the near-environment of the SL shows a slightly greater instability than the environment of the TC and IT. In the sub-cloud and cloud layers, the wind shear and the turning of winds with height are somewhat greater in the case of TC than in the cases of SL and IT. This may account for the greater asymmetry and three-dimensionality of the TC. An appreciable difference in the storms' environment is the height at which the MLJ is observed, the height being smaller in the case of SL than in the cases of TC and IT

The modification of the environment, as deduced from changes in the dry static energy, moist static energy, latent heat content and relative winds, is much greater in the case of SL than in the other cases. This is possibly related to the storm size, the squall lines being much bigger systems than the TC and IT. It is important that all these differences are taken into account when making budget studies of cumulonimbus convection.

The speed of the MLJ is a good empirical predictor for the speed of the Venezuelan storms. In addition, the direction of the MLJ might help in predicting empirically the direction of motion of such storms.

Although a few differences in the near-environmental conditions associated with different types of storms have been found, it is not known for certain how the environment organizes the storms in lines or clusters. The organization in different storm types is very possibly related to synoptic factors and orography. The synoptic situation frequently forms regions of moisture and instability aligned in distinct tongues (Newton, 1963). On the other hand, when surface heating is the primary mechanism, orography plays a very important role in determining where the first convective elements will form. In

order to elucidate this aspect, detailed synoptic and mesoscale analysis of many study cases would be required, and this constitutes a topic for further research.

CHAPTER 3

ENVIRONMENTAL CONDITIONS AND STRUCTURE OF THE WEST AFRICAN AND EASTERN TROPICAL ATLANTIC SQUALL LINES*

3.1 Introduction

One of the most prominent weather systems identified by meteorologists working in West Africa is the disturbance line (DL) or squall line. This consists of a line of thunderstorms oriented roughly north-south, moving westwards, which develop to the north of the intertropical convergence zone (ITCZ). Sometimes less organized convective systems formed in the interior of the ITCZ are also included under the name of disturbance lines. The distinction is quite arbitrary, since there is much variation in detail from one DL to another, and possibly even along the length of an individual DL. According to Hamilton and Archbold (1945), a DL may consist of: (a) a long continuous belt of thunderstorms; (b) a long belt of isolated storms; (c) a line of showers; (d) a line of heavy cloud, or (e) a line made up of parts, each of which may be any one of types (a)-(d), although naturally consecutive parts will be of neighbouring types.

The DL have been described by several authors (Hamilton and Archbold, 1945; Eldridge, 1957; Tschirhart, 1958; Dohnneur, 1971, 1974; Obasi, 1974; LeRoux, 1976) and their climatological aspects are, in general, well known (Aspliden et al., 1976). An experiment carried

---

* A slightly modified version of this chapter has been submitted for publication in the Archiv für Meteorologie, Geophysik und Bioklimatologie, Serie A.

out by the Agence pour la Sécurité de la Navigation Aérienne en Afrique et à Madagascar (ASECNA) during the period 1-10 August, 1973 and called Operation Pre-GATE ASECNA (OPGA), provided valuable data to study some aspects of these convective systems. Final reports of the experiment (ASECNA, 1974, 1975) include an analysis of the fields of several meteorological parameters and a description of the evolution of some DL. Riehl et al. (1974) used the data collected in the experiment to make composites of the synoptic fields of divergence and balances of energy, moisture and vorticity associated with the DL. A case study of a DL based on GATE (GARP Atlantic Tropical Experiment) satellite pictures has also been made by Fortune (1977).

Some characteristics of the DL are the following:

1) The DL is primarily a continental phenomenon; genesis also occurs over the ocean, but very infrequently. From 176 DL observed during the three phases of GATE (a total of 63 days), Aspliden et al. (1976) found that 162 and 130 generated and decayed over land, respectively. Over the ocean, only 14 formed and 46 decayed.

2) They may occur at any time during the year, but they are more frequent in the summer when the southwest monsoon extends farthest northward. At this time of the year, the trade winds of the southern hemisphere cross the equator and their track curves towards the NE so that they arrive over West Africa as a moist southwesterly current. This current is overlain by dry and hot easterly winds leaving the Sahara; the separation surface (frequently called a front) slopes to the south. In the northern part of this zone, the moist southwesterly current is too shallow and no significant convection occurs, while farther south, around the Guinea coast, it is quite deep and appreciable instability is not present. The DL occur between these limits, where the moist

layer is moderately deep and, with the dry easterlies above, marked convective (potential) instability exists. In the winter season the moist air does not penetrate far inland, and the DL are infrequent.

3) There are some preferred areas of formation. Cumulonimbus clouds produced over hills frequently move away and develop into DL. Plateaus in the Agadez region, the Jos Mountains in Nigeria, the Cameroon Mountains and the Marra Mountains in Sudan, are among the areas favoured for the formation of DL.

4) It appears that the genesis of the DL is affected by the presence of synoptic-scale easterly waves. These waves develop somewhere around 15^{o} to 30^{o} E and cross the tropical regions of Africa from mid-June until early October (Burpee, 1972). Their wavelengths are in the 1500-4000 km range, the periods in the 2.2 - 5.5 days range, and the westward speed in the 5-10 m s^{-1} range. The average wavelength and period are about 2500 km and 3.5 days. According to Burpee (1977), they first appear near 700 mb, but as they propagate westward they intensify and influence an increasingly greater depth of the atmosphere. In the latter part of August and September they arrive at the west coast of Africa, at latitudes of about 10^{o} to 16^{o} N, with a maximum amplitude of about 5 m s^{-1}. Aspliden et al. (1976) determined the distribution of the locations of genesis of cumulonimbus and DL in relation to the cyclonic axis at 700 mb of easterly waves. They found that the region from the 700 mb wave trough axis to about 750 km ahead of the trough, at latitudes of 10^{o} to 15^{o} N, was a preferred area for the generation of DL. In this region Burpee (1975) found that an upward motion exists at low levels (925 mb). Payne and McGarry (1977), using satellite data from Phase III of GATE, tracked 36 squall lines that had an average lifetime of 10 hours. They also found that the occurrence of squall lines was most frequent in the region approximately one-fourth of a wavelength

ahead of the wave-trough axis. The squall lines were most likely to form in this region in the early afternoon over land, and they were observed to move westward through the wave at about twice the wave phase speed, and terminate just to the east of the 700 mb ridge. As the DL are formed more frequently in the afternoon hours (1400-1700 LST), it follows that in their genesis the simultaneous influence of strong surface heating and low-level convergence is very important.

5) The DL move westwards faster than the winds at all levels. Their mean speed is about 15 m s^{-1}, with a tendency to move faster during the day than during the night. Inland they move faster than when they approach the coast (ASECNA, 1975). It has been suggested (Hamilton and Archbold, 1945) that the DL propagates as a gravity wave, the propagation speed depending on the height and intensity of the interface between the moist layer and the overlying drier and warmer air. This point will be expanded later on in this chapter.

6) The distance travelled is very variable, from about 150 to 3000 km. A distance of 1000 to 1200 km appears to be a frequent mean trajectory between the first and latest manifestations of the DL, the bigger systems travelling a longer distance.

7) The DL may split in two parts, or two neighbouring storms may merge. The splitting in two parts is favoured when the line becomes elongated meridionally (ASECNA, 1975).

8) The patterns of precipitation are discontinuous and very irregular, with separate nuclei of appreciable amounts of rainfall. It has been observed (ASECNA, 1975) that precipitation nuclei of different DL do not interact with each other. This fact confirms the idea that in the tropics rain of more than 10 mm does not fall twice in the same place in 24 hours (Henry, 1974).

9) Over the oceans the squall lines generally form in early

morning (0300-1000 LST) and they move, in general, a little slower than the DL moving over land (Aspliden et al., 1976).

Fig.3.1 is a sequence of METEOSAT infrared satellite pictures taken every three hours, which shows the movement and evolution of a West African disturbance line. The line structure is not clearly defined in satellite pictures because of the cirrus shield formed by cumulonimbus anvils. The DL originated sometime in the 1500-1800 GMT period (a little time before the first satellite picture of Fig.3.1 was taken) near 5^{o} West and 15^{o} North. It moved westwards with a mean speed of about 19.8 m s^{-1}, travelling a distance of about 2360 km (from about 4^{o}E to 18^{o}W) during the period considered in the Figure (33 hours). This speed is quite large compared with the mean speed shown for most of these disturbances (about 15 m s^{-1}). A diurnal variation of the convective system is clearly observed in Fig.3.1. In the period 0000-1500 GMT on 30 June, it becomes disorganized and moves more slowly at a mean speed of about 17.7 m s^{-1}, while during the period 1500-2400 GMT on 30 June it is well organized and moves very fast at a mean speed of about 28 m s^{-1}.

In this chapter we will describe, as we did before with some types of convective mesosystems observed over Venezuela, the near-environmental conditions in advance of three West African and three Eastern tropical Atlantic squall lines, as well as the modification of the environment during the passage of the storms. We will also examine some aspects of the structure and motion of these convective systems, and a comparison with the Venezuelan squall lines will be made. The values quoted for the Venezuelan storms are those given in Chapter 2.

Fig.3.1 Sequence of METEOSAT infrared satellite pictures showing the movement and evolution of a West African disturbance line. The cross marks in the figure are at 10^{o} North with a separation of 10^{o} of longitude; the middle cross indicates the 0^{o} of longitude. The top of the first picture is about 16^{o} North.

29 Jun - 1 Jul 1979

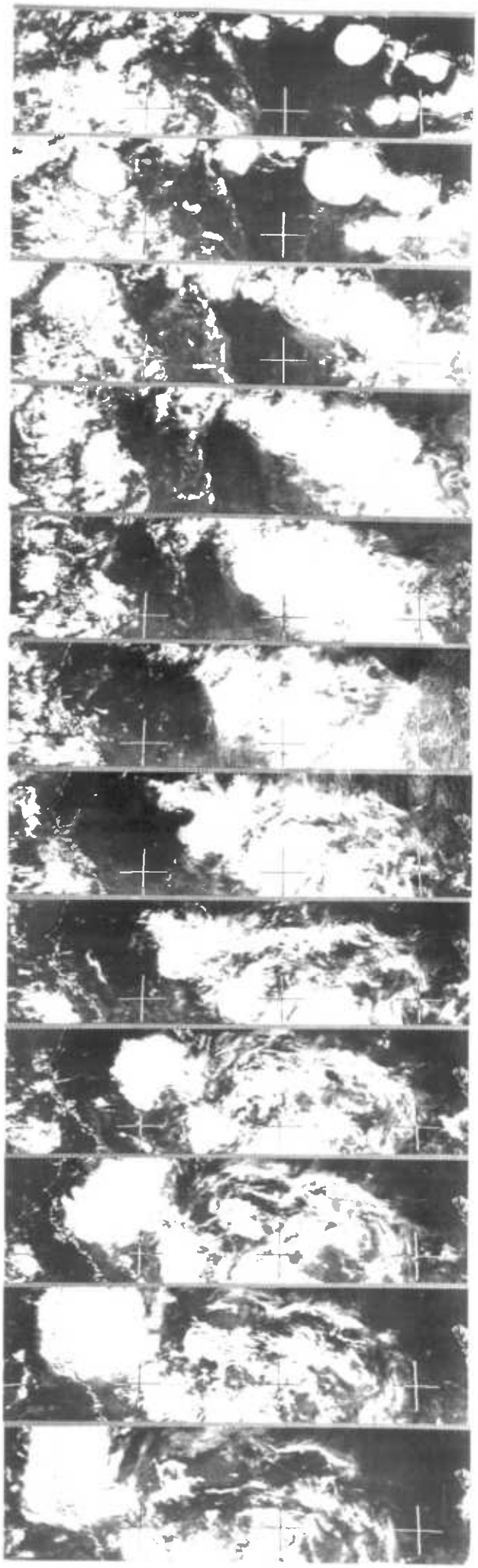

18

21

24

03

GMT

06

09

12

15

18

21

24

03

3.2 Description of observational data

Three DL observed over land during OPGA and three squall lines observed over the ocean during GATE have been selected for this study. A description of the DL observed in OPGA may be found in ASECNA (1975). The squall lines observed in GATE have been described by Houze (1975, 1977) and Mansfield (1977). These case studies have also been used by Fernandez and Thorpe (1979) in their evaluation of two analytical theories of storm motion (see Chapter 5).

The rawinsondes of OPGA were launched at Bamako ($12^{o}38'$ N, $08^{o}02'$ W), Mali, and those of GATE were launched from the ship 'Oceanographer' ($7^{o}45'$ N, $22^{o}12'$ W). At Bamako radiosonde ascents were made every six hours, but on one occasion (on 10 August 1973) they were made every three hours. At 'Oceanographer' they were made every three hours. During GATE, in addition to the rawinsonde observations, data from a variety of sources such as radar, satellites, surface stations, cloud photography and acoustic sounders were also available. With this data a detailed study of a squall line observed over the ocean on 4-5 September, 1974 has been made by Houze (1977). For this reason in this chapter we will put a little more emphasis on the characteristics of the DL observed over land.

Tables 3.1 and 3.2 show some data on the characteristics of the West African and Eastern Atlantic squall lines selected for this study. The West African DL observed over land have a longer lifetime (about 40 hours on average) than the squall lines observed over the Eastern Atlantic (about 10 hours). However, the West African DL selected in this study have a longer lifetime than other DL observed by Payne and McGarry (1977) from satellite pictures. The average lifetime of the type of squall cluster observed by them was about 10 hours, similar to the Eastern Atlantic squall lines. The lifetime for the Venezuelan

TABLE 3.1 Some characteristics of three West African disturbance lines.
σ is the standard deviation

Name	Life-time	Meridional extension*	Zonal extension*	Distance travelled	Max. precipitation	Movement Dir. (from)	Movement Speed
	hours	km	km	km	mm	deg.	m s^{-1}
Brigitte	63	800	400	3400	60	90	15.0
Dominique	18	700	500	1000	40	68	15.3
Fabienne	38	750	400	1900	70	68	14.0
Mean	39.7	750	433	2100	56.7	76	14.8
σ	22.6	50	58	1212	15.3	13	0.7

* as deduced from satellite pictures

TABLE 3.2 Some characteristics of three Eastern Atlantic squall lines.
σ is the standard deviation

Storm index	Date 1974	Life-time	Length of squall line*	Movement Dir. (from)	Movement Speed
		hours	km	deg.	m s^{-1}
G	Sept. 4	14	> 250	45	12.7
H	Sept.11	> 6	300	53	16.0
I	Sept.12	> 9	300	45	15.1
Mean		9.7	283	48	14.6
σ		~ 4.0	~ 29	5	1.7

* as deduced from radar

storms was about 3 hours. The DL observed over land have also a much greater length (about 750 km) than those observed in the Eastern Atlantic (about 350 km). The average length for the Venezuelan squall lines was about 100 km. The storm speed is similar for the West African and Eastern Atlantic squall lines (about 15 m s^{-1}). The mean speed for the Venezuelan squall lines was a little smaller, about 13.5 m s^{-1}.

3.3 Environmental thermodynamic and windfield characteristics

3.3.1 Thermodynamic variables

Table 3.3 shows some thermodynamic characteristics of the storms' near-environment in advance of the squall lines. The values of CAPE and ΔT at 500 mb (as defined in Chapter 2), corresponding to the West African DL, are very large (mean values of 2093 J kg^{-1} and 5.4°C respectively). These values are much greater than those corresponding to the Eastern Atlantic squall lines (mean values of 930 J kg^{-1} and 2.4°C), as well as those corresponding to the Venezuelan squall lines (mean values of 1006 J kg^{-1} and 3.1°C). The largest value of CAPE corresponds to Dominique, which produced a very complex pattern of rainfall distribution (ASECNA, 1975).

The mean value of specific humidity in the subcloud layer for the West African DL is about 18.6 g kg^{-1}, which is greater than those corresponding to the Eastern Atlantic and Venezuelan squall lines (about 15 g kg^{-1}).

The height of the lifting condensation level (LCL) for the West African DL is about 800 m above ground level, while for the Eastern Atlantic storms it is about 570 m on average. For the Venezuelan

TABLE 3.3 Thermodynamic variables of the near-environment of West African and Eastern Atlantic squall lines. σ is the standard deviation

Storm	CAPE	ΔT at 500 mb	$\overline{q}$ sub-cloud layer	LCL AGL	TEL AGL
	$J\ kg^{-1}$	^{o}C	$g\ kg^{-1}$	m	m
Brigitte	1740	4.5	18.5	615	13900
Dominique	3150	6.5	20.4	600	13700
Fabienne	1390	5.3	16.8	1175	12150
Mean	2093	5.4	18.6	797	13250
σ	932	1.0	1.8	328	958
G	738	2.5	15.7	420	11740
H	1681	3.8	15.7	562	12960
I	373	1.0	14.4	734	10620
Mean	930	2.4	15.3	572	11773
σ	675	1.4	0.8	157	1170

squall lines it was about 1275 m. The mean heights of the thermodynamic equilibrium level (TEL) for the West African and Eastern Atlantic convective systems are about 13.3 and 11.8 km respectively.

3.3.2 Windfield variables

Table 3.4 shows the mean values of wind, turning of wind with height and wind shear for the layers' surface to 900 mb and 900 to 200 mb, which are taken here as being representative of the subcloud and cloud layers respectively.

Subcloud layer: The mean winds for the West African and Eastern Atlantic storms are about 3.2 and 3.6 m s^{-1}. They are smaller than those corresponding to the Venezuelan squall lines (about 5.6 m s^{-1} on average). However, from Figs. 2.1, 3.2 and 3.3 it can be seen that the mean relative winds along the direction of motion (U_r) in the subcloud layer are much greater for the West African and Eastern Atlantic squall lines (about 15 m s^{-1}) than for the Venezuelan squall lines (about 8 m s^{-1}). As the values of U_r are much greater in the cases of West African and Eastern Atlantic squall lines, a larger mass flux may enter the system. This may be the reason for the greater intensity of the West African and Eastern Atlantic convective storms.

The turning of wind with height is somewhat greater for the Eastern Atlantic squall lines (about 64^{o}) than for the West African DL (about 23^{o}). For the Venezuelan squall lines it was, on average, -15^{o}, but the standard deviation is greater in the case of these Venezuelan storms (about 43^{o}, compared with 21^{o} for the West African and Eastern Atlantic squall lines). In all cases of West African and Eastern Atlantic squall lines considered here, the wind turned in a

TABLE 3.4 Near-environmental windfield variables for some squall lines observed over West Africa and the Eastern tropical Atlantic ocean.
σ is the standard deviation

Storm	Sub-cloud layer			Cloud layer		
	Mean wind $m\ s^{-1}$	Turning deg.	Wind shear $10^{-3}s^{-1}$	Mean wind $m\ s^{-1}$	Turning deg.	Wind shear $10^{-3}s^{-1}$
Brigitte	2.3	0	4.2	10.2	-30	1.5
Dominique	3.9	30	4.0	9.7	170	1.3
Fabienne	3.5	40	3.8	8.2	170	1.7
Mean	3.2	23	4.0	9.4	103	1.5
σ	0.8	21	0.2	1.0	94	0.2
G	5.2	40	3.8	6.6	117	2.0
H	3.3	77	4.6	6.3	112	2.3
I	2.2	76	3.8	4.3	-104	1.7
Mean	3.6	64	4.1	5.7	42	2.0
σ	1.5	21	0.5	1.3	103	0.3

clockwise sense. In the cases of the Venezuelan squall lines, the wind turned as frequently in a clockwise as in a counterclockwise sense. The wind shear in the subcloud layer is similar for the West African, Eastern Atlantic and Venezuelan squall lines (about 4×10^{-3} s^{-1}).

Cloud layer: The mean wind in this layer is greater for the West African DL (about 9.4 m s^{-1}) than for the Eastern Atlantic and Venezuelan squall lines (about 5.7 and 6.3 m s^{-1}, respectively). This difference in the mean wind for the cloud layer is a consequence of the wind profiles associated with these storms. In the Eastern Atlantic and Venezuelan cases the wind profiles exhibit a mid-level jet (MLJ), which is not clearly defined in the West African cases considered here. The magnitude of the MLJ for the Eastern Atlantic and Venezuelan squall lines is about 14.7 and 11.8 m s^{-1}, respectively. The heights corresponding to these values are 3.2 and 2.8 km, respectively.

The mean turning of wind with height is about 103 degrees for the West African DL and about 42 degrees for the Eastern Atlantic squall lines, but the standard deviations are very large (94^{o} and 103^{o} respectively). Nevertheless, the turning of wind with height is somewhat smaller in the cases of West African and Eastern Atlantic squall lines than in the cases of Venezuelan squall lines (mean value of 177 degrees with a standard deviation of 57 degrees). The magnitude of the wind shear in the cloud layer is about 1.5×10^{-3} s^{-1} for the West African DL and 2.0×10^{-3} s^{-1} for the Eastern Atlantic squall lines. The corresponding value for the Venezuelan squall lines is about 1.5×10^{-3} s^{-1}.

3.4 Modification of the environment

In order to study the modification of the environment caused during the passage of the squall lines, we will make use of dry and moist static energies, as it was in Chapter 2.

Figures 3.2 and 3.3 show the mean profiles of dry static energy, moist static energy, latent heat content, and relative winds along and perpendicular to the direction of motion for the West African and Eastern Atlantic squall lines respectively. The composites include all the storms selected for this study: three West African disturbance lines and three Eastern Atlantic squall lines. We will assume here that soundings taken before and after the passage of the convective systems are sufficiently representative of the unmodified inflow and unmodified outflow. A discussion of the main points follows.

3.4.1 Dry static energy

As expected, there is a decrease in dry static energy (implying a cooling) after the passage of the storms, for the reasons mentioned in Chapter 2. The top of the layer over which this decrease is observed, is about 870 mb for the West African DL, and about 950 mb for the Eastern Atlantic squall lines. The corresponding top for the Venezuelan squall lines is similar to that of the West African DL. The change in dry static energy is thus greater in the cases of squall lines occurring over land than in the cases occurring over the ocean. This is due to the dry air from the Sahara at mid-levels giving a stronger potential cooling at lower levels. An increase in dry static energy at mid-levels (implying a warming) is observed in the cases of the West African and Eastern Atlantic squall lines. This was also observed in the case of the Venezuelan squall lines. This increase in in dry static energy at mid-levels appears to be smaller in the squall

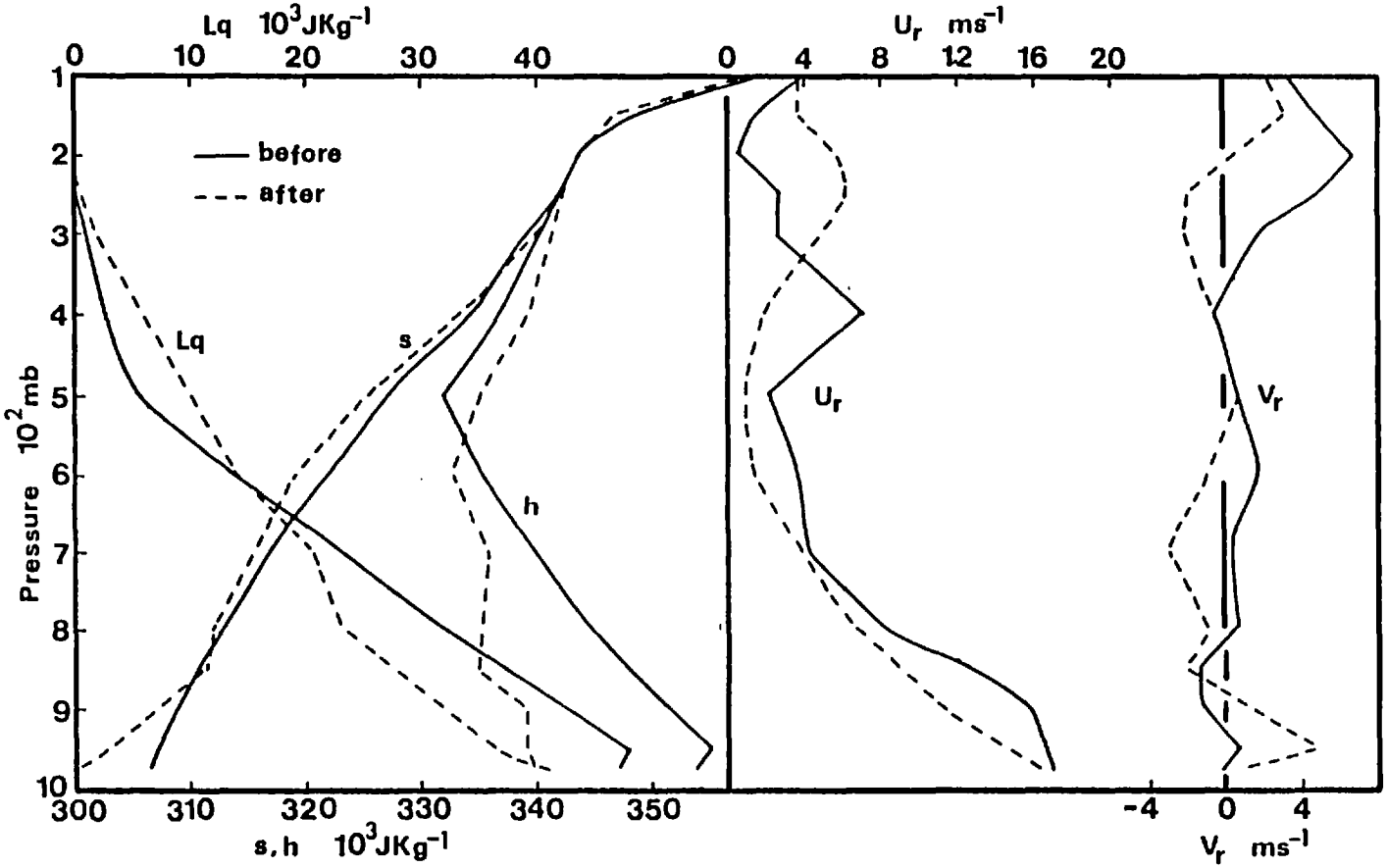

Fig.3.2 Mean profiles of dry static energy (s), moist static energy (h), latent heat content (Lq), and relative winds along (U_r) and perpendicular (V_r) to the direction of motion before and after the passage of a West African disturbance line over the rawinsonde site. Mean motion vector is $76^o/14.8$ m s^{-1}. Composite includes the storms mentioned in Table 3.1.

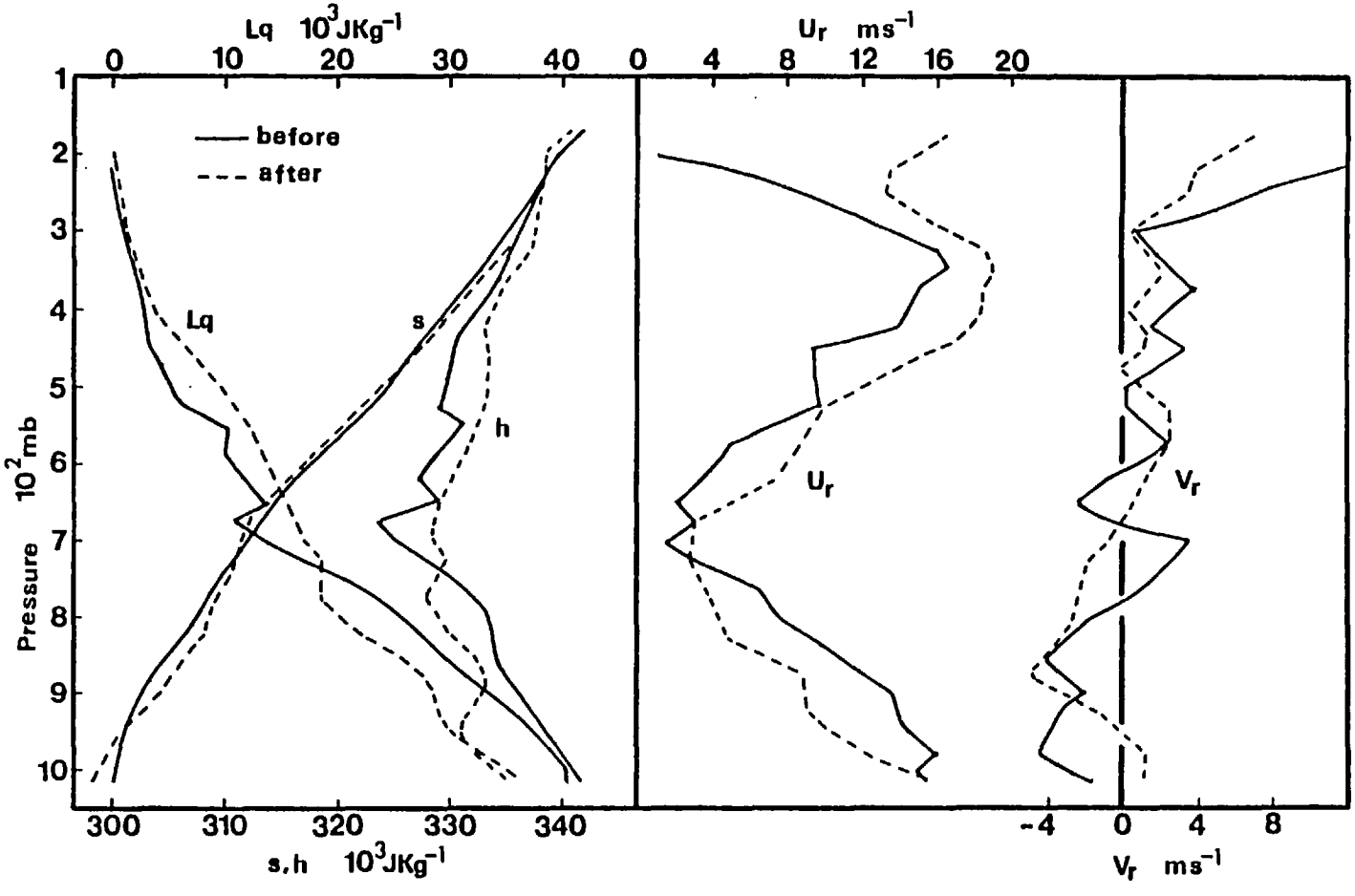

Table 3.3 As Fig.3.2 but for an Eastern Tropical Atlantic squall line. Mean motion vector is $48^{o}/14.6$ m s^{-1}. Composite includes the storms mentioned in Table 3.2.

lines occurring over land than in those occurring over the ocean. These changes in dry static energy at lower and middle levels were explained in Chapter 2 in terms of the two kinds of downdraught which Zipser (1977) has described as being distinct components of the convective systems. One of them is a convective-scale saturated downdraught which produces a shallow layer of cool, near-saturated air in the lowest few hundred metres; the other is a mesoscale unsaturated downdraught which is responsible for the drier air found over the shallow, near-saturated layer mentioned above. In the next chapter we will examine some mechanisms that might produce such a mesoscale downdraught.

At upper levels (above 200 mb) the West African and Eastern Atlantic squall lines show a decrease in dry static energy, which might be produced by radiative cooling of the cloud top.

3.4.2 Moist static energy and latent heat content

As in the cases of the Venezuelan storms, a fall of moist static energy at low levels and an increase at upper levels is observed in the cases of the West African and Eastern Atlantic squall lines. The changes associated with the West African DL are much greater than the changes associated with the Eastern Atlantic squall lines, and also with those associated with the Venezuelan storms.

The fall in latent heat content at lower levels is greater in the case of the West African disturbance lines than in the case of the Eastern Atlantic squall lines. The increase in latent heat content at upper levels is somewhat similar for the West African and Eastern Atlantic squall lines.

3.4.3 Changes in the windfield

The mean wind profiles corresponding to the West African and Eastern Atlantic squall lines show relative inflow at all levels at the front of the system and relative outflow at all levels at the rear. This is also observed in the individual cases, except for one Eastern Atlantic squall line in which relative inflow (above 800 mb) at the rear is observed. This supports the analytical model of Moncrieff and Miller (1976), which not only requires relative inflow at all levels at the front of the system, but also relative outflow at the rear. In contrast, the Venezuelan squall lines, as pointed out in Chapter 2, often show appreciable inflow at the rear of the system in the 950-675 mb layer.

An increase of easterly momentum at lower levels and westerly momentum at upper levels is observed. However, the layer over which the increase of easterly momentum is observed is much deeper in the case of the West African disturbance lines than in the case of the Eastern Atlantic squall lines. The increase of easterly momentum at lower levels is much greater in the case of the Venezuelan squall lines (see Fig.2.1) than in the cases of the West African and Eastern Atlantic convective systems. The reason for this difference is not clear, but it could be related to the synoptic situations associated with the convective systems in those areas. The difference, however, explains why the Venezuelan squall lines show some relative inflow at the rear.

It could be inferred from Fig.3.2 that the near-environment of the West African squall lines do not show a well defined mid-level jet, as is observed in the Eastern Atlantic and Venezuelan cases. However, meteorologists in West Africa are familiar with two circulation features consisting of two currents overlying the monsoon flow. One of these currents, the Tropical Easterly Jet (TEJ), is observed

in mean charts of upper levels as a well developed jet stream. The other current is the African Easterly Jet (AEJ), which is found at mid-levels (700-600 mb). The structure of the AEJ is not well understood, but it appears that some atmospheric systems, such as the African Easterly waves, are associated with this jet (see, for example, Burpee, 1977). From cross sections of the windfield given by Burpee (1972), it can be inferred that the easterly flow at mid-levels generally increases from east to west near 15^{o}N. It is relatively weak at 35^{o}E, but becomes organized into a well defined easterly maximum over most of the western part of Africa (say between 8^{o}E to 14^{o}W). Therefore the reason why this mid-level jet is not observed in soundings taken before the passage of the DL being studied here, requires some explanation.

Figs. 3.4 and 3.5 show cross-sections of the windfield components at Bamako during 10 August, 1973. These cross sections were made with soundings taken every three hours during the period being considered. The U-component field (Fig.3.4) shows a well defined easterly jet centred about the 600 mb level, with maximum intensity at about 1200 GMT. In the immediate vicinity of the storm (the arrow in Fig.3.4 indicates the time of arrival at Bamako) the intensity of the mid-level jet is nevertheless relatively small. Therefore this appears to indicate that once these large convective systems have formed and start moving at a speed comparable to that of the mid-level jet, they perturb the windfield in their surroundings in such a way that the mid-level jet is not well defined. A diurnal variation in the intensity of the mid-level jet with maximum values at 1200 GMT and 0000 GMT may be inferred from Fig.3.4. However, cross-sections covering all periods of the OPGA experiment (ASECNA, 1974) do not show such a diurnal variation of the mid-level jet. The V-component field (Fig.3.5) shows some relatively large values below the 700 mb level in the

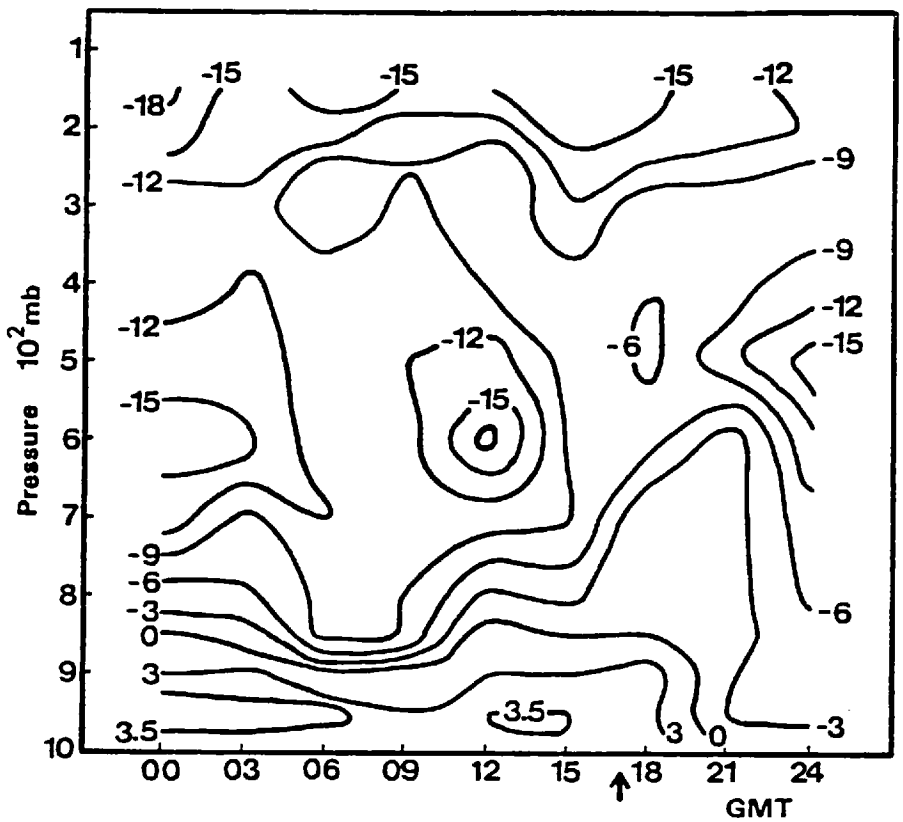

Fig.3.4 Cross section of the zonal wind (U) in m s^{-1} at Bamako (12° 38'N, 08° 02'W) on 10 August 1973. The arrow indicates the time of arrival of the disturbance line Fabienne at Bamako.

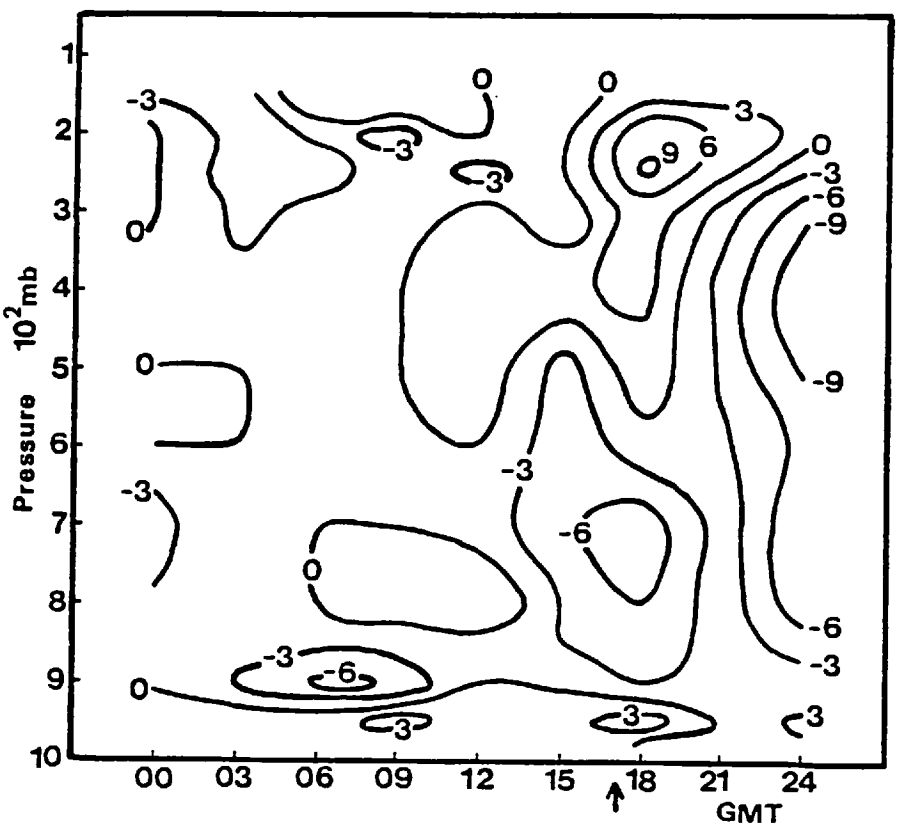

Fig.3.5 As Fig.3.4, but for the meridional wind (V).

1500-1800 GMT period. This is possibly related to the increase of intensity of the monsoon flow due to surface heating. Another feature observed in Figs. 3.4 and 3.5 is the presence of a well defined southwesterly current at low levels (about 900 mb) in the period 0600-0900 GMT, which could have been responsible for the development of local convection during such a period in the Bamako area.

Since the moist static energy is a conservative property in adiabatic processes, Figs. 3.2 and 3.3 may be used to construct conceptual models of the dynamical structure of the convective systems. We will illustrate this for the case of the West African DL.

Fig.3.6 is a conceptual model of the flow in a West African DL. Assuming that the storm is moving towards 270^{o}, air that enters the system at 950 mb with relative velocity $90^{o}/16.5$ m s^{-1} becomes part of the updraught and leaves the system at about 115 mb, with relative velocity $60^{o}/4.3$ m s^{-1}. The turning of the relative winds through the depth of the system is thus relatively small. The downdraught air that arrives at the surface and leaves the system at the rear with relative velocity $90^{o}/16.5$ m s^{-1} has originated from about 700 mb where it enters the system with relative velocity $90^{o}/4.2$ m s^{-1}. The downdraught structure, however, is much more complicated because when the air arrives at the surface it may spread out in all directions. Air that enters the system at 550 mb with relative velocity $90^{o}/4.2$ m s^{-1} leaves the system at the same level with relative velocity $90^{o}/1.2$ m s^{-1}.

3.4.4 Surface changes associated with the passage of West African DL

Figures 3.7 and 3.8 show the surface changes observed at Bamako

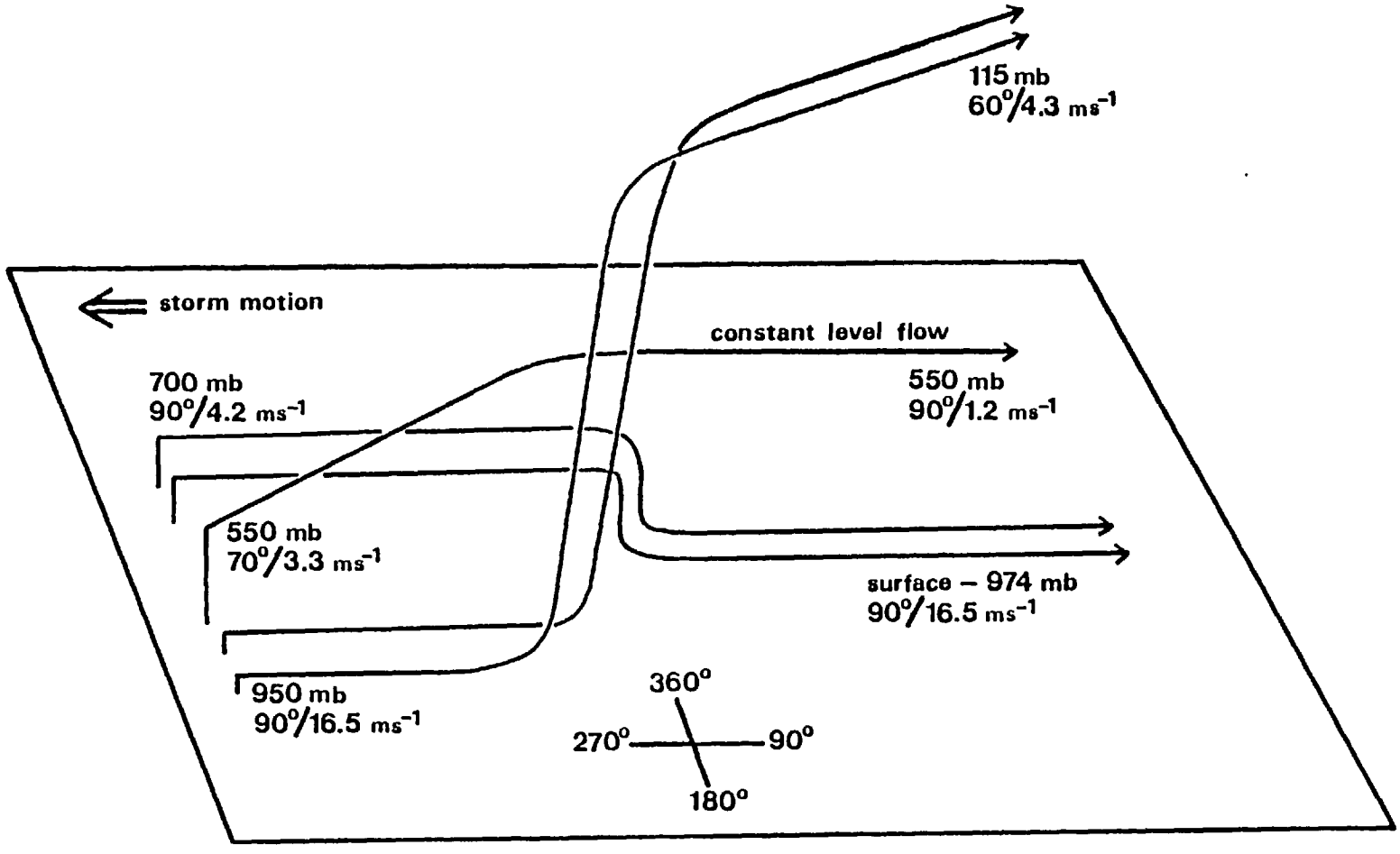

Fig.3.6 Model of the relative airflow within a West African disturbance line. The storm's speed with respect to the ground is 14.8 m s^{-1}.

during the passage of two West African squall lines (Brigitte and Fabienne). These figures were constructed with hourly data, but information on the maximum surface winds was also available. The weather elements plotted are wind speed and direction, relative humidity, temperature, pressure (reduced to sea level) and rainfall. With the arrival of the squall lines a sharp decrease in temperature and increase in relative humidity is observed. A gust in the wind speed and an abrupt change in wind direction are also observed. These changes are clearly related to the rainfall.

The temperature may decrease by as much as $9^{o}C$ in one hour or less, and the relative humidity may increase from values below 70% to saturation in the same period. The increase in wind speed is about 8 m s^{-1} and the change in wind direction is in the $120\text{-}150^{o}$ range. The amount of rainfall is similar for both storms (about 48 mm) but the period over which precipitation fell at Bamako might have been greater in the case of Brigitte than in the case of Fabienne. After the storms have passed the station, the thermodynamic conditions at the surface stay constant for a long period of time. The observed pressure change is due to the cold air at the surface produced by the downdraught.

3.5 Some aspects of storm movement

3.5.1 Movement in relation to the maximum wind in the cloud layer

In studying the Venezuelan convective systems (Chapter 2) we found that such storms move approximately with the maximum wind at mid-levels (the mid-level jet). Although the wind profiles associated with the West African DL dealt with in this study do not show

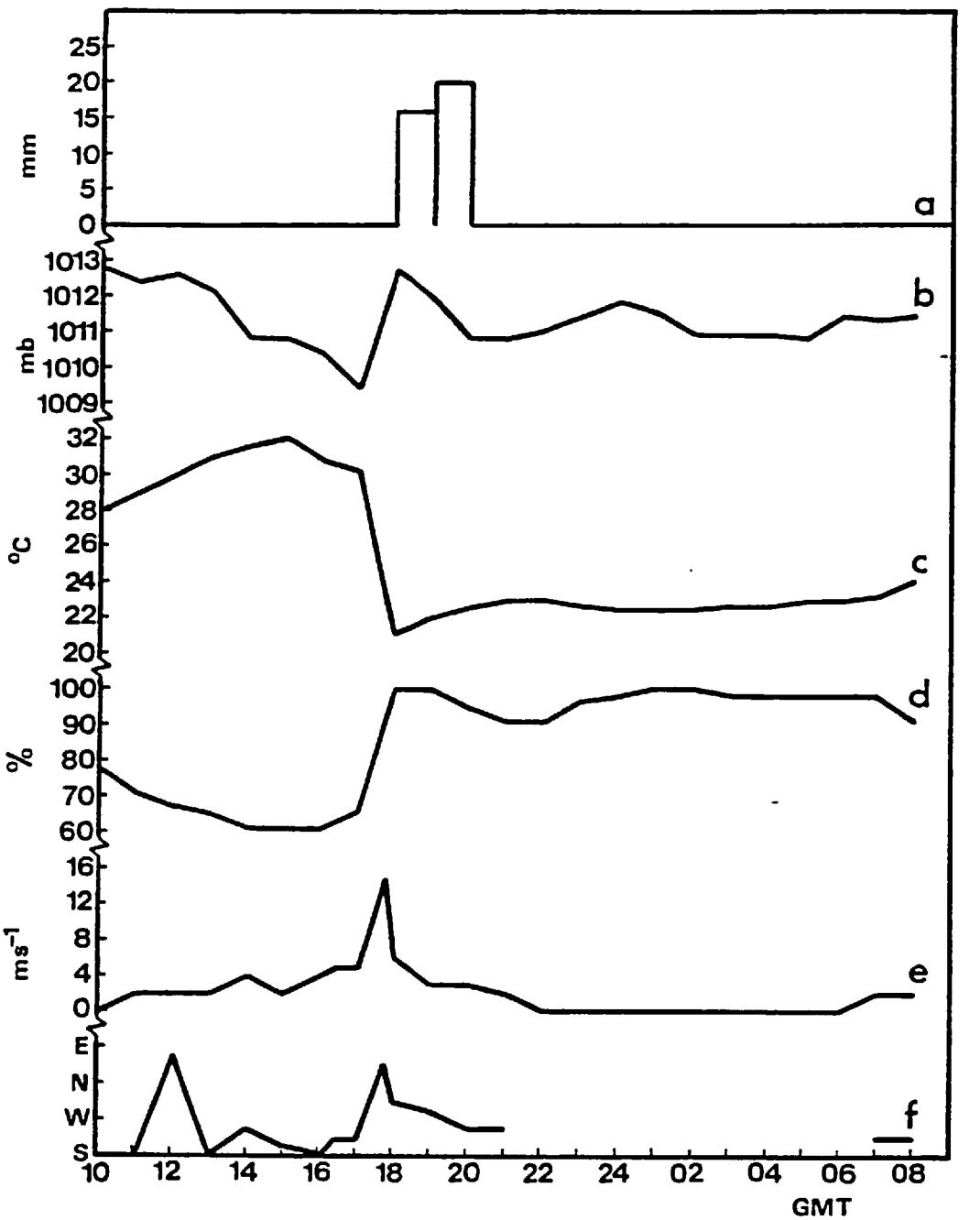

Fig.3.7 Surface changes associated with the passage of the West African disturbance line Brigitte over Bamako (12^{o} 38'N, 08^{o} 02'W). The data include wind direction and speed (m s^{-1}), relative humidity (%), temperature (^{o}C), pressure reduced at sea level (mb), and rainfall (mm). The time period shown is for 3-4 August 1973.

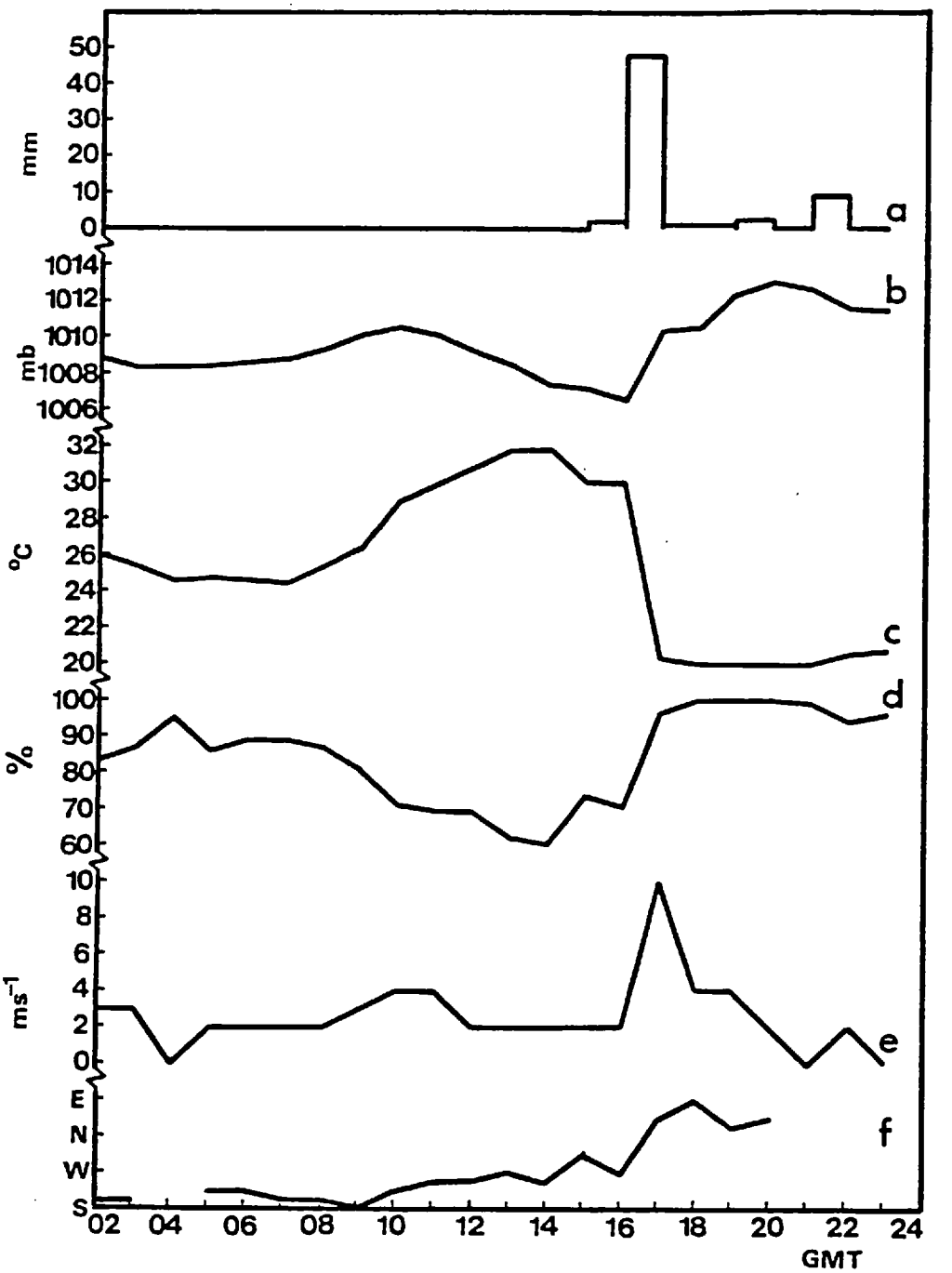

Fig.3.8 As Fig.3.7 but for the West African disturbance line Fabienne on 10 August, 1973.

a well defined maximum at mid-levels, it is still interesting to compare the observed storm velocity with the maximum wind in the cloud layer.

In Table 3.5, an evaluation of the maximum wind in the cloud layer (C_{Max}) as an empirical predictor for the storm velocity is made. It can be seen that C_{Max} is a good empirical predictor for the speed (C_{ob}) of the West African and Eastern Atlantic squall lines. In addition, the deviation with respect to the maximum wind in the cloud layer is relatively small, which emphasizes the importance of the maximum wind as a predictor for the storm velocity in tropical regions.

From the last column of Table 3.5 it could be inferred that the West African and Eastern Atlantic systems have a preference to move to the right of the maximum wind, in contrast to the Venezuelan convective systems that show a preference to move to the left of the maximum wind.

3.5.2 The hydraulic jump analogy

Hamilton and Archbold (1945) suggested that the DL propagates as a gravity wave, the propagation speed depending on the height and intensity of the interface between the moist layer and the overlying drier air. They approximated the situation to the one of wave motion along a rectangular canal in which an incompressible liquid is overlain by a layer of liquid of small density. Independently, Tepper (1950) developed in more detail the hydraulic jump analogy, following the work of Freeman (1948). Freeman discussed the motion of a disturbance, induced by accelerations of a piston, which propagated along an inversion. If a vertical plane piston is accelerated, the level of the inversion in its immediate vicinity will rise as a bump,

TABLE 3.5 Evaluation of the maximum wind as an empirical predictor for the velocity of the West African and Eastern Atlantic squall lines.
σ is the standard deviation

Storm	C_{Max} m s^{-1}	C_{ob} m s^{-1}	$\frac{C_{ob}}{C_{Max}}$	Deviation w.r.t. Max. wind deg.
Brigitte	13.0	15.0	1.15	0
Dominique	16.0	15.3	0.96	+12
Fabienne	12.0	13.9	1.16	+12
Mean	13.7	14.7	1.09	+ 8
σ	2.1	0.7	0.11	7
G	12.0	12.7	1.06	+17
H	15.3	16.0	1.04	- 1
I	16.8	15.1	0.90	+31
Mean	14.7	14.6	1.00	+16
σ	2.5	1.7	0.09	13

TABLE 3.6 Results obtained with the hydraulic jump analogy (Eq. 3.1) and comparison with the observed storm speeds (C_{ob}).

Storm	H (AGL) m	$\overline{\theta}'$ K	$\overline{\theta}$ K	C m s^{-1}	C_{ob} m s^{-1}
Brigitte	1213	304.4	309.0	13.3	15.0
Dominique	700	299. 5	304.7	10.8	15.3
Fabienne	700	304.2	309.2	10.5	14.0
G	1260	296.8	302.0	14.6	12.7
H	1264	298.4	303.8	14.8	16.0

producing a wave which would travel downstream as a gravity wave with a speed greater than the wind speed. Since the velocity of the various parts of the wave is a monotonically increasing function of their height, the slope of the leading edge of the wave would approach the vertical, thus creating a jump. When the piston starts to decelerate, a rarefaction wave would be formed, and it would follow the original wave with a speed greater than the speed of the jump. Tepper proposed that such a mechanism described by Freeman was applicable to squall lines. He visualised the atmosphere in the warm section of a cyclone as being composed of two layers separated by a stable interface. To complete the picture, Tepper assumed that a cold front acts as the piston, that is, the initial impetus required for the formation of the squall line is accomplished by a sudden and temporary acceleration of a cold front. However, as Tepper pointed out, strictly speaking the piston itself is not required, but rather any mechanism which would yield sudden accelerations of the wind below the inversion. The eventual dissipation of the pressure jump is implicit in such a mechanism, because the rarefaction wave, moving faster than the jump, eventually overtakes it and destroys it. Thus the lifetime of the squall line would depend on the intensity and duration of the acceleration, and on the nature of the deceleration which follows the acceleration. The jump would travel at a speed given by

$$C = \left[gH\left(1 - \frac{\theta'}{\theta}\right) \right]^{\frac{1}{2}} \qquad \text{—(3.1)}$$

where g is the gravity acceleration, H the depth of the lower layer (height of the inversion), and θ' and θ the potential temperatures of the fluid layers adjacent to the interface (the lower layer being potentially cooler).

Since it is common to observe an inversion at about 900-850 mb in soundings taken in advance of squall lines occurring over West Africa and the Eastern tropical Atlantic, an evaluation of Eq.(3.1) using the observations of the squall lines considered in this study has been made. In applying Eq.(3.1), mean values of θ' and θ were used, the depth of the upper layer taken to be the same as the depth of the lower one. Table 3.6 shows the details of the computations. The values obtained with Eq.(3.1) are, with one exception (storm G), smaller than the observed storm speeds (C_{ob}). The predictions are reasonable considering the approximate nature of the analogy and the consequent uncertainties in the computations. Storm I was not included in the evaluation of Eq.(3.1) because an inversion was not present in the sounding taken in advance of this storm.

3.5.3 Density current model

The cold air mass that flows outward from severe convective storms has been related to density or gravity currents by several authors (Simpson, 1969; Charba, 1974; Miller and Betts, 1977) and it has been suggested that a relationship may exist between the storm speed and that of the density current (Tepper, 1950; Charba, 1974). Charba examined the physics of such a cold air mass by comparing its structure with density currents observed in laboratory experiments carried out by Keulegan (1958), Middleton (1966) and Simpson (1969, 1972). He also compared the gust front's forward speed with that predicted from applications of empirical and dynamical theory of density currents (e.g. Keulegan, 1958; Benjamin, 1968). Miller and Betts made a similar comparison using observations of tropical convective systems over Venezuela.

The density current speed relative to still air is given by

$$C^* = \kappa C_\rho \qquad \text{—(3.2)}$$

where C_ρ is the densimetric speed (see Charba) given by

$$C_\rho = \left[gd(\rho_2 - \rho_1)/\rho_1 \right] \qquad \text{—(3.3)}$$

where ρ_2 and d are the density and mean depth of the gravity current, ρ_1 is the density of the ambient medium and g is the gravity acceleration. κ is the square root of the ratio of inertial to gravitational forces and it is, therefore, the square root of the Froude number of the density current. For practical purposes it is essentially an empirical constant.

Miller and Betts expressed C_ρ as

$$C_\rho = \left[- H_\rho \frac{\Delta s_v}{\overline{\rho}\,\overline{s_v}} \right]^{\frac{1}{2}} \qquad \text{—(3.4)}$$

where H_ρ is the pressure depth (Pa) of the layer of cooling, as deduced from soundings taken before and after the passage of a storm over a site, and $\overline{\Delta s_v}$ is the mean fall of virtual static energy in such a layer. The virtual static energy is defined as

$$s_v = s + \delta c_p Tq \qquad \text{—(3.5)}$$

where $\delta = 0.608$ and the other variables are those used in Eqs.(2.2) and (2.3). $\overline{\rho}$ and $\overline{s}_v$ in Eq.(3.4) are the mean values of density and virtual static energy in advance of the storm over the layer of depth H_ρ. Eq.(3.4) is simple to apply when soundings taken before and after the passage of a storm over a site are available.

In the studies of Charba and Miller and Betts, it was pointed out that more case studies are needed in order to test the general applicability of the density current model to cumulonimbus outflows. For this reason Eqs. (3.2), (3.4) and (3.5) have been applied to compute the density current speeds of the West African and Eastern Atlantic squall lines dealt with in this chapter, and compared them with the observed speeds (C_{ob}). Following Miller and Betts, the density current speed has also been compared with the maximum surface gust, G (when it is available) and the mean wind in the subcloud layer (depth H_B) along the direction of motion in advance ($\bar{u}_0$) and behind ($\bar{u}_1$) the storm system. The results obtained are shown in Table 3.7. The mean values obtained by Miller and Betts for the Venezuelan storms (VE) are also included in Table 3.7 for comparison purposes. The main points are:

a) The layer of cooling for the West African disturbance lines is much deeper than the subcloud layer. This contrasts appreciably with the Venezuelan storms for which H_B and H_ρ are comparable. For the Eastern Atlantic squall lines, H_ρ is much larger than H_B in two cases (storms G and H) but it is much smaller in the case of storm I.

b) The mean fall in virtual static energy is comparable for the West African and Venezuelan convective systems. As was pointed out before, the degree of cooling is greater for convective systems occurring over land than for those occurring over the ocean.

c) The values of C_ρ are, in general, much greater for storms occurring over land. For the Eastern Atlantic squall lines, C_ρ is very small because $\overline{\Delta s_v}$ and H_ρ are much smaller in these convective systems:

TABLE 3.7 Storm and sounding parameters derived for density current model.
σ is the standard deviation

Storm	H_B 10^2Pa	H_ρ 10^2Pa	$\overline{\Delta s}_y$ 10^3 J kg^{-1}	C_ρ ms^{-1}	C_{ob} ms^{-1}	$\overline{u}_0$ ms^{-1}	$\overline{u}_1$ ms^{-1}	G ms^{-1}	C_{ob}/C_ρ	$\overline{u}_0/C_\rho$	u_1/C_ρ	G/C_ρ
Brigitte	66	112	-3.3	10.5	15.0	1.5	-2.9	15.0	1.43	0.14	0.28	1.43
Dominique	64	450	-3.5	22.9	15.3	-3.2	2.3	--	0.67	0.14	0.10	--
Fabienne	121	271	-3.5	17.2	14.0	-2.3	-2.5	10.0	0.81	0.13	0.15	0.58
Mean	84	278	-3.4	16.9	14.8			12.5	0.97			1.01
σ	32	169	0.1	6.2	0.7			3.5	0.40			0.60
G	47	112	-1.4	6.8	12.7	0.9	-3.9	7.0	1.87	0.13	0.57	1.03
H	62	105	-3.7	10.6	16.0	-2.7	6.0	--	1.51	0.25	0.57	--
I	88	22	-1.2	2.9	15.1	-0.2	3.0	--	5.21	0.07	1.03	--
Mean	66	80	-2.1	6.8	14.6				2.86			
σ	21	50	1.4	3.9	1.7				2.04			
Mean	135	150	-3.2	11.8	13.5	5.4	12.4	10.9	1.08	0.44	1.02	0.88
VE σ	23	42	1.3	3.7	2.1	2.1	3.8	2.3	0.14	0.15	0.16	0.16

d) The values of C_{ob}/C_{ρ} show that for the West African disturbance lines, as well as for the Venezuelan storms, a close relationship exists between the storm speed and the speed of the density current. This relationship does not hold, however, in the case of the Eastern Atlantic squall lines. Therefore it appears that the density current model mentioned above is not applicable to convective systems occurring over the oceans.

e) A comparison of the values of $\overline{u}_0$ and $\overline{u}_1$ with C_{ρ} for the Venezuelan storms (Miller and Betts) appears to be irrelevant in the West African and Eastern Atlantic squall lines, because in these cases the mean flow in the subcloud layer may be in an opposite direction to that of the density current. This is also true if, instead of taking mean values of u_0 and u_1 over H_B, they are taken over H_{ρ}. The reason for this is that in the West African and Eastern Atlantic cases there is frequently a westerly flow at lower levels and an easterly flow at upper levels. For this reason a relationship between C_{ρ} (or C_{ob}) with $\overline{u}_0$ and $\overline{u}_1$ is not observed. For the Venezuelan storms the mean value of $\overline{u}_1/C_{\rho}$ is 1.02, but the mean value of $\overline{u}_0/C_{\rho}$ is 0.44.

f) The last column of Table 3.7 shows the values of G/C_{ρ} for the cases in which observations of the maximum surface gust were available to the author. The maximum surface gust for the Eastern Atlantic squall line (storm G) was obtained from data given by Houze (1977). The number of observations is not sufficient to arrive at a conclusion, but it appears that a relationship between G and C_{ρ} may exist.

3.6 Summary and conclusions

In this chapter the environmental conditions in advance of some West African and Eastern tropical Atlantic squall lines have been examined, as have the changes in atmospheric structure during the passage of such storms over a site. A comparison with other tropical convective systems observed over Venezuela has been made. Some aspects of storm motion were examined and a model of the relative airflow within a West African disturbance line was presented. The main conclusions are:

1. The near-environment of the West African disturbance lines shows a much greater instability than the environment of the Eastern Atlantic and Venezuelan squall lines. The humidity at lower levels is also greater in the West African cases than in the Eastern Atlantic and Venezuelan cases.

2. The relative winds along the direction of motion in the subcloud layer are much greater for the West African and Eastern Atlantic squall lines (about 15 m s^{-1}) than for the Venezuelan squall lines (about 8 m s^{-1}). This indicates that a larger mass flux may enter the system, which would account for the greater intensity of the West African and Eastern Atlantic squall lines.

3. The wind shear in the subcloud layer is similar for the West African, Eastern Atlantic and Venezuelan squall lines (about 4×10^{-3} s^{-1}).

4. In the cloud layer the mean wind is greater for the West African disturbance lines (about 9.4 m s^{-1}) than for the Eastern Atlantic and Venezuelan squall lines (about 6 m s^{-1}). The wind shear in the cloud layer is similar for the West African, Eastern Atlantic and Venezuelan storms (about 1.5×10^{-3} s^{-1}).

5. The turning of wind with height is somewhat smaller in the West African and Eastern Atlantic squall lines than in the Venezuelan storms.

6. The thermodynamic modification of the environment is much greater in the West African disturbance lines than in the Eastern Atlantic and Venezuelan squall lines. The cooling at lower levels is greater for convective systems occurring over land than for those occurring over the ocean.

7. The dynamical modification of the environment, as deduced from changes in the relative winds, is greater in the Venezuelan squall lines than in those in West Africa and the Eastern Atlantic. The wind profiles corresponding to the West African and Eastern Atlantic squall lines show relative inflow at all levels at the front of the system and relative outflow at all levels at the rear of the system. This contrasts with the Venezuelan squall lines, which show relative inflow at the rear of the system in the 950-675 mb layer.

8. There are sharp surface changes in the meteorological variables with the passage of a disturbance line over a station. The temperature may decrease by as much as $9^{o}C$ in one hour or less. The wind speed may increase by as much as 8 m s^{-1} and the change in wind direction is greater than 120^{o}. A sharp pressure rise is observed, which is due to the cold air at the surface produced by the downdraught.

9. It is found that the maximum wind in the cloud layer is a good empirical predictor for the West African disturbance lines, as well as for the travelling convective systems occurring over the Eastern tropical Atlantic.

10. The hydraulic jump analogy proposed by Tepper (1950) gives reasonable predictions for the speed of the West African and Eastern Atlantic squall lines.

11. The results obtained with a density current model show that for the West African disturbance lines, as well as for the Venezuelan storms, a close relationship exists between the storm speed and the speed of the

density current. As this relationship is not observed in the Eastern Atlantic squall lines, it appears that the density current model is not applicable to convective systems occurring over the ocean. A comparison between the maximum surface wind and the densimetric speed, show that a relationship between such variables may exist.

More case studies are needed in order to test the applicability of the hydraulic jump analogy and the density current model to tropical convective systems. Other aspects of storm movement, besides those considered in this chapter, have been examined by Fernandez and Thorpe (1979) and they will be discussed in Chapter 5. Further research on the West African disturbance lines should put special emphasis on the mechanism of their formation and the environmental conditions at the places and times of origin. Observational data from WAMEX (West African Monsoon Experiment) will be very useful for such purposes. Studies of the internal structure of the storms are also needed. The model of relative flow within a West African disturbance line deduced in this study must be interpreted with care, taking into account that there is much variability from one disturbance line to another. Numerical simulations, using realistic input data, may help in studying the dynamical structure of the storms and the author plans to carry out research on this matter.

CHAPTER 4

DOWNDRAUGHTS AT THE REAR OF TROPICAL SQUALL LINES

4.1 Introduction

In recent years much effort has been applied to the study of the interaction between small scale cumulus convection and the large scale environment. It has been assumed that cumulus convection with a length scale of about 1 to 10 km, responds in some way to a forcing by the large scale flow (length scale of about 10^3 km). Theories of cumulus parameterization have been developed (e.g. Ooyama, 1971; Arakawa and Schubert, 1974) and some diagnostic studies of the interaction processes have been carried out (e.g., Yanai et al., 1973; Ogura and Cho, 1973; Nitta, 1975; Johnson, 1976). In most of these studies, the cumulus cloud has been modelled as a one-dimensional, steady-state entraining plume updraught and the effects of precipitation evaporation have not been taken into account. However, Johnson (1976) developed a method to estimate the contribution to the total convective mass, heat and moisture transports by *convective scale* precipitation downdraughts. He found that convective-scale downdraughts contribute significantly to the total convective mass transport in the lower troposphere and that their omission leads to the diagnosis of excessively large populations of shallow cumulus clouds in highly convective situations.

An aspect that has not been taken into account in the studies mentioned above, is the role of *mesoscale* downdraughts (length scale of about 10^2 km) as an interaction mechanism between the convective scale and the large scale. For example, Zipser (1969), using data from the Line Islands Experiment, showed that highly unsaturated downdraughts

produced first on the convective scale and the mesoscale may become organized over the entire extent of the system. Cumulus development is then suppressed in the downdraught air and thus may produce a rapid decay of the weather system. Zipser (1977) has described the two kinds of downdraught (convective scale and mesoscale downdraughts) which are frequently observed at the rear of some squall lines. His study shows that a layer of cool, near-saturated air occupies the lowest few hundred meters, and is separated by a marked stable layer from a deep layer of highly unsaturated air. The lowest layer is the result of convective scale downdraughts, while the drier air is shown to be the result of mesoscale unsaturated downdraughts. Zipser (1969, 1977) and Riehl (1969) propose evaporation of anvil rain as the mechanism that produced such unsaturated downdraughts, and this is supported by the numerical study of Brown (1979). Miller and Betts (1977) have postulated, from a numerical experiment, that the drier air results from a dynamical response to the outflowing density current, rather than anvil rain.

In this chapter a review of the mechanisms proposed for the formation of downdraughts at the rear of tropical squall lines will be made. However, before presenting such mechanisms, some observational aspects of the downdraughts will be considered.

4.2 Observational evidence of downdraughts at the rear of tropical squall lines

Several studies have been made in relation to tropical squall lines (Betts, 1976a; Betts et al., 1976; Moncrieff and Miller, 1976; Miller and Betts, 1977; Zipser, 1969, 1977; Houze, 1977; Mansfield, 1977; Fernandez, 1980a, b). From such studies it is possible to visualise the basic features of a tropical squall line system. The typical

tropical squall lines behave in a different manner from those typical of *mid-latitudes* because they move faster than the wind at all levels in contrast to the mid-latitude systems which travel at nearly the speed of the mean wind. Air rich in moist static energy (potentially warm) from the boundary layer enters at the front, rises in the updraught and leaves at high levels at the rear. Thus the anvil trails behind the system in contrast to the typical mid-latitude squall lines where the anvil is at the front. However, in some mid-latitude cases, such as those studied by Newton (1950), Sanders and Paine (1975) and Sanders and Emanuel (1977) there is relative inflow at the front through a deep layer in a manner such that a significant depth of the anvil trails behind the squall line. Since the tropical squall line moves faster than the wind at all levels, the downdraught air may also arrive from the front and leave the system at the rear (e.g., Moncrieff and Miller, 1976; Fernandez, 1980 a, b). In some cases the squall lines may show relative inflow at the rear of the system (Zipser, 1969, 1977; Betts et al., 1976; Fernandez, 1980a) but not in others (Fernandez, 1980b). The tropical squall line moves by the discrete growth of new convective elements ahead of the old ones. This growth takes place at the leading edge of the gust front, formed by downdraught air from decaying cells whose remnants become part of the anvil cloud (Houze, 1977). The thickness of the anvil is quite large; in the region 30 to 100 km behind the squall line it may be about 8 km thick (Zipser, 1977; Houze, 1977). The base of the anvil in this region is located in the 4-6 km range, which includes the melting level. Beyond 100 km behind the gust front, the anvil tapers gradually to a thin cirriform cloud. The extension of the anvil, as deduced from satellite pictures, is quite large: 250 and 350 km in the cases studied by Zipser (1977) and Houze (1977), respectively, and about 400 km in some West African disturbance lines (Fernandez, 1980b). The region below the anvil's base is, in

general, free of significant convective clouds (Zipser, 1977). House (1977) estimated that about 40% of the precipitation from a squall line system observed in GATE (GARP Atlantic Tropical Experiment) fell from the trailing anvil cloud and pointed out that this precipitation was stratiform in character. He suggested that the large amount of rain falling from the anvil cloud may have resulted from the successive incorporation of precipitation-laden old squall line elements into the anvil region or from mesoscale ascent throughout the anvil cloud, as suggested by Brown's (1979) numerical model results. Brown found from a numerical study that mesoscale ascent in the middle and upper troposphere may exist behind the squall line, which would help in the maintenance of the anvil. On the other hand, the studies by Zipser (1969, 1977) show that mesoscale descent under the anvil takes place in the lower troposphere. Zipser (1977) found that wind divergence of about 1 to 5 x 10^{-4} s^{-1} over distances of 30-100 km behind the squall line, exists in the surface and mixed layer. He estimated that the speed of the mesoscale downdraught air was in the 5-25 cm s^{-1} range at 500 m. The mechanisms for the formation of this mesoscale downdraught are not clear, and some possible explanations will be discussed later.

Evidence of downward motion behind the squall line comes from data taken from aircraft penetrations at low levels, and from comparisons of soundings taken before and after the passage of the convective systems over a site. Data collected on aircraft penetrations at low levels (about 150 m altitude) through tropical squall line systems, as discussed by Zipser (1977), show that a well defined squall front separates ambient subcloud layer air from cool, near-saturated air in the heavy rain area (typically 10-30 km behind the squall front). The air in the heavy rain area is called by Zipser (1977) the *saturated downdraught air*. The aircraft data also show that there are some regions under the raining anvil with very low wet-bulb potential temperature values, low relative

humidity values and sometimes, but not always, higher temperature values than those found anywhere else at the same level. This air, with low values of wet-bulb potential temperature and relative humidity, is called by Zipser (1977) the *unsaturated downdraught air*. Zipser has pointed out that the area under the anvil occupied by unsaturated downdraught air is quite variable. The area tends to be larger with altitude and with the age of the system. It also appears to be larger at distances in the 100-200 km range behind the squall front.

Soundings taken behind tropical squall lines (see, for example, Zipser, 1977) show that a stable layer (with its base in the 400-500 m altitude range) separates cool and near saturated air close to the surface from very warm and dry air just above. The different properties of these two layers suggests two distinct origins for the air found in such layers. The cool and near-saturated air found close to the surface is likely to have descended in *convective scale* downdraughts in the squall line, while the warm and dry air above is likely to have descended in *mesoscale* downdraughts.

Figs. 4.1 to 4.3 show some profiles of dry static energy ($s = c_p T + gz$) and moist static energy ($h = s + Lq$) taken before and after the passage of two West African squall lines over Bamako, Mali, and one squall line over Carrizal, Venezuela. As the speeds of the squall lines in these cases are known, it is possible to deduce the distances in front or behind the squall line front at which the soundings were launched. The relative winds along (U_r) and perpendicular (V_r) to the direction of motion are also shown in Figs. 4.1 to 4.3. A comparison of the profiles of dry static energy (s) show that a warming has taken place in some regions behind the squall lines, say above 900 mb. The depth of the layer over which the warming is observed, the altitude of the base of this layer, and the magnitude of the warming, are quite variable. The

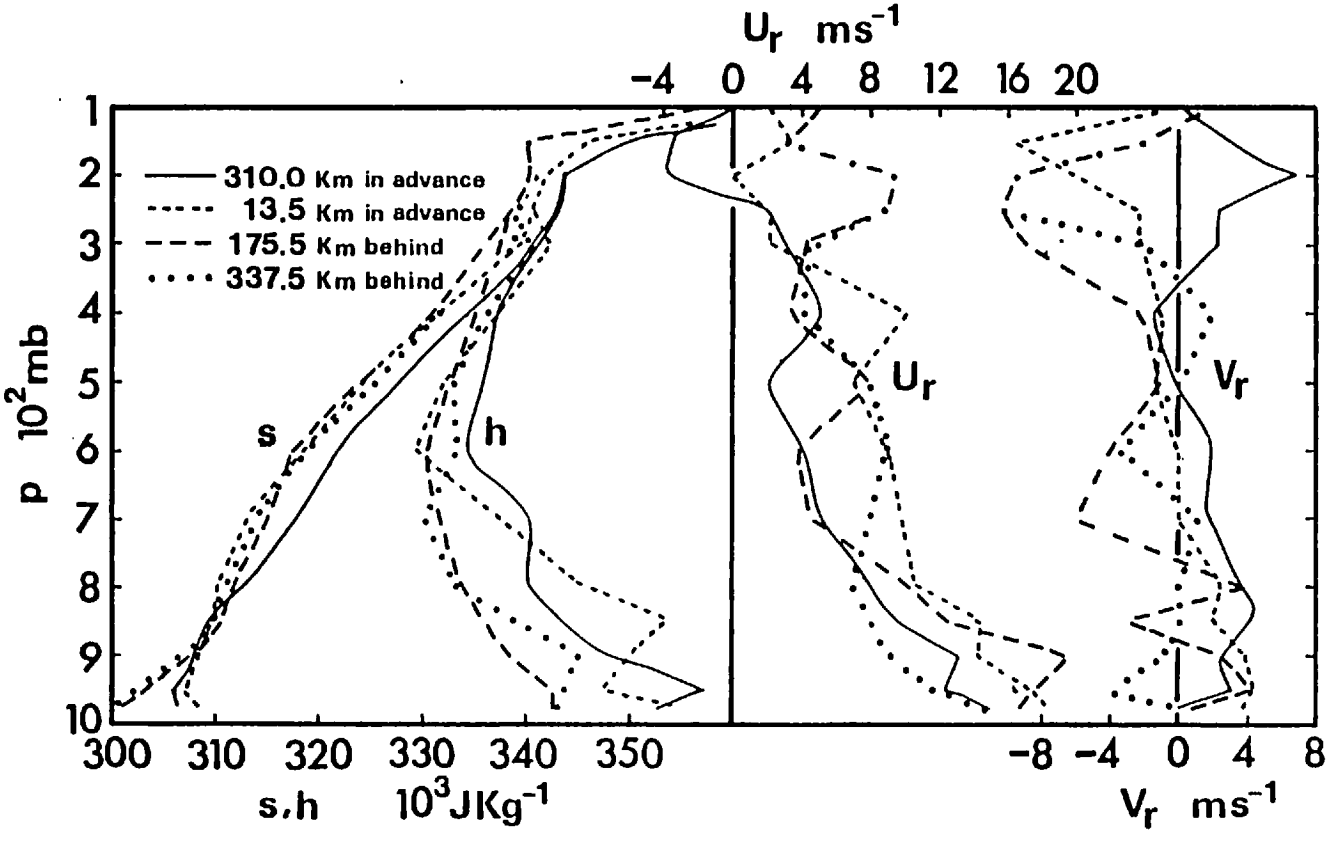

4.1 Profiles of dry static energy (s), moist static energy (h), and relative winds along (U_r) and perpendicular (V_r) to the direction of motion in advance and behind the West African squall line "Brigitte", which passed over Bamako (12° 38'N, 08° 02'W) Mali, on 3 August 1973. The mean storm velocity was 90°/15.0 m s^{-1}.

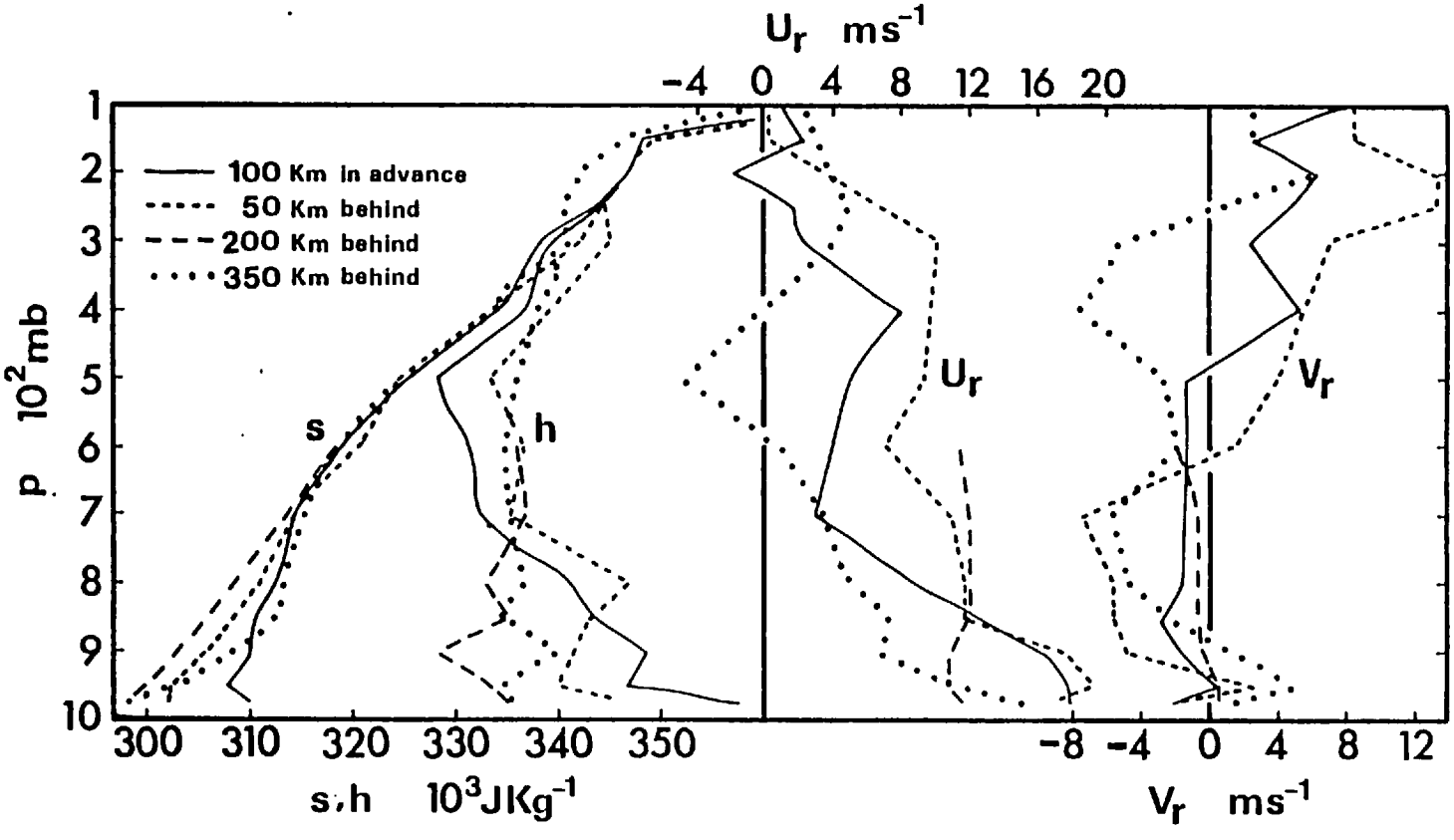

Fig.4.2 As Fig.4.1 except for the West African squall line "Fabienne" on 10 August 1973. The mean velocity of the storm was $68^{o}/14.0$ m s^{-1}.

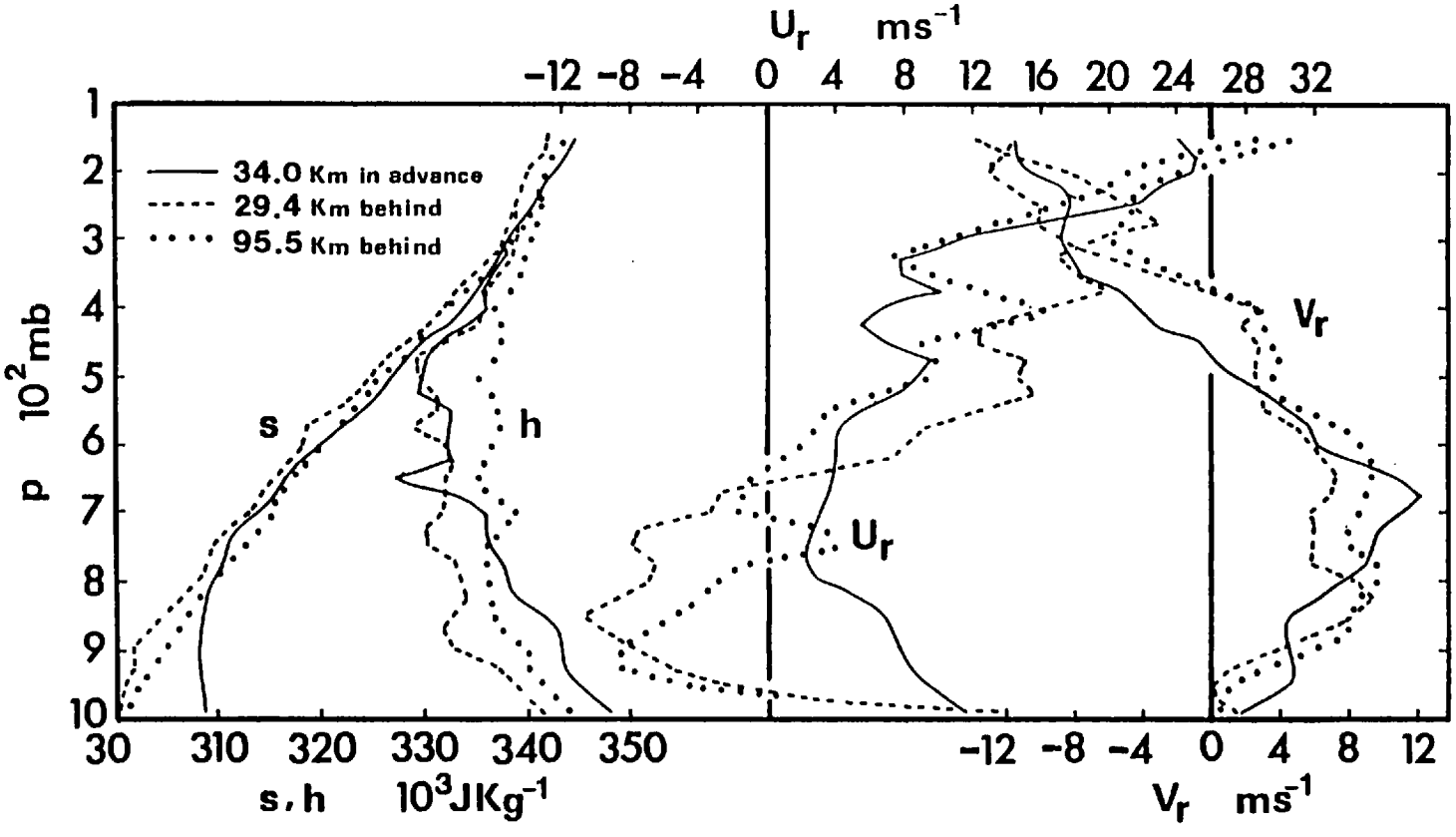

Fig.4.3 As Fig.4.1 except for storm 47 of VIMHEX, which passed over Carrizal (9° 22.8'N, 66° 55'W), Venezuela, on 24 July 1972. The mean velocity of the storm was 65°/15.3 m s^{-1}.

warming at some levels may be as much as 2^{o}K and it tends to be more significant at distances beyond 100 km behind the squall line front. In some regions, behind the squall line, such warming is not observed and, on the contrary, the s-profiles indicate that a cooling has taken place up to high levels. The warming, however, appears in most of the individual cases in which comparisons of soundings taken before and after the passage of a squall line have been made, and it is especially apparent in composite soundings which include several case studies (e.g. Betts et al., 1976; Miller and Betts, 1977; Mansfield, 1977; Fernandez, 1980 a, b). The existence of these regions of warming behind the squall lines and the fact that such a warming is observed far behind the squall line front, indicate the existence of mesoscale downdraughts.

The origin of the low-level air behind a tropical squall line may be deduced approximately from the profiles of moist static energy (h), taken before and after the passage of the convective system over a site (Figs. 4.1 to 4.3). The low values of moist static energy (or equivalent potential temperature, θ_e) found behind the squall lines at low levels, indicates that air at these levels originates in mid-levels, where air with the same values of h is found in front. However, there may also be some relative inflow from the rear, as pointed out before. Betts (1976a) suggested that the downdraught inflow layer is the 100-150 mb deep layer above the inflow subcloud layer. However, in the cases studied by Zipser (1969, 1977) the downdraught air originated somewhat higher, above 750 mb. In tracing the origin of the downdraught air using h values (or θ_e values) no distinction is made, in principle, between the different scales of downdraughts. The low values of h at low levels are found, nevertheless, in most of the anvil area, even at distances quite far from the squall line front. This also suggests the existence of mesoscale downdraughts beneath the

anvil of tropical squall lines.

The relative wind profiles for the West African squall lines (Figs. 4.1 and 4.2) show relative outflow at all levels at the rear. The Venezuelan squall line (Fig.4.3), however, shows appreciable relative inflow at the rear in the 950-675 mb layer, approximately. As has been pointed out elsewhere (e.g. Fernandez 1980 a, b), all these tropical squall lines show relative inflow at all levels at the front, and they move at a speed comparable to the maximum wind in the cloud layer. Fig.4.3 indicates that relative inflow at the rear might take place at significant distances (about 100 km) behind some tropical squall lines. Thus the mesoscale downdraught may originate from the front or the rear of the squall line, or from both directions. Downdraughts originating from the front would require air passing between cumulonimbus updraughts in order to arrive behind the squall line below the anvil. If there is relative inflow from the rear, air would enter directly to the region underneath the anvil.

4.3 Mechanisms for the formation of downdraughts at the rear of tropical squall lines

4.3.1 Evaporation of rain

Riehl (1969) and Zipser (1969, 1977) have suggested that evaporation of rain falling from cumulonimbus anvils may be sufficient to produce a mesoscale downdraught in the region below the anvil. The reasons for this are that the air found below the anvils is unsaturated and that evaporation of rain cools the surrounding air. Observations by Zipser (1977) show that the relative humidity in the rain observed behind tropical squall lines may be as low as 40-50%, which indicates that air may descend while remaining highly unsaturated. As pointed out previously, Houze (1977) estimated that about 40% of the precipi-

tation from a squall-line system observed in GATE fell from the trailing anvil cloud. The anvil rain is sometimes observed at great distances behind the cumulonimbus towers of the squall line system and this rain may persist for some hours after the cumulonimbus towers have disappeared. In the case studied by Houze (1977) rain was observed for 2-3 hours after the passage of the squall line.

Unsaturated downdraught thermodynamics has been discussed by Betts and Silva Dias (1979). They constructed a thermodynamic model for a downdraught trajectory which may be applicable to different scales of downdraught (though for different ranges of microphysical and kinematic variables). Betts and Silva Dias show that the thermodynamic structure of unsaturated downdraughts driven by the evaporation of falling rain can be parameterized using an evaporation pressure scale which is related to the speed of the downdraught, rain-rate and raindrop population. The larger this evaporation scale, the more unsaturated the downdraught.

Brown (1979) designed a time-dependent hydrostatic numerical model to test the hypothesis that evaporation of precipitation falling from an extensive thick anvil is sufficient to drive a mesoscale downdraught. In his model the flow dynamics is governed by the hydrostatic unfiltered equations. He parameterizes cumulus convection using a one-dimensional (updraught-only) plume model, which takes into account the vertical transport of water substance in the vapour and liquid phases. The governing equations are integrated in an east-west section assuming that there is present a large-scale wave disturbance of wavelength 1000 km. The initial conditions were taken from the Line Islands Experiment and were based partly on Zipser's (1969) study of 7 April 1967 squall line. All the computations have the same initial temperature sounding and a geostrophic easterly current of 5 m s^{-1} at 975 mb. Superimposed upon this is a meridional current of amplitude

$\pm$ 5 m s^{-1}, varying sinusoidally in x but independent of height, except for frictional modification.

A pair of runs (S1 and S2 in Brown's terminology) in which there is appreciable shear in the zonal geostrophic wind, permit examination of the role of the evaporation of rain as a possible driving mechanism for the formation of mesoscale downdraughts. These runs are similar except that in one (S2) rain falls to the surface without evaporation. The initial ageostrophic streamfunction in the region of convection, obtained by solving $\partial\psi/\partial p = -(u - u_g)$ and $\partial\psi/\partial x = \omega$, is shown in Fig.4.4, together with the initial 975 mb profile of v. The highest convective cloud top is initially within the 450-500 mb layer.

Runs S1 and S2 are very similar up to about 1½ hours, when appreciable precipitation starts falling from the anvil. After this time the original ascent region in run S2 continues to narrow significantly as can be seen by comparing Figs. 4.5a and 4.5c with Fig. 4.4. Fig.4.5 shows that by three hours there are some differences below the 600 mb level between S1 and S2. At this time the temperature in S1 is falling at 587.5 km and 875 mb and a mesohigh is starting to develop at low levels, with a consequent weakening of upward motion. This condition leads to the formation of a mesoscale downdraught between 4 and 5 hours in a location where there was strong upward motion at 3 hours. Thus a mesosystem has formed within the synoptic-scale disturbance. Since the initial humidity in Brown's simulations is high and the liquid water loading in convection is large, detrainment brings the large scale to saturation during the first 30 minutes of both experiments. Thus the anvil becomes warm core and, as a result of latent heat release, a mesoscale updraught develops in the middle and upper troposphere (see Fig.4.5). This makes the anvil's top extend above the 300 mb level, much higher than the highest initial convective cloud top.

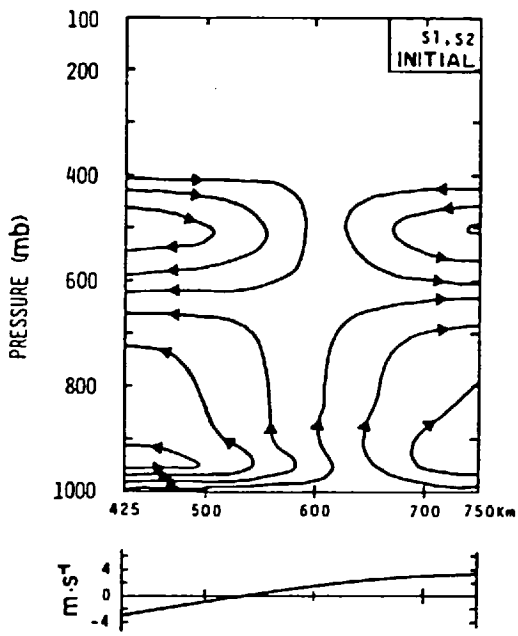

Fig.4.4 Initial ageostrophic streamfunction and 975 mb v-profile for runs S1 and S2. Mass flow between like-pointing streamlines is 1.02 x 10^3 kg m^{-1} s^{-1} (from Brown, 1979).

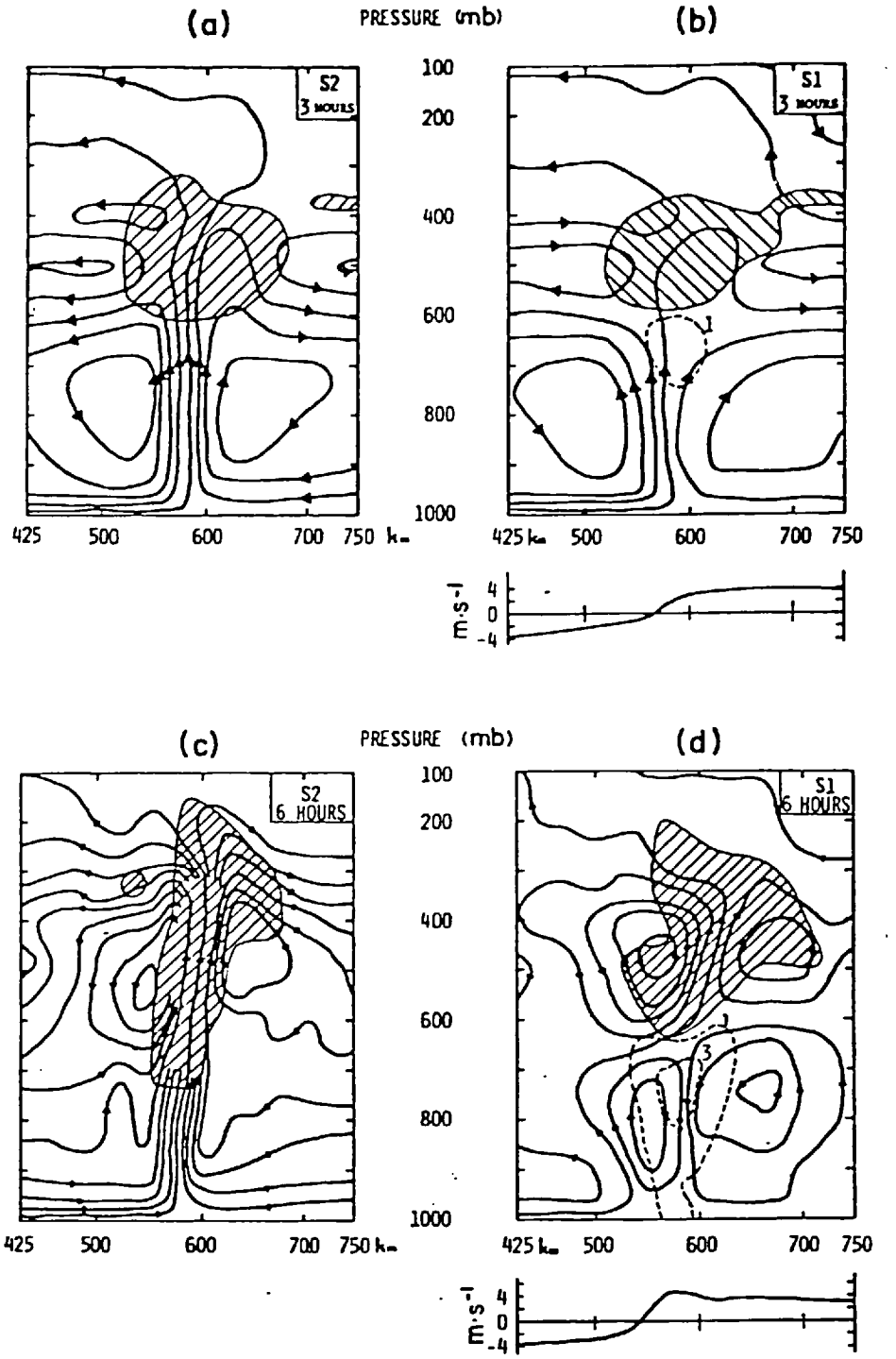

Fig.4.5 Ageostrophic streamfunction (streamlines are solid lines with arrows), large-scale cloud (hatched) and isotherms of cooling by evaporation of large-scale precipitation during the preceding 3h (dashed, K) for runs S1 and S2 :
(a) S2, 3h; (b) S1, 3h; (c) S2, 6h; (d) S1, 6h.
Below each diagram depicting conditions in experiment S1, the v-profile at 975 mb is included. Mass flow between like-pointing streamlines is 1.02×10^3 kg $m^{-1} s^{-1}$
(from Brown, 1979).

Some of Brown's results (not shown here) indicate that by 6h the anvil ascent becomes much stronger in run S2 than in S1. They also show that in run S1 condensation associated with mesoscale ascent provides about 44% of the anvil's liquid water and probably a similar fraction of the mesoscale precipitation. The downdraught produced by evaporation of rain persists in the region of 600 km at 9h (see Fig.11e of Brown's paper). At this time the downward transport of air with low θ_e from mid-levels is evident in Figs. 14 and 15 of Brown's paper.

An interesting aspect in the S1 experiment discussed by Brown is the formation of a surge in the low-level easterlies by 6h, which moves westwards at about 5 m s^{-1}. Subsidence above this surge together with a near cessation of precipitation, produces a warm and dry layer at 9h between 850 and 950 mb. Surface friction produces weakening of the surge by 9h of simulation.

The most important aspects of experiments S1 and S2, as deduced from the above discussion and other results decribed by Brown are the following:

1) Evaporation of anvil precipitation forms a mesoscale downdraught of about 10 cm s^{-1}, which transport low θ_e air from mid-levels.

2) Evaporation of precipitation produces a weakening of the disturbance.

3) Mesoscale ascent in the middle and upper troposphere contributes significantly to anvil precipitation.

4) The evaporation of precipitation limits the growth of strong ascent within the anvil.

In the last section it was pointed out that regions of warming are observed behind the squall lines at mid-levels. This may suggest descent forced by processes other than evaporation. However,

the results obtained by Brown indicate that the observed warming may be a consequence of continued subsidence in the presence of decreased evaporation.

The time required to transport low θ_e air from mid to low levels is quite long in Brown's numerical experiment. If the vertical velocity is 0.1 m s^{-1}, it would take 8.3 hours to bring air down through a distance of 3000 m. This appears not to be consistent with some observations, which indicate that warming at the rear of the squall line may be produced in shorter time periods (say about 3 hours). In these cases it could be that evaporation of rain does not play a primary role in the formation of the downdraught.

4.3.2 Response to a density current

Moncrieff and Miller (1976) described a numerical simulation of a squall line which was initiated using a sounding that preceded a squall line observed in Venezuela. From the fields obtained in the simulation, Miller and Betts (1977) computed trajectories through the simulated squall line, which they used to study the structure of the downdraught air.

Many of the trajectories starting in the 650-850 mb layer entered the system and descended to the lowest 50-100 mb layer in convective (or cell) scale downdraughts produced by evaporative cooling and water loading. A typical value for the vertical velocity was -3 m s^{-1} with values ranging from -1 to -6 m s^{-1}.

Miller and Betts found that much of the air behind the system in the layers above the lowest 50-100 mb had small motion relative to the system. Air moved in from the sides and descended at approximately -0.5 to -1 m s^{-1}, while warming nearly adiabatically. Since the simulated squall line did not have a large precipitating anvil, the

effect of evaporation of rain was very small. Thus the air was dynamically, rather than evaporatively, driven.

The analysis of Miller and Betts shows that it is reasonable to differentiate between two types of downdraught, which they called *cell* and *system* downdraughts. The cell downdraught is driven by the evaporation of rain and water loading, and produces cooling and drying of the air. The system downdraught is dynamically driven and produces warming and drying of the air. The results of Miller and Betts suggest that the system downdraught is forced to descend as a response to the spreading density current.

An important aspect to be emphasised here is that the response to the spreading density current, as shown by the results of Miller and Betts, appears to be significant only at distances close to the squall line. This may be the result of limitations in the horizontal domain of the model (30 x 30 km). However, it is not possible to conclude from the results of Miller and Betts that the response to the spreading density current may be an important factor for the formation of downdraughts with a scale, say, of about 100 km. Nevertheless, some areas of heavier rainfall in the anvil region (as observed by Zipser, 1969, 1977) would produce spreading of air at low levels, which may produce subsidence in a similar manner to the mechanism by Miller and Betts. This may explain the regions of warming observed at distances quite behind the squall line.

4.3.3 Momentum balance considerations in a dynamical model

Moncrieff and Miller (1976) developed an analytical model, applicable to tropical squall lines, in which there is relative inflow at all levels at the front of the squall line and relative outflow at all levels at the rear. In this model, Moncrieff and Miller used a set of nonlinear conservation equations, which are useful for describing organized convection provided that:

a) the explicit effects of the earth's rotation may be neglected;

b) the motion is steady in some appropriate reference frame;

c) subcloud-scale turbulence is neglected (macro-scale structure is sought);

d) microphysical and diabatic processes are required in the thermodynamic equation in the form of a heating function, $Q(x,y.z)$, which is proportional to the vertical velocity (w);

e) motion is hydrostatic at great distances from the updraught/downdraught region.

Their paper shows that such a set of equations is very useful for understanding updraught/downdraught regimes on the *convective-scale* Moncrieff and Miller showed that given the inflow conditions (kinematic and thermodynamic state) it is possible to ascertain the propagation speed of the squall line and the modified outflow. Their analytical results have been compared with observations (Betts et al., 1976; Fernandez and Thorpe, 1979) and numerical model results (Moncrieff and Miller, 1976) with fairly good agreement. However, an important aspect of Moncrieff and Miller's analytical model is that there is momentum imbalance on the mesoscale. In other words, on the mesoscale there exists a momentum excess. Moncrieff (1979) has proposed the hypothesis that this momentum excess is balanced by a forced response

of a special form in a "wake" region behind the squall line. He has expanded the approach used by Moncrieff and Miller on the convective-scale to the interactive cloud-mesoscale system, that is, the whole tropical squall line system (the squall line and the anvil region behind it). He has developed a dynamical response model which is matched to the analytical model of Moncrieff and Miller.

In his treatment, Moncrieff obtains an equation for the outflow displacement in the vertical in terms of the inflow displacement. The important role of the dynamical response model can be seen by solving the displacement equation for a special case in which the inflow speed and the environmental static stability (B) are constant, and the parcel lapse rate (γ) is zero. The form of the solution, when the normalised travel speed $\left[\Gamma = c/(CAPE)^{\frac{1}{2}} \right]$ is 0.5π and the pressure change across the system (Δp_s) is less than zero, is shown in Fig. 4.6. There is descent and warming in the lower troposphere and ascent and cooling in the upper troposphere, which qualitatively agree with observations. The ascent in the upper troposphere would help in the maintenance of the anvil from which stratiform rain would fall. The descent in the lower troposphere would produce an unsaturated down-draught. Thus the mesoscale momentum imbalance provides the pressure field which produces a mesoscale response of a type which is consistent with observations.

Fig.4.7 shows a schematic picture of the interactive model. The main points are:

a) the outflow from the squall line model defines inflow to the dynamical response model: the cloud-scale momentum source provides a dynamical forcing to drive the mesoscale response.

b) the whole system propagates at the speed (c) of the squall line;

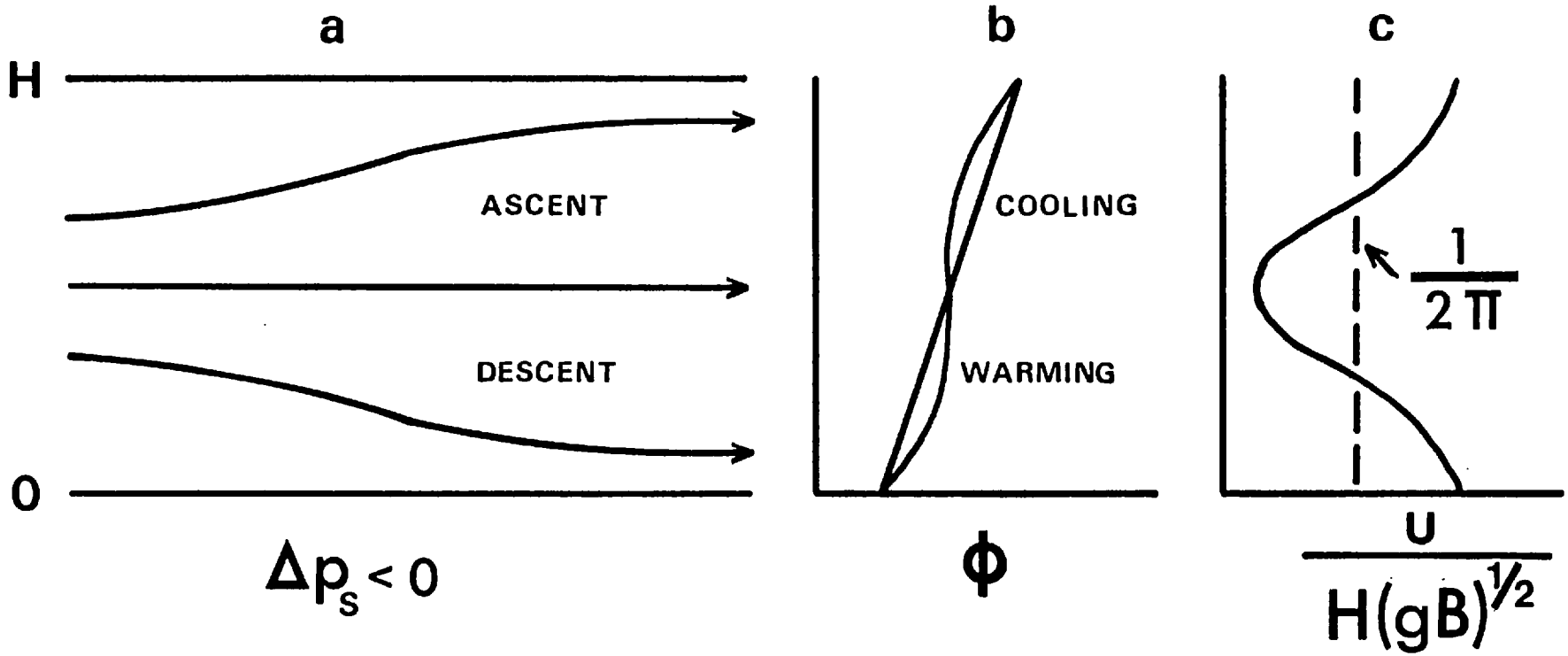

Fig.4.6 Schematic form of the solution of the displacement equation when $F = 0.5\pi$ and $\Delta p_s < 0$ in the case of constant inflow speed ($u_0/c = 1$), $\gamma = 0$, and B = constant.

(a) schematic representation of the flow,

(b) modification of the log potential temperature (ϕ) profile, and

(c) modification of the wind profile (after Moncrieff, 1979).

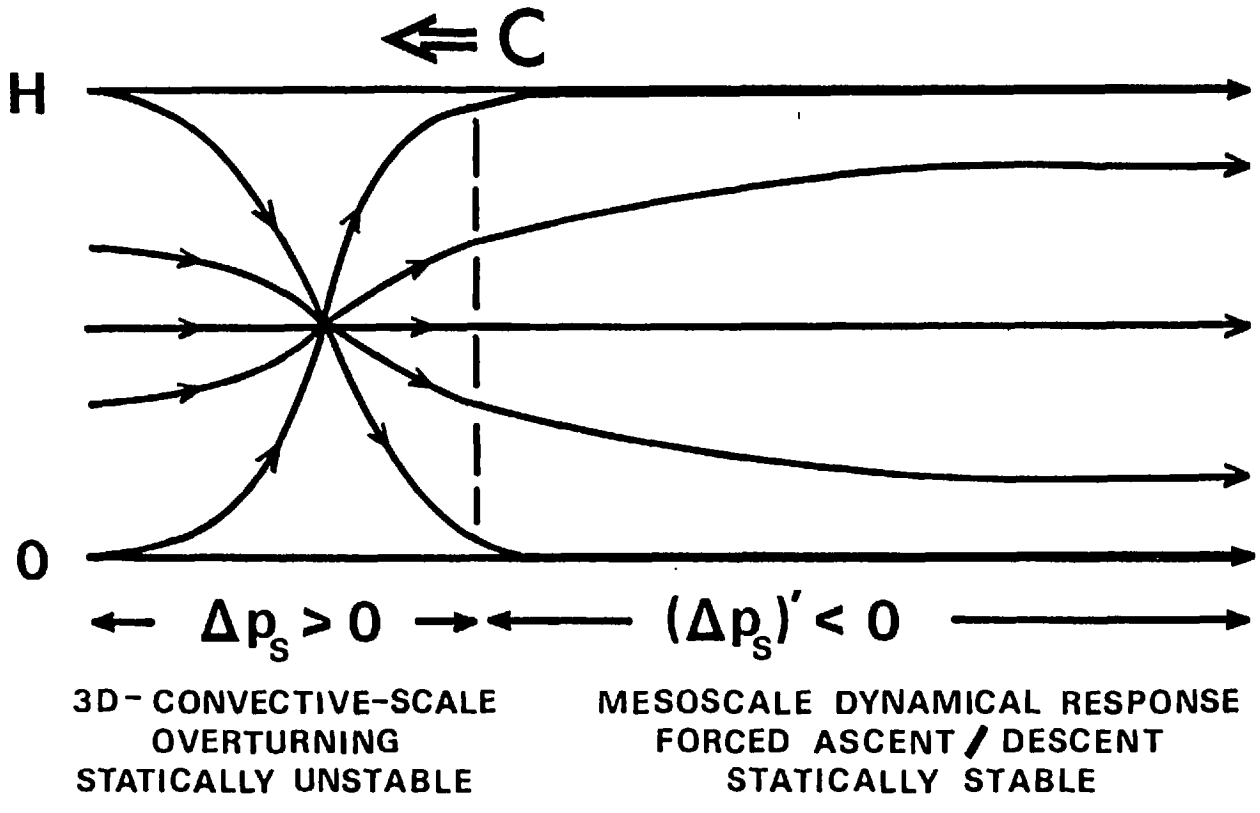

Fig.4.7 Schematic representation of the interactive cloud-mesoscale model of a tropical squall line system (after Moncrieff, 1979).

c) the system is closed (say) by imposing the constraint

$$\Delta p_s = -(\Delta p_s)'$$

d) the total outflow from the whole system is different from that of the squall line sub-system.

4.4 Conclusion

In this chapter, the observational evidence of unsaturated downdraughts at the rear of tropical squall lines has been reviewed. However, much more observational data are needed in order to study the downdraught structure in more detail. Three distinct possible mechanisms for the formation of the downdraughts have been examined. These are: evaporation of rain, response to a spreading density current and response to momentum imbalance on the mesoscale in a dynamical model. Although these mechanisms are different, it is likely that in a tropical squall line system all of them act together to produce the observed downdraughts. Purely dynamical processes with no evaporation of rain would produce a greater warming than the one actually observed. Therefore, even if the downdraught is dynamically driven, some evaporation of rain would be required to produce a warming consistent with observations. As in the case of convective-scale downdraughts, there exists a competition between two effects: evaporative cooling and adiabatic compressional warming. The observations show that in the case of downdraughts occurring at the rear of tropical squall lines, the latter effect dominates the former, contrary to that which occurs in convective-scale downdraughts.

The response to the density current appears to be significant in a scale of a few tens of kilometres, while the evaporation of anvil rain operates on a scale larger than 100 km. Assuming that the recovering of the pressure field when a squall line passes over a site takes about

2 hours and that the speed of the squall line is about 15 m s^{-1} (54 km h^{-1}), it is deduced that the horizontal scale of the dynamical response to momentum imbalance on the mesoscale is about 100 km. Therefore the dynamical response model and evaporation of rain are related because the results of the dynamical response to momentum imbalance show that there is ascent in the upper troposphere and descent in the lower troposphere. The ascent in the upper troposphere helps to maintain the anvil, from which precipitation may develop. The evaporation of anvil rain and the dynamical response to momentum imbalance on the mesoscale would act together to produce the observed mesoscale downdraughts in the lower troposphere.

The analytical results of Moncrieff's dynamical response model are very interesting. Since the model results are consistent with observations, it could be used as a method of partitioning the transports of momentum and energy between the convective-scale and the mesoscale. This may be very useful in parameterization schemes for large-scale models.

More numerical experiments with mesoscale models should be carried out using realistic data. The comparison of numerical and analytical results with observations should be an important aspect in any further research of downdraughts associated with tropical squall lines.

CHAPTER 5

AN EVALUATION OF THEORIES OF STORM MOTION USING OBSERVATIONS OF TROPICAL CONVECTIVE SYSTEMS*

5.1 Introduction

There have been a number of attempts to derive a theory of storm motion but, even after decades of research, there are only two approaches which are anywhere near complete in their treatment of this topic. These are based on the equations of motion for atmospheric flow, and they consider the entire storm system. The two approaches can be labelled as being of steady state and wave-CISK type. The former was introduced in the literature by Moncrieff and Green (1972, hereafter MG) and Moncrieff and Miller (1976, hereafter MM), and the latter by Raymond (1975, 1976, hereafter RY).

Several field experiments have been carried out recently in the tropics in order to study the interactions between convection and the large scale fields, and thereby to produce observational models. Among these experiments are those of VIMHEX-1972 (Second Venezuelan International Meteorological and Hydrological Experiment), GATE (GARP Atlantic Tropical Experiment) and OPGA (Operation Pre-GATE ASECNA). These field projects have provided data which are especially useful in evaluating the predictions of the theoretical models of severe storms, and will help in the development of more complex models. An important aspect to be evaluated is the accuracy of the predicted propagation velocity, this being a funda-

---

* A slightly modified version of this chapter has been published in collaboration with A. J. Thorpe in Monthly Weather Review, *107*, 1306-1319, 1979.

mental problem dealt with by the theories. In this context it is worth mentioning the work of Betts et al. (1976) who made a comparison of the results predicted by the theory of MM with observations of some tropical squall lines over land observed during VIMHEX-1972. They found considerable agreement between the predictions and observations, despite significant differences in the outflow profiles and overall mass transports. The propagation speeds were fairly well predicted. Mansfield (1977) in his study of squall lines observed in GATE, has pointed out that the structure and transport of heat, water vapour and momentum are consistent with the MM model. Unfortunately a complete evaluation of this model was not made as there were no comparisons of the observed propagation speeds with those predicted by the theory.

In this chapter the wave-CISK model will be applied to some tropical convective storms and the propagation velocities predicted by the model compared with the observed ones. Nine convective storms observed in Venezuela during VIMHEX-1972, three Eastern Atlantic squall lines observed in GATE, and three WEST African disturbance lines observed in OPGA, will be considered. The interest in Raymond's model lies in the fact that it is based on the wave-CISK concept, which may be useful in studying convection in the tropics (Lindzen, 1974). Indeed, there is a need for the theory to be tested in the case of tropical convective storms (Lilly, 1979). The MM model will also be applied to these tropical convective storms in order to compare the predictions of both models. It is important to realise, however, that the RY and MM models are conceptually distinct. The RY model is linear and can predict the propagation of a wide range of convective systems; it cannot describe the circulation explicitly. The model of MM, on the other hand, represents the dynamical aspects in greater detail, but is restricted to well-developed systems.

Finally, by way of clarifying the difference between the models, a comparison of the models' predictions in the case of the idealised wind

profile of constant shear will be made.

5.2 The wave-CISK model

In the wave-CISK model proposed by RY, the entire storm is represented as a packet of forced internal gravity waves. The gravity wave serves to generate regions of low level convergence and divergence. The resulting concentration of convection into convergent regions provides a driving mechanism for the wave itself. Convection provides the potential energy, whilst the wave provides the organisation. The wave packet consists of one convergent and one divergent region, with a dominant wavelength comparable to the diameter of the storm. RY supposes that below cloud base, water vapour transport is dominated by plumes with a horizontal scale perhaps ten times smaller than the horizontal storm scale. The plumes possibly arise from some internal convective instability in the storm-scale flow. They develop in the convergent region, pass into the divergent region as they decay, and produce rain. Thus the storm-scale motions control the internal convective motions which, in turn, play the main role in energy release and material transport.

The model uses linear theory to predict the modes of maximum growth rate. An exponential dependence is assumed for all perturbation variables, i.e. $\exp\left[i(\underline{k}.\underline{r}-\sigma t)\right]$, where $\underline{k}$ is the wave vector in the horizontal plane and σ is the wave frequency.

With the relevant assumptions, the governing equations may be reduced to a single equation for the vertical velocity w'. Defining an auxiliary variable $\tilde{w}(z)$ such that

$$w' = \tilde{w} \exp\left[\left(\mu^* - \frac{\mu}{2}\right) z\right] \qquad (5.1)$$

where $\mu^* = 1.4\,\mu = \frac{1}{8}\ km^{-1}$

The resulting equation for $\tilde{w}$ has the form

$$\frac{d^2\tilde{w}}{dz^2} + q(c,z)\tilde{w} = N S \tag{5.2}$$

where

$$q(c,z) = \frac{1}{(c-V_K)}\left\{\frac{d^2V_K}{dz^2} + \mu\frac{dV_K}{dz}\right\} + \frac{gB}{(c-V_K)^2} \tag{5.3}$$

with

$$S = g\,B\,J\,\exp(\mu z/2)\Big/(c-V_K)^2 \tag{5.4}$$

and

$B = \frac{1}{\bar{\theta}}\frac{d\bar{\theta}}{dz}$ static stability

$c = c_r + ic_i = \frac{\sigma}{k}$ complex phase speed of the eigenmode

V_K = component of $\underline{v}$ along $\underline{k}$

$k = |\underline{k}|$ total horizontal wavenumber

J = vertical mass flux per unit area due to the plumes.

If the regions between plumes are without vertical motion, continuity requires that J be equated to the mass flux through cloud base. This mass flux through cloud base is represented as the surface convergence times b, the height of the cloud base:

$$J = b\frac{dw'}{dz}\bigg|_{z=0} = b\frac{d\tilde{w}}{dz}\bigg|_{z=0} \tag{5.5}$$

N is called the duty cycle of the convective forcing and it is a correction factor that was initially introduced to take into account how much of the storm-scale divergence is accompanied by penetrative down-

draughts. Its scope, however, has been extended to counteract some difficulties common to all CISK models. As RY has pointed out, if there should exist a significant mass flux of quiescent air downward across cloud base (the air surrounding the plumes has been assumed to have no vertical motion), then the mass flux would be larger than that given by (5.5). RY evaluated N empirically and found that a value of 1.5 gave optimum agreement between calculated and observed propagation velocities.

The solution of Eq.(5.2) is an eigenvalue problem defining a dispersion relation $c = c(\underline{k})$ for forced gravity waves, which gives the phase speed $\mathrm{Re}(c)$ and the growth rate $k\mathrm{Im}(c)$ of each eigenmode. A realistic representation of a localized disturbance may be constructed by linearly superimposing eigenmodes into a wave packet. The propagation velocity of such a packet is the group velocity and as the procedure is restricted to $k = 0$ (which can be justified by scale analysis), it is a function of the direction of $\underline{k}$ only. This restriction allows a curve in the horizontal velocity plane to be defined, which is called the propagation velocity curve. It represents the locus of all possible storm propagation velocities for a given sounding.

In the published work connected with this model, only realistic soundings were considered and no attempt was made to explore idealised profiles and hence to derive simple analytic expressions for storm speed. This interesting and important topic will be dealt with later in this chapter.

5.3 Results of the wave-CISK model

In applying the wave-CISK model, the height interval for which rawinsonde data are input was taken to be 1000 m for the Venezuelan

and West African storms and 500 m for the Eastern Atlantic storms. Eleven sounding levels, starting at the surface, were used for the storms observed in VIMHEX and OPGA and 21 for the storms observed in GATE.

The results obtained with this model are given in Table 5.1. It may be seen that the values corresponding to the mode with the largest $Im(c)$ do not agree with those observed. In three cases (storms 14, 27 and Fabienne) the wave front corresponding to the most unstable mode is not tangential to the propagation velocity curve. This may be because the storms selected in this study may have arisen from some large amplitude perturbation and, indeed, rainfall during VIMHEX was strongly controlled by the synoptic situation (Riehl and Lueckefedt, 1976). The squall line which developed in the numerical simulations carried out by MM was found to be generated by a large amplitude perturbation involving the gust front from the initial cell, producing enhanced boundary layer convergence. In this case, as has been pointed out by RY, it may be necessary to calculate all the unstable eigenmodes and not just the one with the largest growth rate. Because of this, the observed speeds will be compared with the model closest prediction C_R, defined here as that point on the propagation velocity curve corresponding to the observed direction of motion. The tangent to the curve on that point will give the predicted orientation of the squall lines.

The choice of C_R as defined above, is also justified because the most unstable growth rates do not differ significantly from the growth rates associated with C_R for all the storms. It was found that $Im(c)$ is a weak function of ϕ for the tropical convective storms dealt with in this chapter. The values of $Im(c)$ corresponding to the most unstable mode and those associated with C_R do not differ by more than 2 $m\,s^{-1}$ and in most of the storms the difference is less than 1 $m\,s^{-1}$. For this

Table 5.1

Results of Raymond's wave-CISK model for the propagation characteristics of some tropical convective storms. Direction indicates motion from.

Storm number or index	Raymond's prediction for velocity with maximum Im(c)			Raymond's closest prediction			Observed velocity		
	Speed ($m\ s^{-1}$)	Direction (deg)	Orientation (deg)	Speed (C_R) ($m\ s^{-1}$)	Direction (deg)	Orientation (deg)	Speed (C_{obs}) ($m\ s^{-1}$)	Direction (deg)	$\frac{C_{obs}}{C_R}$
14	*	*	*	18.6	104	—	11.7	104	0.63
27	*	*	*	14.6	79	155–335	15.0	79	1.03
33	10.0	55	138–318	12.0	97	4–184	14.7	97	1.22
35	8.6	163	90–270	11.7	85	174–354	10.7	85	0.91
47	**	**	**	**	**	**	15.3	65	—
53	7.2	149	90–270	10.0	110	34–214	9.9	110	0.99
56	**	**	**	**	**	**	14.7	92	—
60	8.0	122	60–140	10.8	95	35–215	13.8	95	1.28
64	**	**	**	**	**	**	15.5	79	—
Brigitte	8.0	118	30–210	7.4	90	170–350	15.0	90	2.03
Dominique	7.0	10	120–300	5.0	68	175–355	15.3	68	3.06
Fabienne	*	*	*	10.0	68	170–350	14.0	68	1.40
G	**	**	**	**	**	**	12.7	45	—
H	3.8	360	120–300	2.2	53	164–344	16.0	53	7.27
I	5.4	23	97–277	5.4	45	135–315	15.1	45	2.80

* For these cases, the wavefront corresponding to the mode with the largest Im(c) is not tangent to the propagation velocity curve.
** For these cases, the distribution of wave-fronts does not define a propagation velocity curve.

reason the choice of the most unstable mode is somewhat arbitrary in the case of these tropical storms. This contrasts strongly with the mid-latitude cases studied by RY in which Im(c) was a strong function of ϕ.

Figures 5.1 and 5.2 illustrate the results obtained for two cases. It can be seen that the most unstable mode gives a poor prediction for the *velocity* of the storms. However, the point on the propagation velocity curve corresponding to the observed direction of motion gives a good prediction for the storm *speed*. For storm 33 (Fig.5.1) the value of Im(c) for the most unstable mode is 5.1 $m\,s^{-1}$, the value corresponding to the closest prediction is 4.3 $m\,s^{-1}$, and the maximum difference over all angles is 0.8 $m\,s^{-1}$. For storm 35 (Fig.5.2), such values are 6.7, 5.1 and 1.6 $m\,s^{-1}$, respectively.

5.3.1 Venezuelan storms

It can be seen from Table 5.1 that the model's closest predictions agree fairly well with the observed values for storms 27, 33, 35, 53 and 60. The propagation speed for storm 14 is poorly predicted. For the other three VIMHEX cases (storms 47, 56 and 64) the wavefronts obtained are distributed in such a way that no determination of the propagation velocity curve is possible. The orientation of the squall line is fairly well predicted for storms 27, 33, 35 and 53, if the observed orientations are assumed to be normal to the direction of motion, which appears to be the case (Betts and Stevens, 1974; Mansfield, 1977).

5.3.2 West African disturbance lines

The propagation speeds for these storms (Brigitte, Dominique and Fabienne) are poorly predicted, as can be seen from Table 5.1. However, the observed values were determined from satellite pictures and maps

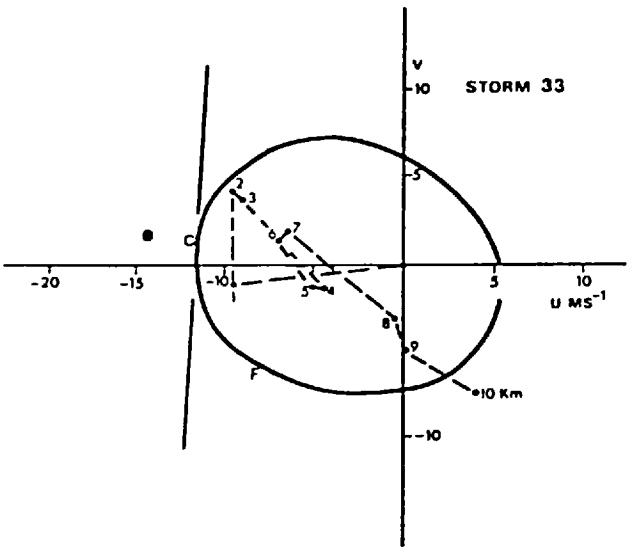

Fig.5.1 Propagation velocity curve for storm 33, calculated for N = 1.5. The mode with maximum Im(c) is indicated with the letter F. The diamond surrounded by a circle represents the observed velocity of the storm. The closest prediction as defined in the text is indicated with the letter C and the solid line tangent to the curve gives the orientation of the squall line. The dashed line is the wind hodograph associated with the storm. Heights on the hodograph are in kilometres above ground level.

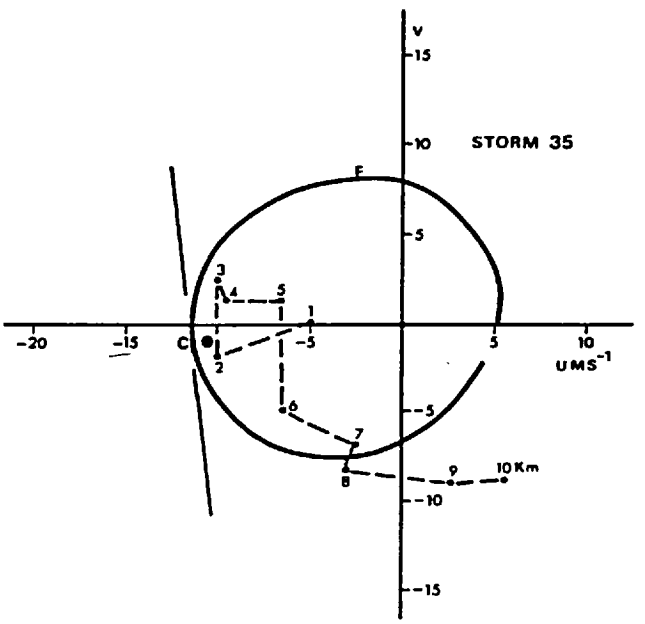

Fig.5.2 Same as Fig.5.1, except for storm 35.

of isochrones and isohyets, and thus an error of $\pm 3\ m\ s^{-1}$ is likely. For the VIMHEX and GATE storms the observed values were determined from radar films and the error is somewhat smaller, $\sim \pm 2\ m\ s^{-1}$. The orientation of these storms is, however, well predicted.

5.3.3 Eastern Atlantic squall lines

For the squall lines observed in GATE (storms G, H and I in Table 5.1) the model's closest predictions do not agree with the observed values. In addition, the distribution of wave fronts for storm G does not give a propagation velocity curve. In all these squall lines the cloud bases are very low compared with the VIMHEX storms. It is possible that a poor estimate of the mass flux across cloud base could be responsible for the model's failure. This point will now be examined in more detail.

5.3.4 The role of mass flux due to the plumes

In order to see how the mass flux due to the plumes (J) affects the wave-CISK model predictions, experiments have been carried out changing the value of the parameter b in Eq.(5.5). This appears preferable to varying N which is not easy to justify in physical terms. The parameter b presumably represents something physically understandable, namely the height at which the large scale flow breaks down into plumes. In retrospect there seems to be no reason why b should be the height of cloud base, as assumed originally by RY.

Calculations for all storms for which the model failed to give good predictions were carried out. Some of the results are illustrated in Fig.5.3 in which the predicted propagation speed is plotted against b for two storms observed in GATE. This figure shows that as b is increased (which implies an increase in J), the model predictions become

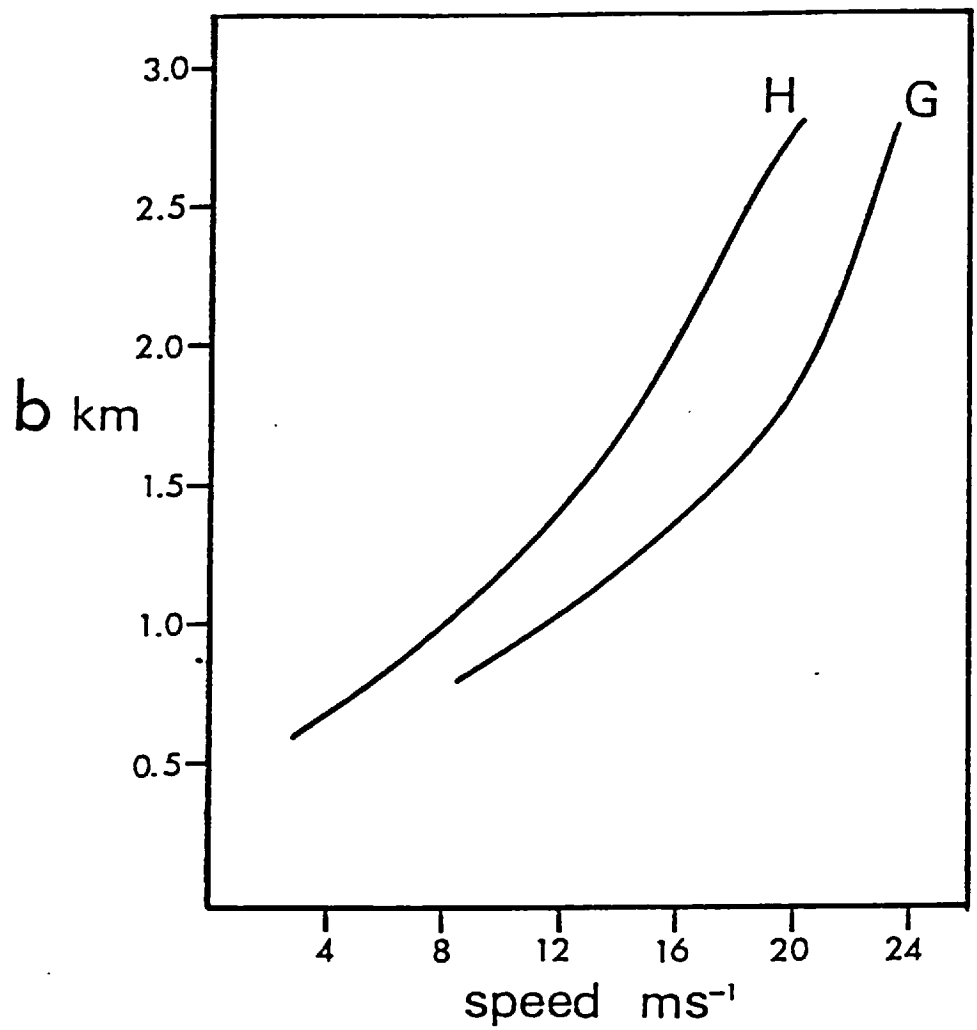

Fig.5.3 Predicted values of the storm speed as a function of the parameter b for two Eastern Atlantic squall lines (storm G and H).

closer to those observed. This is true not only for the GATE storms but also for storms 47, 56 and 64 of VIMHEX and the three West African disturbance lines. (An exception is storm 14 of VIMHEX, which is the only case in which b should be lowered in order to get good agreement.) In other words, J is underestimated for almost all storms. In the cases observed in GATE (Fig.5.3), b should be increased by a factor of about 2.5 in order to get good predictions. For the West African and Venezuelan storms the factor is about 1.8 and 1.1 respectively. This is interesting because it has been suggested (Hamilton and Archbold, 1945) that the West African squall lines may be generated by gravity waves propagating in the interface separating the lower moist south-westerly winds from the overlying dry and hot easterly winds leaving the Sahara.

The above discussion indicates that the assumption of the large scale flow breaking out into plumes *at cloud base* may not be a good one. The flow possibly breaks into plumes at a higher level, which the present results indicate to be more related to the top of the moist layer. This conclusion is important, not only to the model proposed by RY, but in general to all wave-CISK models, which are used in parameterization schemes.

5.4 Steady state models

This section will briefly describe some aspects of two related theoretical models which are based on the assumption of steady state dynamics. In this context "steady" means that the form of the storm does not change with time, although its position relative to the earth's surface may do so. The first model proposed by MG is intended to apply in strongly sheared environments, while the second one proposed by MM

is intended to apply in relatively weakly sheared environments, such as those found in the tropics. Both models are nonlinear; MG is two dimensional and MM is quasi three dimensional.

In the MG and MM models, simple expressions for the storm velocity are obtained for idealized profiles. The mathematical methods of solution which can be found in their papers are not relevant for our purposes and will be omitted. However, attention is drawn to the following points.

5.4.1 The MG model

The MG model for severe storm motion arose from the observational work of Browning and Ludlam (1962). The conclusions from that work lead to three important simplifications in the equations of motion for the flow in severe storms: neglect of viscous terms which represent mixing processes, neglect of the partial derivative with respect to time because such storms remain in a steady state for many hours, and the use of two dimensionality. These approximations led MG to their analytic solutions for storm motion and structure. Some important aspects of the model are:

i) The model deals with constant shear, A, and a non-dimensional number, R, similar to the Richardson number, determines the properties of the storm;

ii) the thermodynamics of each parcel is determined by latent heat release equal to the parcel vertical velocity multiplied by a constant pseudo-saturated adiabatic lapse rate, γ. The environmental profile of potential temperature is characterised by constant static stability B. These conditions imply a linear (increase/decrease) of parcel potential temperature upon (upward/downward) displacement. The realism of such a thermodynamic parameterization and its implications

will be the subject of further discussion in this chapter;

iii) the model gives the following expression for the speed of the storm relative to the surface wind:

$$c = AH\left[\frac{1+(1+4R)^{\frac{1}{2}}}{3+(1+4R)^{\frac{1}{2}}} - 0.11\frac{H}{H_0}\right] \qquad (5.6)$$

where H is the depth of the convective layer

$R = g(\gamma - B)/A^2$

H_0 is the density scale depth

This convective overturning can only take place for $0 \leq R \leq 1.0$ and is thus a large wind shear phenomenon.

Moncrieff (1978) shows that the storm has an updraught slope *downshear*. This important result shows that the two-dimensional model cannot be used to describe this feature of the storm structure because as the updraught slopes downshear, rain will fall into the inflow air and inhibit steady convective overturning. However, it is probably incorrect to discard the results of this model at this stage in its development. It is an analytical model which predicts a reasonable speed for some mid-latitude severe storms - observations indicate that such storms move at an average wind speed in the atmosphere. Also, work carried out by Tam (1979) indicates that most storms are a complex three dimensional amalgamation of the MG and the MM regimes of overturning. Indeed, first results suggest that certain storms can be thought of as consisting of two normal planes in which the MG circulation takes place in the plane of maximum shear and the MM circulation occurs in the plane of minimum shear. Thus, although certain inconsistencies arise in the MG model, it may still be of use in hybrid models, and for completeness, the results of this model will be included in this study.

5.4.2 The MM model

This model is applicable to a different regime of convection in which the storm moves faster than the wind at all levels. The model now considers a two-dimensional relative inflow at all levels at the front of the system and calculates the relative outflow profile at the rear, which is again two-dimensional. The internal dynamics is now, however, necessarily three-dimensional, otherwise the streamlines will intersect, an impossibility in two dimensions. In this analytical model, the storm speed relative to the surface for constant shear is given by

$$C = U_m + \tau(CAPE)^{\frac{1}{2}} \tag{5.7}$$

where U_m is the mid-level wind, and CAPE is the convective available potential energy

$$CAPE = \int_o^H g\,\delta\,\phi_p\,dz$$

where H is the height of cloud top and $\Delta\phi_p$ is the log potential temperature difference between parcel and undisturbed flow. If a pseudo-saturated ascent is assumed, then CAPE is proportional to the positive area on a tephigram. The parameter τ is a function of the non-dimensional number (R) of the large-scale flow. The authors showed that for a convective circulation of maximum mechanical efficiency, $\tau = 0.32$.

CAPE is related to R through the relation

$$R = CAPE \Big/ \left[\tfrac{1}{2}(\Delta u)^2\right]$$

where Δu is the wind difference between top and bottom of the convective system.

Eq.(5.7) strictly only applies for constant wind profiles, but is

found to be a good approximation over the wide range of wind shear such that $R \geq 3$. The accurate expression depends only weakly on the wind shear (or R), as will be shown in later figures. It should be particularly noticed that the storms move faster than the flow (for constant wind) by an amount depending essentially on the available *potential* energy, and that storm speed is nearly independent of wind shear.

The steady analytic model results can be categorized as follows:

$R \leq 1$: the storm is two-dimensional. Its speed is proportional to the wind shear and is weakly dependent on CAPE.

$R > 1$: the storm is three-dimensional. It speed is proportional to $(CAPE)^{\frac{1}{2}}$ and depends weakly on shear.

5.5 MM model results

Betts et al. (1976) used Eq.(5.7) to calculate the propagation speed of six VIMHEX storms. Eq.(5.7) has been used to calculate the propagation speeds of all the storms selected for this study, including the ones studied by those authors, in order to compare these results with those obtained with the wave-CISK model. The results are shown in Table 5.2. CAPE for the VIMHEX storms was determined, following Betts et al. (1976), by measuring the energy released by pseudo-saturated ascent at the mean equivalent potential temperature (θ_e) of the 980-900 mb layer. For the GATE and OPGA storms, CAPE was determined by raising a parcel with values of pressure, temperature and mixing ratio representative of a layer close to the surface. The choice of θ_e might affect substantially the positive area in a thermodynamic diagram, which is proportional to CAPE. However, small differences in CAPE do not substantially affect the second term of Eq.(5.7). The values of U_m are those corresponding to the values

Table 5.2

Moncrieff-Miller's analytical model predictions and comparison with observed and Raymond's predicted propagation speeds.

Storm number or index	Mean value of wind component along direction of motion ($m\ s^{-1}$)	Mid-level wind U_M ($m\ s^{-1}$)	CAPE ($J\ Kg^{-1}$)	Moncrieff-Miller's predicted speed C_{MM} ($m\ s^{-1}$)	Observed speed C_{ob} ($m\ s^{-1}$)	Raymond's predicted speed C_R ($m\ s^{-1}$)	$\frac{C_{obs}}{C_{MM}}$	$\frac{C_{obs}}{C_R}$	$\frac{C_{obs}}{C'_{MM}}$
14	9.8	11.9	920	21.6	11.7	18.6	0.54	0.63	0.60
27	6.9	7.9	797	16.9	15.0	14.6	0.89	1.03	0.94
33	4.0	6.7	940	16.5	14.7	12.0	0.89	1.22	1.06
35	4.1	3.1	1388	15.0	10.7	11.7	0.71	0.91	0.67
47	7.8	9.7	662	17.9	15.3	—	0.85	—	0.96
53	6.0	6.0	—	—	9.9	10.0	—	0.99	—
56	6.2	10.1	691	18.5	14.7	—	0.79	—	1.01
60	5.3	7.4	991	17.5	13.8	10.8	0.79	1.28	0.90
64	4.4	2.0	1485	14.3	15.5	—	1.08	—	0.93
Brigitte	9.6	10.8	1740	24.2	15.0	7.4	0.62	2.03	0.65
Dominique	8.9	10.3	3150	28.3	15.3	5.0	0.54	3.06	0.57
Fabienne	7.1	8.3	1390	20.2	14.0	10.0	0.69	1.40	0.73
G	6.4	10.4	738	19.1	12.7	—	0.66	—	0.84
H	4.2	3.3	1681	16.4	16.0	2.2	0.98	7.27	0.92
I	2.5	6.3	373	12.5	15.1	5.4	1.21	2.80	1.74

observed at a height equal to half the height of the cloud tops. The cloud tops for VIMHEX storms were taken as those corresponding to the maximum heights (as determined from radar). For the GATE and West African storms the height H was taken to be given by the thermodynamic equilibrium heights for a parcel rising unmixed from the sub-cloud layer. This was done because of stability problems on the ship "Oceanographer", which make the observed maximum echo heights of GATE storms uncertain, and because of lack of radar data for the West African storms. However, as pointed out by Mansfield (1977), where data were available in the GATE cases, the maximum echo heights were seen to be close to the cloud tops, as determined from the parcel theory.

The height-mean value of the component of wind along the direction of motion is included in Table 5.2 in order to compare these values with U_m. With a few exceptions they are normally smaller than U_m. If, instead of using U_m in Eq.(5.7) the mean value of the component of wind along the direction of motion is used, better predictions for the storm propagation speed are obtained. This is shown in the last column of Table 5.2, where the values for C_{ob}/C'_{MM} are given (C'_{MM} is the predicted speed using the mean wind component rather than U_m). Therefore it appears that the mean value of the component of wind along the direction of motion is better than the mid-level wind for the prediction of the storm propagation speed. This may be due to uncertainties in the evaluation of U_m (especially errors in estimating cloud tops).

In the case of the West African squall lines, the MM prediction gives poor agreement. As pointed out in Chapter 3, the wind profiles corresponding to the West African squall lines show an increase of easterlies to high levels, contrasting with the wind profiles of the Venezuelan and Eastern Atlantic storms which show a mid-level jet.

For this reason the mean wind along the direction of motion is, in general, larger in the case of the West African storms. On the other hand, CAPE is very large for these storms and this contributes to the values obtained with Eq.(5.7). It appears, therefore, that the MM formulation for constant shear is not appropriate for the prediction of speed of the West African squall lines.

From Table 5.2 it can be seen that, in general, the MM model overestimates the storm speed. For the storms observed in VIMHEX and GATE this may be due in part to the fact that CAPE was calculated from a tephigram assuming a pseudo-saturated ascent. However, this is not the reason for the West African storms, whose speeds are significantly overestimated. The wave-CISK model, on the other hand, appears to underestimate the storm speed for most of the convective systems considered in this study.

5.6 A comparison between theories in conditions of constant shear

In this section a close intercomparison of the models' predictions in conditions of constant shear will be made. Atmospheric flow is rarely close to constant shear and, indeed, the important property of deviatory motion is probably due to the turning of the wind with height (see, for example, Thorpe and Miller, 1978). However, constant shear is an important idealised case, amenable to analytical study. There has been discussion of the role of shear in severe storm motion which can now be clarified from the existing theories. The understanding of the effects of constant shear represents an important step in the prediction of storm motion.

The variation of the RY model predictions with b will be studied by considering the parameter $b^* = b/b_{obs}$, where b_{obs} is the

observed height of cloud base. In this way the ambiguities discussed in Section 5.3 of defining cloud base can be overcome.

The procedure adopted to compare these theories has been to use thermodynamic soundings from three VIMHEX storms (with correspondingly different values of CAPE) and to calculate from the theories the storm speed relative to the mid-level wind, which is also the mean wind, as a function of a constant shear. These results are shown in Figs. 5.4, 5.5 and 5.6. The following lines have been plotted :

i) The prediction of MG, where appropriate, i.e. $R < 1$, using the compressibility ratio $H/H_0 = D = 1.8$.

ii) The prediction of MM for $D = 0$ and neglecting the slight variation with R, i.e., plot of Eq.(5.7) in the form $C - U_m = \tau(CAPE)^{\frac{1}{2}}$.

iii) The prediction of MM for $D = 1.0$ with the variation with R included.

iv) The prediction of RY for $b^* = 1.10$.

v) The prediction of RY for $b^* = 1.66$.

vi) The line $C = U_{max}$.

A number of interesting properties emerge which are tabulated below:

a) For wind shear $A \leq 1.5 \times 10^{-3} s^{-1}$ RY gives predictions with $C > U_{max}$. Thus, linear theory can model storms which move faster than the flow in the layer. This property which, from the work of MM, had been expected to be essentially a non-linear one, appears to be produced in the forced linear wave model. This similarity, and others to be discussed shortly, between MM and RY, make an understanding of the physical basis for each model fundamental, as evidently *both* may contain the essential physics of cumulonimbus convection.

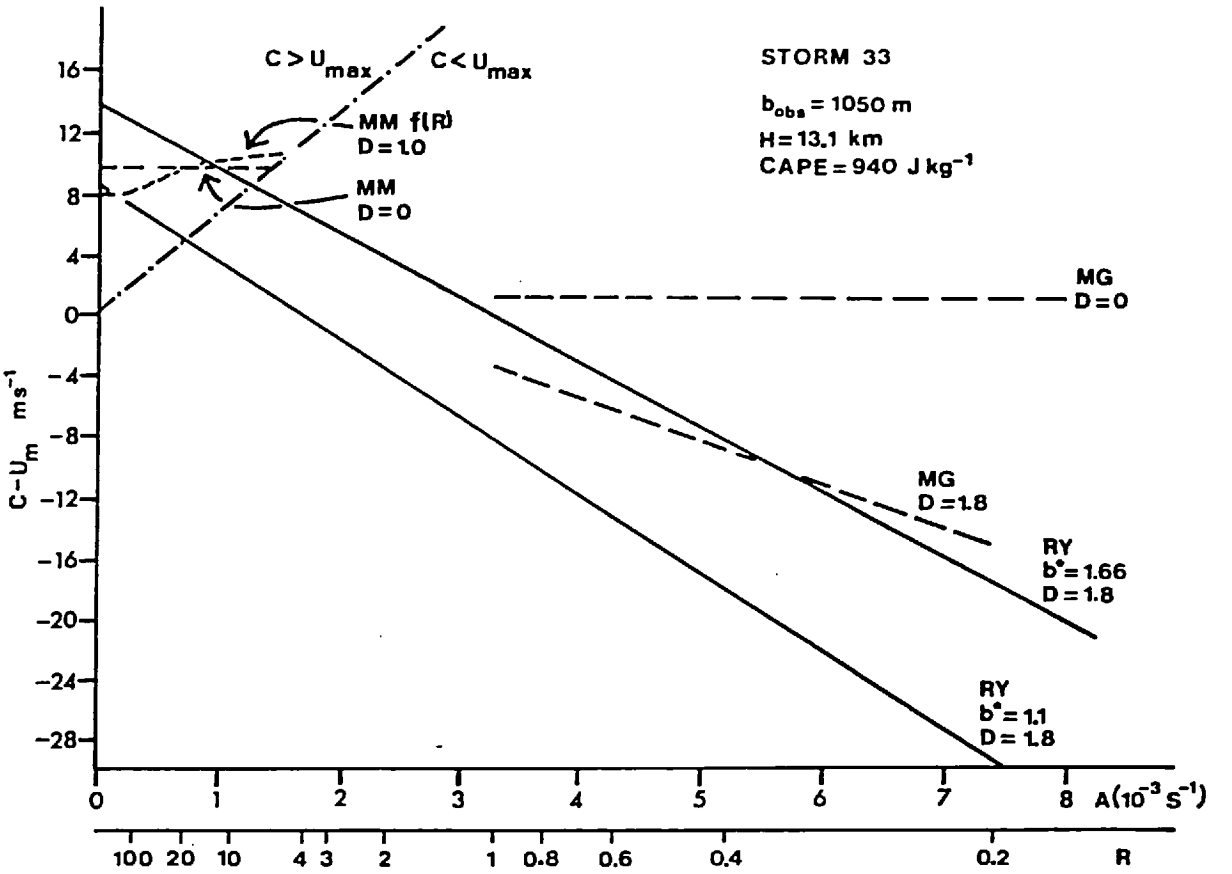

Fig.5.4 Predictions of MG, MM and RY models for the storm speed relative to the mid-level wind as a function of the wind shear (and R) for storm 33. See text for further details.

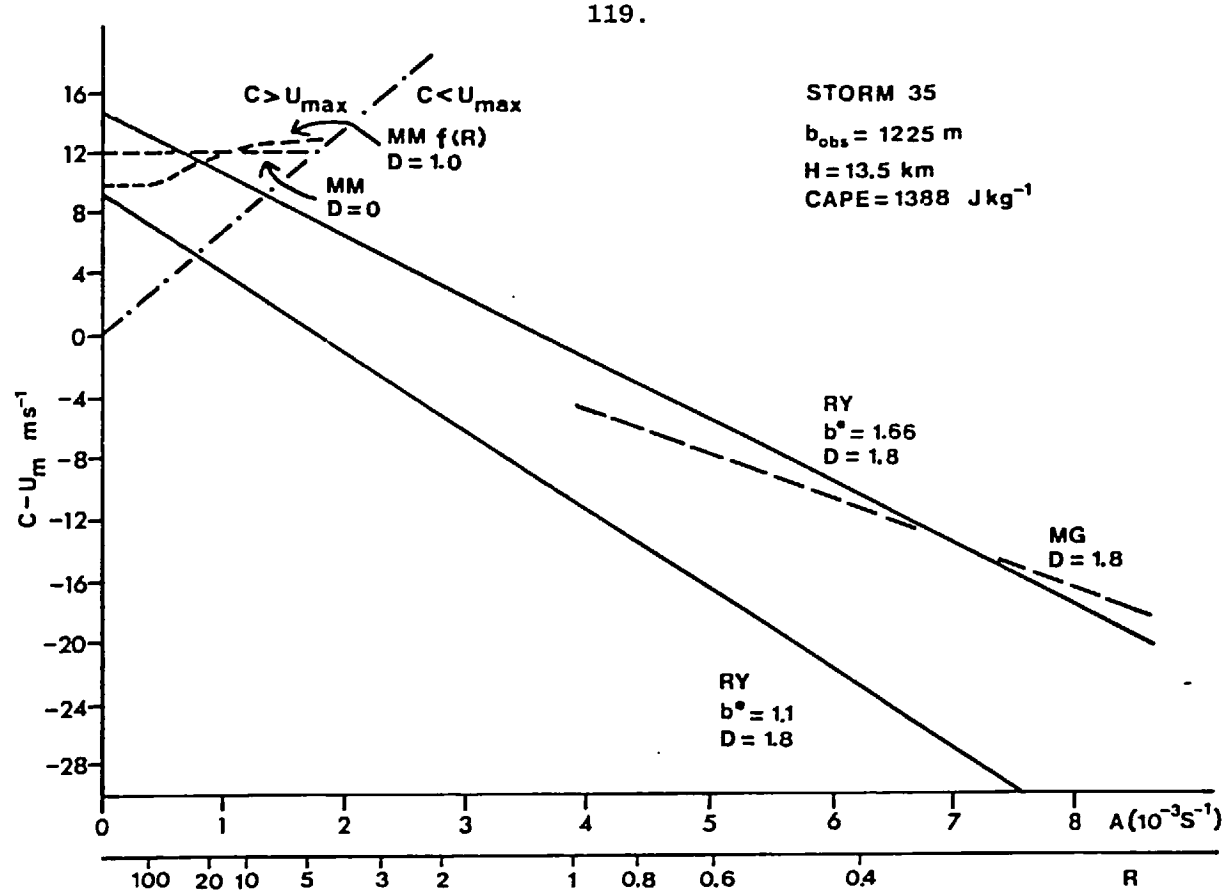

Fig.5.5 Same as Fig.5.4, except for storm 35.

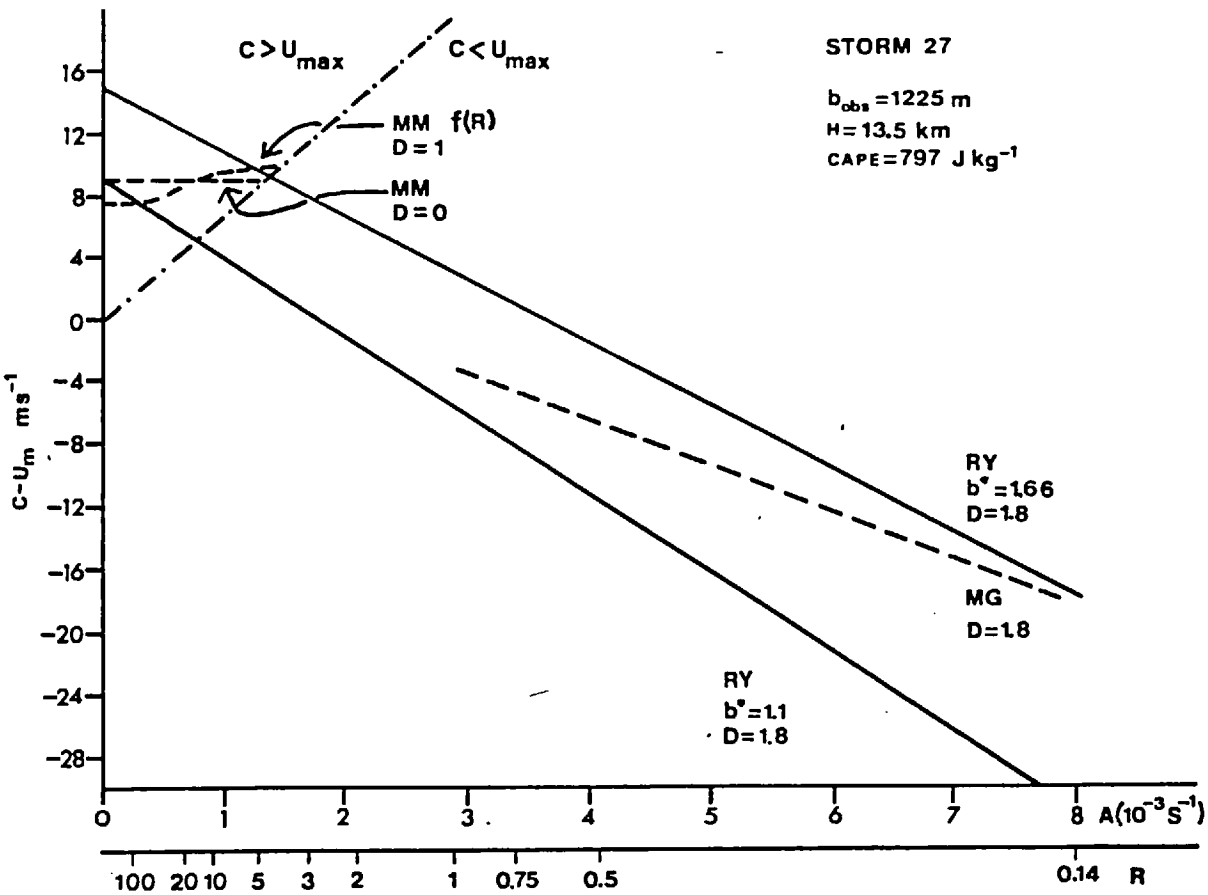

Fig.5.6 Same as Fig.5.4, except for storm 27.

b) The predictions of RY can be approximated very accurately with the formula

$$C - U_m = \beta - \alpha A \qquad (5.8)$$

For the three storms, values of β and α, for various values of b^* are shown in Table 5.3. Eq.(5.8) has interesting similarities with those of the steady models. It is the sum of a part proportional to the shear, a feature common to Eq.(5.6) of MG, and a constant which can be likened to the right-hand side of Eq.(5.7) of MM. Thus it appears to be a form of amalgamation of the two formulae. This hypothesis of the similarity of the expressions will be examined more closely in the following discussion.

c) Before comparing the two models, the variation of the wave-CISK model results with the parameter b^* must first be considered. The work of Section 5.3 showed that $C - U_m$ was a monotonically increasing function of b^* and, for the range of b^*-values in this study, can be approximated by a linear variation. The results quoted here indicate that α is a very weak function of b^*, whereas β is a strong function of b^* :

$$\beta \simeq \beta_0 b^* \qquad (5.9)$$

It is probable that β is a function of the available potential energy of the particular storm in question.

d) In conditions of constant wind, i.e. $A = 0$, the two models give very similar predictions for the storm speed, as indicated in Table 5.4. Thus it appears that the models are very similar in their prediction for constant wind. It is therefore possible to postulate that :

Table 5.3

Values of α and β for three storms

	$b^* = 1.0$		$b^* = 1.10$		$b^* = 1.66$	
Storm	α (km)	β (m s^{-1})	α (km)	β (m s^{-1})	α (km)	β (m s^{-1})
33			5.1	8.6	4.4	14.0
35			5.1	9.0	4.0	14.4
27	5.4	7.6	5.0	8.6	4.0	14.5

Table 5.4

Comparison of speed predictions using

$b^* = 1.1$ and zero shear

Storm	$\frac{(C - U_m)_{RY}}{(C - U_m)_{MM}}$	$(CAPE)^{1/2}$ (m s^{-1})
33	1.08	31
35	0.91	37
27	1.15	29

$$\beta \simeq 0.26\ (CAPE)^{\frac{1}{2}}$$

by comparing Eqs.(5.7) and (5.8).

e) When the shear is increased from zero, the behaviour of the models (RY and MM) are distinct. MM predicts a slight increase in storm speed as shear increases, whereas RY predicts a linear decrease. This clear difference in behaviour is in sharp contrast to the other close similarities.

f) For large shear ($R < 1$) we can compare MG and RY. Both theories give linear decreases in storm speed as the shear increases and the results indicate that the most appropriate value of b^*, to ensure the best agreement between MG and RY models, is 1.66. This is rather different from the 1.10 of the tropical small shear storms. It is of interest to compare the gradients of the two lines, these being respectively:

Wave-CISK : α

Steady : $$\alpha_s = -H\left[\frac{1 + (1+4R)^{\frac{1}{2}}}{3 + (1+4R)^{\frac{1}{2}}} - 0.11\frac{H}{H_0} - \frac{1}{2}\right]$$

Using the appropriate value $b^* = 1.66$, the value of α/α_s for storm 33 is 1.48, and for storms 35 and 27 it is 1.33. Thus the two models differ more than for zero shear, but their proportionality to the shear is the important similarity.

5.7 An alternative forced gravity wave model

Perhaps the two most important results to emerge from this study are that the linear wave-CISK model predicts storms to move faster than the ambient flow for small shear, thus agreeing with the steady model in this limit, and that for large shear both models predict a linear decrease of speed, relative to the mid-level flow, with shear. These results

indicate that the two models are consistent with each other, even though one is linear and therefore considers the growth phase, whereas the other is non-linear and considers the mature steady phase. Thus it may be that the forcing in the linear model adequately parameterizes the extra advective terms which are not included explicitly. The gravity waves are " forced" in that there is a non-adiabatic term included in the equations of motion. This term is of the form

$$Q/\bar{\theta} = 0 \qquad 0 < z < b$$

$$Q/\bar{\theta} = B N b \left(\frac{dw'}{dz}\right)_{z=0} \qquad b < z < H$$

where Q is the heat source/input, b and H are the heights of "cloud base" and cloud top respectively, B the static stability. The thermodynamics of upward motion (imagined to be in the form of plumes) is determined by latent heat release proportional to the product of the static stability, the parameter b, and the surface convergence/divergence. Thus the only vertical dependence is through the vertical variation of B above cloud base, which is small in most atmospheric cases.

In order to understand better the forced gravity wave model, an alternative parameterization of the latent heat release is considered which, although probably less realistic than that of RY, provides analytic solutions. The heat source/sink will be made proportional to the vertical velocity at the middle level :

$$Q/\bar{\theta} = \varepsilon \tilde{w}_{H/2} \qquad 0 < z < H$$

This form of thermodynamic parameterization is suggested because it is related to those in both models. The heat source is proportional to vertical velocity, as in the steady model, but is a constant

with respect to height, as in the RY model. The extent to which this function is a different form from $\tilde{w}(z)$ seems to be the crucial factor considering the conspicuous inability of unforced growing gravity waves to move faster than the mean flow; in the unforced model Q has exactly the form of $\tilde{w}(z)$. The choice of the mid-level vertical velocity is arbitrary and any level, or even an average value, could have been chosen. However, particularly simple analytical solutions are obtained for the mid-level case, and this we use as sufficient justification.

For convenience take $V_k = \bar{u}$, ε and B to be constants and consider the flow between two rigid lids at $z = 0, H$. The solution for $\tilde{w}$ can be written as :

$$\tilde{w} = f\tilde{w}_{H/2}\left[1 - \left[\frac{\sin(\nu z) + \sin(\nu(H - z))}{\sin(\nu H)}\right]\right] \tag{5.10}$$

where $$\nu = \left[\frac{g B}{(\bar{u} - c)^2} - k^2\right]^{\frac{1}{2}}$$

Application of the consistency condition that $\tilde{w}(z = H/2) = \tilde{w}_{H/2}$ gives the dispersion relation to be

$$\cos(\nu H/2) = f/(f - 1), \quad f \neq 1 \tag{5.11}$$

where $$f = \frac{\varepsilon}{B}\,\frac{\nu^2 + k^2}{\nu^2}$$

For growing solutions, c is required to be complex and hence ν is not necessarily real in Eq.(5.11). Approximate solutions can be found for $k^2 << \nu^2$ (which is the limit used in RY):

$$f \simeq f^* = \varepsilon/B$$

Solving Eq.(5.11) in the complex plane, gives :

$$c_i = \tfrac{1}{2}(gB)^{\frac{1}{2}} H \frac{\cosh^{-1}\left[(-1)^n f^*/(f^*-1)\right]}{(n\pi)^2 + \{\cosh^{-1}\left[(-1)^n f^*/(f^*-1)\right]\}^2}$$

$$c_r = \bar{u} \pm \tfrac{1}{2}(gB)^{\frac{1}{2}} H \frac{n\pi}{(n\pi)^2 + \{\cosh^{-1}\left[(-1)^n f^*/(f^*-1)\right]\}^2}$$

and for the vertical wavenumber we obtain :

$$\nu_r H = n\pi \qquad n \text{ integer}$$

$$\nu_i H = 2 \cosh^{-1}\left[(-1)^n f^*/(f^*-1)\right]$$

There are two branches to this solution, for n odd and n even. For these branches, growing waves are obtained for :

n odd requires $\frac{1}{2} < f^* < 1$ for growth

n even requires $f^* > 1$ for growth

The important point to be emphasized is that this model produces growing propagating modes (for $n \geq 1$). (It should be noted, however, that the fastest growing even mode is for $n = 0$, which has $c_r = \bar{u}$. It is not our intention to concentrate on this mode, however, but to describe the ability of the model to produce growing propagating eddies.) It thus gives us direct evidence of such behaviour in linear forced gravity wave models. In the theory of RY, it was assumed that the thermal forcing was proportional to the static stability, and this can be introduced into the present formulation by setting $\varepsilon = NB$. We see that the growing propagating solutions then occur for $N > \frac{1}{2}$ (as now $f^* = N$). As N increases the growth speed decreases and the phase speed increases.

It is of interest to estimate the propagation speed given by this model. Consider the first even mode for $f^* > 1$ which has $n = 2$. It is easy to show that the value of f^* which gives the largest growth speed is approximately 1.0 (to with 1%), and gives a speed :

$$c_r = \bar{u} + (gB)^{\frac{1}{2}} \frac{H}{8\pi}$$

Reasonable atmospheric values $B = 2 \times 10^{-5} m^{-1}$ and $H = 10$ km give $c_r - \bar{u} \simeq 5.7$ m s^{-1}. This value is in reasonable agreement with the other models and, indeed, with the observed motion of squall lines.

Another plausible hypothesis may be to set $\varepsilon = \gamma$, the wet adiabatic lapse rate, as used in the steady model. Now an appropriate value for $f^* = \gamma/B$ is $1.2 \rightarrow 1.5$ which, from the previous discussion, gives growth and propagation.

In summary to this section, it has been shown that the property of propagation relative to the mean flow is not unique to the surface convergence parameterization of RY, and can be reproduced using the alternative parameterization of the present model. It seems that the crucial aspect of the linear forced gravity wave model may be the vertical profile of the latent heat source/sink term.

5.8 Discussion

It has been shown that the wave-CISK model generally underestimates the storm speed, whilst the MM model overestimates it. In some cases the models give good results, but not in others. The predictions of the wave-CISK model for tropical convective storms are not as good as those obtained for some mid-latitude counterparts. In the cases in which this model does not work, it is shown that the responsible factor may be the mass flux due to the plumes, which is not adequately treated

in the model. The MM model gives better results if the mean wind component along the direction of motion is used rather than the mid-level wind.

It has also been shown that the wave-CISK and steady models of storm motion give similar predictions of storm speed in conditions of constant shear. In particular, the storm speed is found to be proportional to the shear, plus a contribution dependent on the available potential energy. An alternative parameterization to that of dependence on surface convergence for latent heat transfer shows growth and propagation to be a general property of forced gravity waves. It appears that the vertical profile of the heating/cooling function is crucial in such models.

A possible interpretation of the relationship of the two models is that the RY model represents the mesoscale aspects of the flow (for example, the speed at which local modifications can propagate), whereas MG and MM represent the dynamics of the local system. When these two coincide, the thermodynamic source term Q appears to be of vital importance.

The steady model essentially considers a pseudo-adiabatic Q, with the motion it predicts occurring in a conditionally unstable environment The wave-CISK model, however, uses a genuine non-adiabatic Q which, although dependent on the motion for its amplitude, has no dependence on the vertical form of the motion. This aspect of the wave-CISK model seems, in some sense, to adequately parameterize the non-linear terms omitted in the linear formulation. This conclusion is somewhat surprising and, at present, is not easy to justify in physical terms.

Another point of interest is the relationship of the wave-CISK model surface convergence parameterization to the forcing produced at the downdraught outflow. Both numerical models (see Thorpe and

Miller, 1978, for example) and observational data (see Miller and Betts, 1977) have shown the convergence produced by the cold downdraught air flowing into the oncoming inflow air to be a very important mechanism in the maintenance and regeneration of severe storms. It appears that the linear wave-CISK model does not represent this process. For example, consider the pressure and potential temperature field produced by a wavelike disturbance :

$$\frac{\delta p}{\rho_0} = \mathrm{Re}\left[\frac{-i(u-c)}{k}\ \frac{\partial w}{\partial z}\right]$$

$$\frac{\delta \theta}{\bar{\theta}} = \mathrm{Re}\left[\frac{-iB}{k(u-c)}\ \left(\frac{Q}{\bar{\theta}} - w\right)\right]$$

where δp is pressure deviation and $\delta\theta$ is potential temperature deviation.

The pressure field, at the surface, is dominated in the small wavenumber approximation by the term :

$$\left.\frac{\delta p}{\rho_0}\right|_{z=0} \simeq \frac{-c_i}{k}\ \mathrm{Re}\left[\left.\frac{\partial w}{\partial z}\right|_{z=0}\right]$$

Thus there is high pressure in the divergent regions of the downdraught and low pressure in the convergent regions of the updraught, at the surface. However, the numerical model data indicate the presence of a meso-high pressure area everywhere at the surface.

The potential temperature is approximated by :

$$\frac{\delta\theta}{\bar{\theta}} \simeq -\frac{B}{kc_i}\ \mathrm{Re}(w) \qquad z < b$$

$$\frac{\delta\theta}{\bar{\theta}} \simeq \frac{B}{kc_i}\ \mathrm{Re}\left[\underset{\text{(i)}}{Nb\ \left.\frac{\partial w}{\partial z}\right|_{z=0}} \underset{\text{(ii)}}{-\ w}\right] \qquad z > b$$

For typical severe storm soundings $B \simeq 0$ in the boundary layer ($z < b$) and thus $\delta\theta/\bar{\theta}$ is zero there. In the free atmosphere $z > b$ and clearly term (i) has to be larger than term (ii) for warming in the updraught and cooling in the downdraught. Thus the near surface temperature structure is unaffected by this motion. Again, this is in sharp contrast to the previously mentioned downdraught mechanism, which gives large negative $\delta\theta$ near the surface.

It is therefore concluded that wave-CISK is probably a completely different maintenance mechanism to that of gust front regeneration. An important test of the theory would be for a numerical simulation to reproduce the features herein described.

The internal forcing near the surface in the steady model has to remain implicit at present, due to the three dimensional nature of the overturning. This represents a serious difficulty in the attempt to evaluate the physical realism of this model and there is indeed a need to examine this problem using numerical and analytical models.

CHAPTER 6

ORGANISATION AND MOTION OF THE SPIRAL RAINBANDS IN HURRICANES

6.1 Introduction

A tropical cyclone is defined as a warm core cyclonic wind circulation in which the maximum sustained winds are 18 m s^{-1} or greater. Tropical cyclones in which the maximum wind equals or exceeds 32 m s^{-1} are called hurricanes when they occur in the Atlantic, and typhoons in the Pacific. In the United States a tropical cyclonic circulation is called a tropical depression if the maximum sustained winds are less than 17 m s^{-1}, tropical storm if the maximum winds are between 17 and 32 m s^{-1}, and hurricane if the maximum winds are greater than 32 m s^{-1}.

The horizontal scale of a hurricane is normally defined by the radius of the longest closed isobaric surface. Characteristic radii vary between 500-1000 km, depending on the hurricane. The average radial extent of hurricane force winds is only about 100 km, but winds greater than 14 m s^{-1} may extend 500 km from the centre.

Following Anthes (1974), we can divide the hurricane into four regions in order to visualise the main aspects of its structure. Fig.6.1 shows these regions. Region I is a relatively inactive region separating regions II and IV, which are respectively the inflow and outflow layers. In this region the vertical velocities and vertical wind shear are small. Radial flow is negligible compared with the tangential flow and the flow is, in general, in gradient balance. Region II is the frictional (Ekman) boundary layer. In this region surface friction destroys gradient balance and produces strong inflow and moisture convergence. Region III includes the eye and eye wall. The air that is accelerated toward low pressure into the centre of the

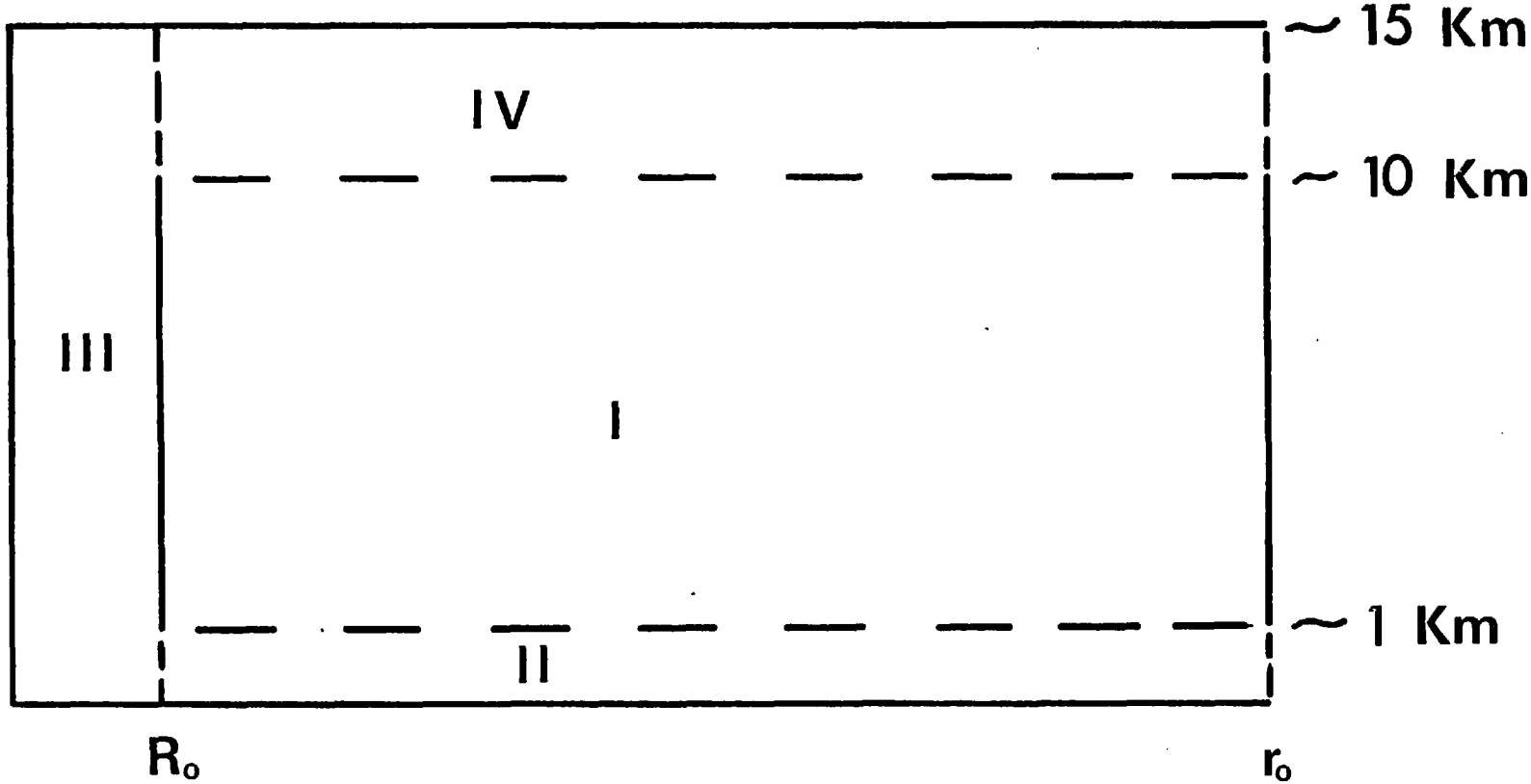

Fig.6.1 Partition of hurricane into four regions. Mass inflow is significant across dashed boundaries and negligible across solid boundaries. R_0 is the radius of maximum wind (about 40 km) and r_0 is the radius of hurricane domain (about 1000 km). (From Anthes, 1974)

storm cannot penetrate beyond some minimum radius because of the excessive velocities required by the conservation law of angular momentum. The air then rapidly rises to the high troposphere in a ring of strong upward motion. This ring is called the eye wall and is characterised by vigorous cumulonimbus clouds and large amounts of precipitation. Latent heat flux in these convective cells produces the warm core structure that is especially pronounced in the upper troposphere. This warm core structure is one of the essential characteristics of the tropical cyclone. Temperature differences between this region and the surrounding environment could be greater than $10^{o}C$ at the 10 km level. The horizontal temperature gradient beyond 100 km is small (approximately $0.5^{o}C$ per 100 km). Inside 100 km the temperature rises sharply and reaches a maximum inside the eye. In the lower troposphere the warm core exists only in the eye. In the eye the winds are light and variable, in sharp contrast to the maximum winds that occur in the eye wall. The eye is typically free of significant cloud cover. Subsidence of upper tropospheric air of high potential temperature is necessary to achieve the extremely low surface pressures observed in the eye. A typical value is 950 mb but a value as low as 887 mb has been registered. In the hurricane about 50% of the total pressure drop occurs within 80 km, which is about twice the radius of maximum winds. Observational studies show that the energy required to drive these systems is derived from the latent heat of condensation released in the eye wall. Latent heat in the warm core maintains the hurricane baroclinic structure and releases available energy, which is continuously converted to kinetic energy. The eye and eye wall typically occupy less than 5% of the total storm volume. Region IV is the outflow layer. Above 10 km to the tropopause, weak radial pressure gradients prevail because of the warm core structure, and the air flows outwards. The outward motion is clearly observed in

satellite photographs by cirrus cloud (Cb anvils) that extend away from the storm to great radii. The diameter of the hurricane's cirrus shield is typically 600-800 km. The circulation in this region is anticyclonic relative to the earth. This anticyclonic circulation is a result of the loss of angular momentum to the sea along the air's low-level inflow trajectory. The outflow layer is quite asymmetric and barotropic processes appear to play an important role in maintaining the kinetic energy of the eddies.

The strongest horizontal winds in the hurricane circulation are located near the top of the boundary layer. Because of the hurricane's warm-core structure, these winds slowly decrease in speed through the troposphere. The mean vertical motion throughout most of the hurricane circulation is weak. Subsidence occurs over a large area surrounding the storm (at radial distances greater than 300 km), as is seen by the nearly cloud-free atmosphere beyond the radius. Diagnostic studies using observations and theoretical models indicate typical mid-tropospheric subsidence values of the order of 1 $cm\,s^{-1}$ Upward motion occurs inside 300 km. The maximum circular mean updraught is of the order 1 $m\,s^{-1}$ and occurs in the eye wall.

The clouds in the hurricane occur mainly in the region of mean upward motion. The dominant cloud type is convective; cumulonimbus clouds erupt in the ascending convectively unstable tropical air. The cloud bases coincide approximately with the top of the Ekman Boundary layer. The many cumulonimbus clouds generate a dense cirrus canopy in the upper troposphere. . The convective elements are organised into spiral bands, as is clearly observed in radar and satellite pictures. These bands appear to originate near the centre of the hurricane and spiral anticyclonically outward to great distances from the centre. The physical mechanism or mechanisms which are responsible for the organisation of convective elements into spiral bands and the outward

propagation of some of these bands relative to the eye, as we will see later, are still uncertain.

In this chapter the main features of hurricane rainbands, as observed on radar and other observational techniques will be described. The discussion is based on observational data of hurricane rainbands reported in the literature, as well as data obtained by the author from radar films and surface data. The author has examined seven radar films of tropical cyclones: Hurricane Donna (1960), Cleo (1964), Betsy (1965) and Caroline (1975), which formed in the Caribbean, Tropical Cyclone Tracy (1974), which struck Darwin, Australia, Typhoon Vera (1959) which struck Japan, and Typhoon Rose (1971), which struck Hong Kong. A review of the ideas concerning the origin of hurricane rainbands will also be made in this chapter.

6.2 Basic Characteristics of Hurricane Rainbands

6.2.1 The hurricane radar weather model

The radar films of many hurricanes reveal a sequence of hurricane radar weather which have been described by Senn and Hiser (1959) as follows (see Fig.6.2):

"The first echoes as seen by a radar well in advance of the storm centre are sharply defined and form narrow pre-hurricane squall lines. In some storms those squall lines are far enough away from the centre so that the tangential motion of the storm, as indicated by the echoes within the lines is small compared with the radial component. In other storms, the hurricane's cyclonic circulation is easily observed in these squall lines several hundred kilometers ahead of the storm centre. Pre-hurricane squall lines are generally separated by 80 km or more from the first echoes of the rain shield, a ragged mass of

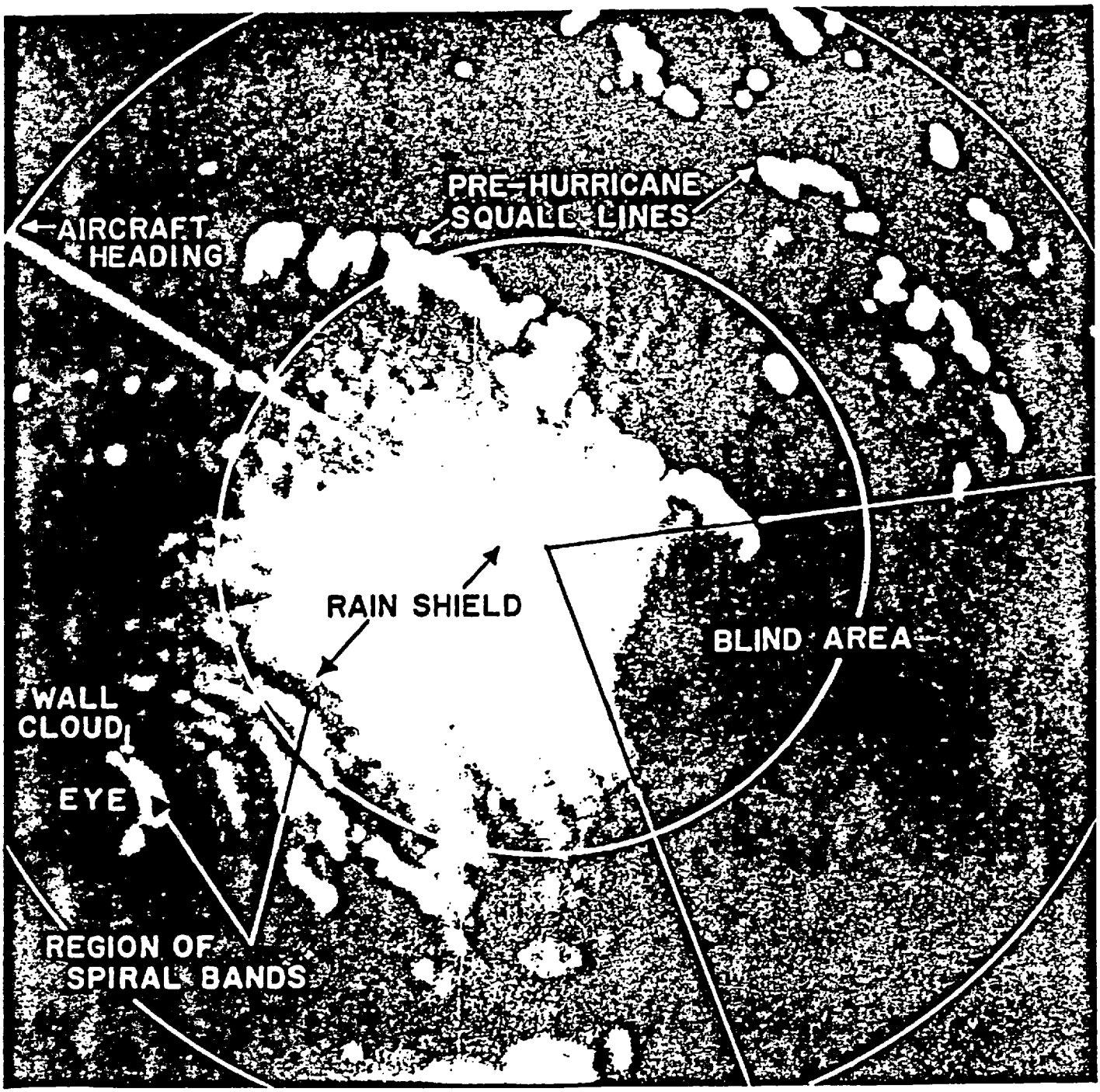

Fig.6.2 Airborne radarscope photograph of Hurricane Daisy, 1946 Z, 27 August 1958, 50 mile range circles. (From Senn and Hiser, 1959)

spiralling weather which extends from 80 to 160 km ahead of the storm centre, or there may also be scattered hard-core echoes between the pre-hurricane squall lines and the lighter precipitation of the rain shield. As the hurricane moves closer and the pre-hurricane squall lines have passed the station, the rain shield, when examined more closely, seems to be composed of many spiral bands which apparently merged as they have been thrown outward from the storm, becoming wider and longer and less well defined in the process. The leading edge of this rain shield has often been observed to have the shape of a well-defined spiral band. As the center of the storm comes into view, it is usually not directly connected to this mass of spiralling weather but is separated from it by a space of 16 to 80 km which is occupied by one or several much more discrete spirals. The spiral bands nearest the storm center are most clearly defined and continuous, and it is these which often define the eye of the hurricane." In the literature, the pre-hurricane squall lines are frequently called outer rainbands, and the bands between the eye wall and the rain shield are called inner rainbands.

In order to illustrate the organisation of rainbands in a hurricane, we will describe the horizontal radar composites of Hurricane Dora (1964). The discussion is based on information given by Sheets (1968).

Fig.6.3 presents the horizontal composites for September 4, 5, 8 and 9, 1964. On September 4 (Fig.6.3a) many spiral bands are observed. A compact eye wall is observed in the northeast quadrant while the other quadrants present only broken echoes. Most of the convective activity is concentrated in the northeast and southeast quadrants. The radar composite shows that the well organised spiral bands are concentrated in a region that extends to a radial distance of approximately 40 n.mi (74 km) north and 60 n.mi (111 km) south

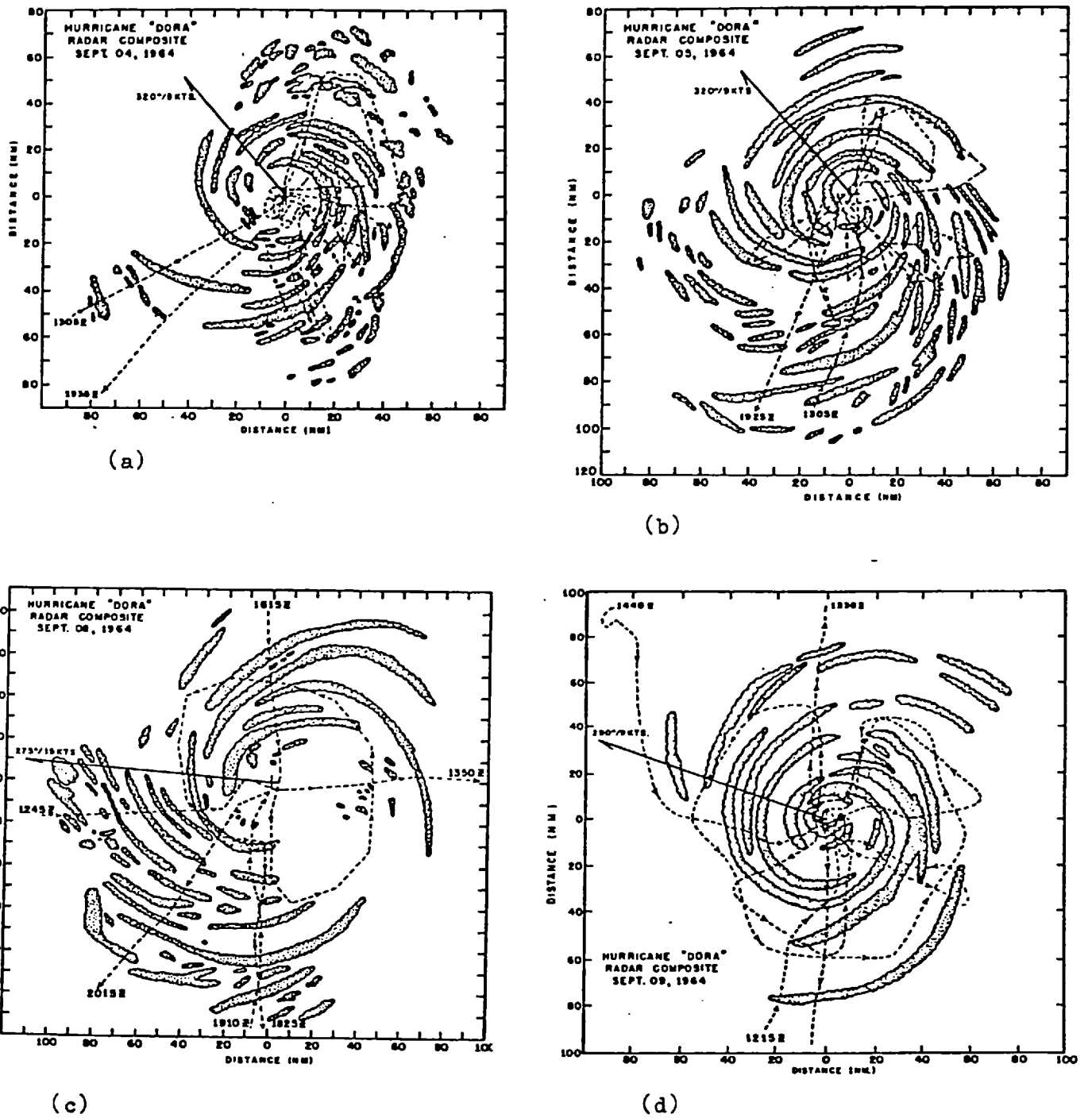

Fig.6.3 Horizontal radar composites for Hurricane Dora (1964): (a) September 4 (b) September 5 (c) September 8 and (d) September 9. (From Sheets, 1968)

of the storm centre. Beyond these limits some broken echoes are observed but are not well organised. According to Sheets, the nose camera film showed considerable layered clouds in the eye, with a small break in the cirrus shield near the centre of the circulation. Large middle level overhanging clouds also extended well into the eye. Below these was a broken-to-overcast stratocumulus cloud deck. The cloud film substantiated the radar structure, with solid clouds and nearly continuous precipitation observed over most of the eastern half of the storm in the region where well organised bands were observed by radar. In the outer regions of the northeast quadrant, where the radar composite indicated broken echoes, the cloud film showed generally layered clouds, with the aircraft being in and out of light-to-moderate precipitation. It also showed layered clouds, with some breaks between the two major rainbands observed by radar in the southwest quadrant.

On September 5 (Fig.6.3b) the storm appears to be well organised. The spiral bands extended to a radial distance of 100 n.mi (185 km) from the storm centre. There is a defined eye wall in the northwest quadrant but not in the other quadrants. Most of the convective activity is in the southern part of the storm, although it is better distributed then than on the previous day. There could have been activity in the northwest quadrant, but the track flown did not cover this area. A band free of echoes is observed at a radial distance of approximately 40 to 50 n.mi (74 to 93 km) south of the storm center. This band spirals into the storm centre, with the width decreasing downstream.

On September 8 (Fig.6.3c) many spiral bands are observed and most of them are concentrated in the western part of the storm. However, on this day no eye wall is defined, and there is a central region free of echoes, which in the west direction extends to a radial distance

of approximately 40 n.mi (74 km).

On September 9 (Fig.6.3d) an eye wall is observed, except in the northeast quadrant. This eye wall had not been seen on the previous day. A band free of echoes is observed in the west part of the storm at a radial distance of approximately 20 to 25 n.mi (37 to 46 km). On this day, well organised bands extended to radial distances of 60 to 80 n.mi (111 to 148 km).

In general, looking at the radar composites of Fig.6.3, one gets the impression that there is a gradual spreading and some rotation of the convective activity.

Penetrative convection in a hurricane is very restricted in area occurring only in the major lines of cumulonimbi. For example, Malkus et al.(1961) found that on the formation day of Hurricane Daisy (1958) about 1% of the rain area ($r < 370$ km) was covered with "hot towers" defined as cumulonimbi with tops above 11 km. This figure had increased to 2.5% on the deepening day, and 4% on the mature day, on which about 200 hot towers were estimated.

6.2.2 Width of the bands

The width of the bands vary not only from storm to storm, but also in time and space in the same storm. Individual inner bands vary in width from 5 to 13 km, while the outer ones are wider, in some cases as much as 32 km. However, in the cases of extreme width, definite evidence of multiple sub-bands is found. The width of these sub-bands is in the 5-13 km range.

Although estimating the width of the bands from radar photographs is rather subjective, the values given above agree fairly well with those obtained by Gentry (1964) from normal traverse flights in hurricanes.

6.2.3 Spacing of the bands

As with the width, the spacing between the bands varies from storm to storm and also in the same storm. The distance between the bands varies in general from 3 to 16 km, with greater spacing for the outer bands.

6.2.4 Inward spiralling of the bands

Radar photographs of hurricanes show that there exists considerable inward spiralling of the bands. Senn et al.(1957) derived a logarithmic spiral in order to provide a realistic fit to some of the radar rainbands. This logarithmic spiral is of the form

$$\ln(r - r_0) = A + B\theta \qquad \text{—(6.1)}$$

where A and B are constants, r is the radial distance from an assumed storm centre to a point on the spiral band, r_0 is the radius of an inner limiting circle which is the origin of the spiral, and θ is the angle between the radius and an assumed axis of origin.

Jordan (1963) evaluated the accuracy of using the equation of the logarithmic spiral mentioned above to determine the position of the hurricane eye. He found a median error of about 32 to 40 km between the eye positions estimated by spiral overlay and the official storm tracks published in the Monthly Weather Review. However, Jordan concluded that the spiral overlay technique is useful when the eye is not observed directly.

Several studies (Fritz et al., 1966; Watanabe, 1963; Sivaramakrisham and Selvam, 1966) show that the crossing angle between the cloud-band and concentric circles decreases as the storm becomes more intense. During the early stage of storm development, a crossing angle of 25 to 30° is usually noted. As the mature stage is reached,

the crossing angle decreases and the bands become tightly coiled. The crossing angle of the mature stage is characteristically between 10 and 15^{o}, with bands approaching concentric circles in the most intense tropical cyclones.

6.2.5 Band life time

The observations of rainbands using radar films show that most of the individual bands have measurable life times only slightly longer than the larger echoes which form them, usually one or two hours. In some exceptional cases, however, the band life time may be as much as 6 or 7 hours.

6.2.6 Band movement

Analysis of hurricane radar films have shown that some hurricane rainbands form near the centre of the hurricane and move outwards, while growing in length. A good example of band movement has been described by Senn and Hiser (1959) who presented the history of a well formed spiral band of hurricane Diane (1955) from its inception to the time it becomes an indistinguishable part of the rain shield. The band moved across the space between the storm centre and the rain shield until it finally merged with the rain shield. They found that the band moved outward from the storm centre at 5 m s^{-1} along the storm path NNW, and at over 8 m s^{-1} normal to the path on the right side of the storm. The outward propagation of the head end in the left front quadrant was slowest, smaller than 3 m s^{-1}; that of the tail end in the right rear quadrant was greater, near 15.5 m s^{-1}. The centre moved at an average speed of 6 m s^{-1} during this period.

Tatehira (1962) made a mesosynoptic and radar analysis of a typhoon rainband. The radar band was initially generated near the eye and was

on the radar PPI photographs at subsequent times. Disregarding the movement of the individual cells composing the band, the main part of the band appeared only in the northeast quadrant of the eye, which moved northeastward with a speed of 12.5 m s^{-1}. The band moved outward at about 4 m s^{-1} relative to the eye.

6.2.7 Movement of individual cells in the bands

Ligda (1955) made a radar study of a Florida hurricane of 23-28 August, 1949. He used in his study a very fine radar film of such a hurricane. The film consisted of pictures taken at about 30 second intervals of the PPI of an SCR 615-B (10 cm) type radar. The tracks of small precipitation areas in various sections of the storm were observed and collected over half-hour periods of storm time. Ligda found that in the storm of 23-28 August, 1949, there was little or no actual rotation of the spiral bands as a whole around the eye. There was, however, motion of small precipitation echoes along the outer spiral bands towards the centre. Protuberances on the bands and small precipitation echoes between the bands near the eye also moved along or parallel to the bands. Fig.6.4 shows six of the thirty vector patterns made by Ligda in the study of precipitation echo motion during this storm. The length of each vector represents the movement of a small precipitation area in one half-hour, so that speed of the echo is directly proportional to the length of the vector. The cross marks the location of the radar relative to the eye of the storm, which is indicated by the hurricane symbol. Because the speed of the eye during the time these tracks were observed varied between 3-11 mph (1.3-5 m s^{-1}), the motion of the storm contributed little to the small precipitation area velocity. Therefore little error exists if these vectors are assumed to be relative to a stationary centre. In the period 0515-0545 EST, 27 August, a small precipitation area velocity of 98 mph (44 m s^{-1}) was found

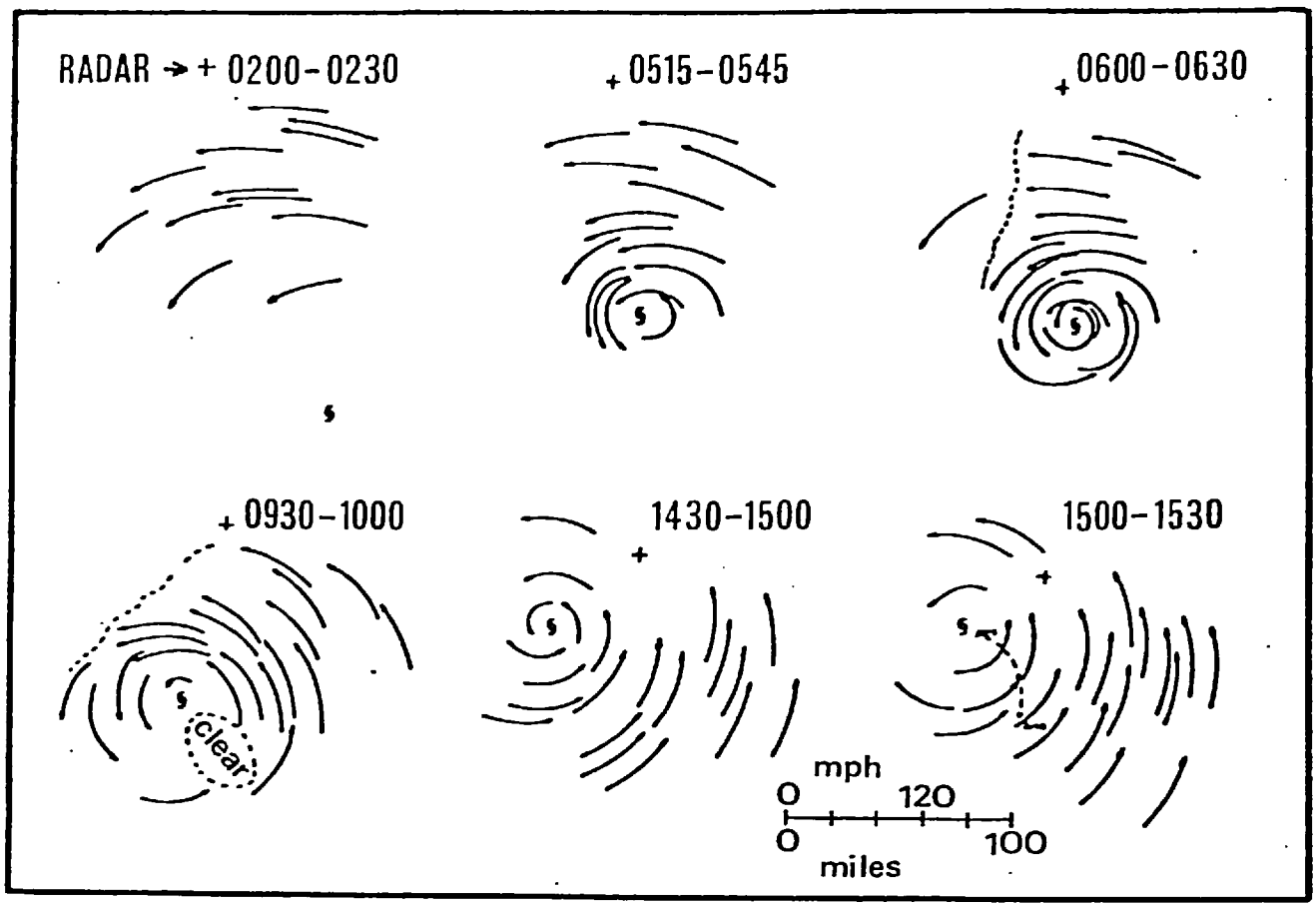

Fig.6.4 Six vector patterns of precipitation echo motion observed in the hurricane of August 23-28, 1949. (From Ligda, 1955)

some 25 miles (40 km) from the eye. In the period 1430-1500 EST, 27 August, except close to the eye of the storm, the length of the vectors is quite uniform, indicating speeds of about 65 mph (29 $m\,s^{-1}$). Ligda compared the speed and direction components of the surface wind and the small precipitation area velocity near three stations There seems to be a fairly consistent difference between small precipitation area and surface wind velocity. Relative to the relationship between small precipitation area and surface wind direction, there exists a fairly consistent difference of about 45^{o} between the two. Apparently in this storm small precipitation areas moved fairly close to the gradient wind direction.

In the study of Tatehira (1962) identification of the individual cells constituting the band was attempted (see Fig.6.5). Only during about one hour was such identification possible, and new cells appeared at the windward (southeast) end of the rainband and the old ones dissipated at the leeward end. The rates of appearance of new cells and disappearance of old ones were about 100 km hr^{-1} (28 $m\,s^{-1}$) measured along the length of the band. This phenomenon is closely related to the apparent divergence of the rainband from the eye.

The facts concerning the displacement of the band studied by Tatehira and the facts concerning the trajectory of the individual cells are summarized in a model shown in Fig.6.6. Although each cell constituting the rainband rotates nearly concentrically around the eye at a high speed, the rainband seems apparently to propagate radially outwards owing to new generation in the windward part and dissipation in the leeward part of the cells and to a non zero crossing angle of the band with a circle about the eye.

Fig.6.7 shows the wind profiles relative to the hurricane's centre of the tangential (V_t) and radial (V_r) components at a distance of about 120 km from the storm's centre. The figure was constructed with

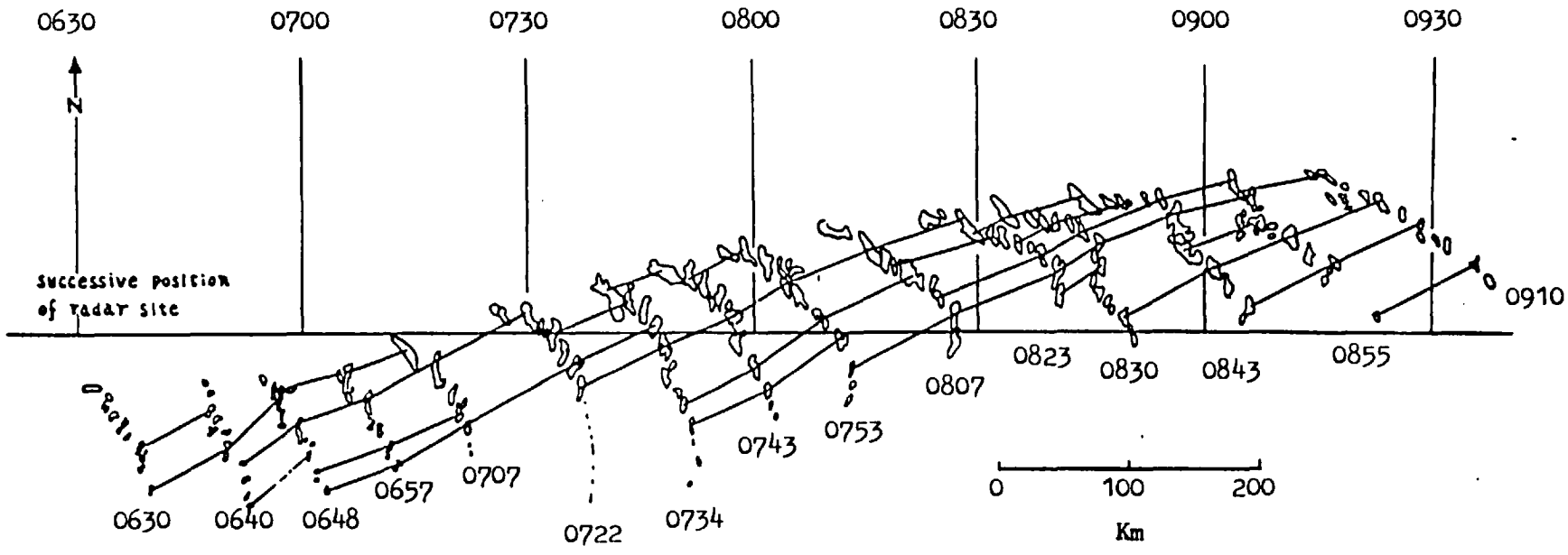

Fig. 6.5 Identification of individual cells constituting a rainband of Typhoon Helen (1958). The cells connected with thin lines are identical. The position of the radar site is shifted with time along an east-west axis. (From Tatehira, 1962)

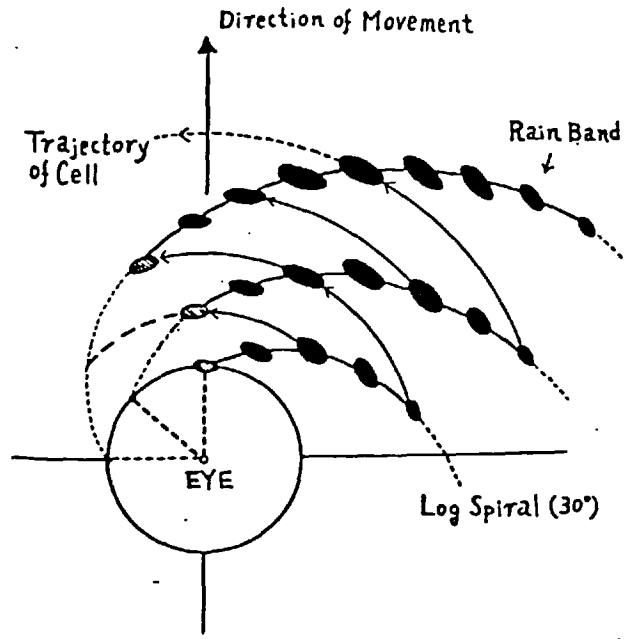

Fig.6.6 Model displacement of a rainband relative to the eye. In this figure the crossing angle of the rainband is exaggerated. (From Tatehira, 1962)

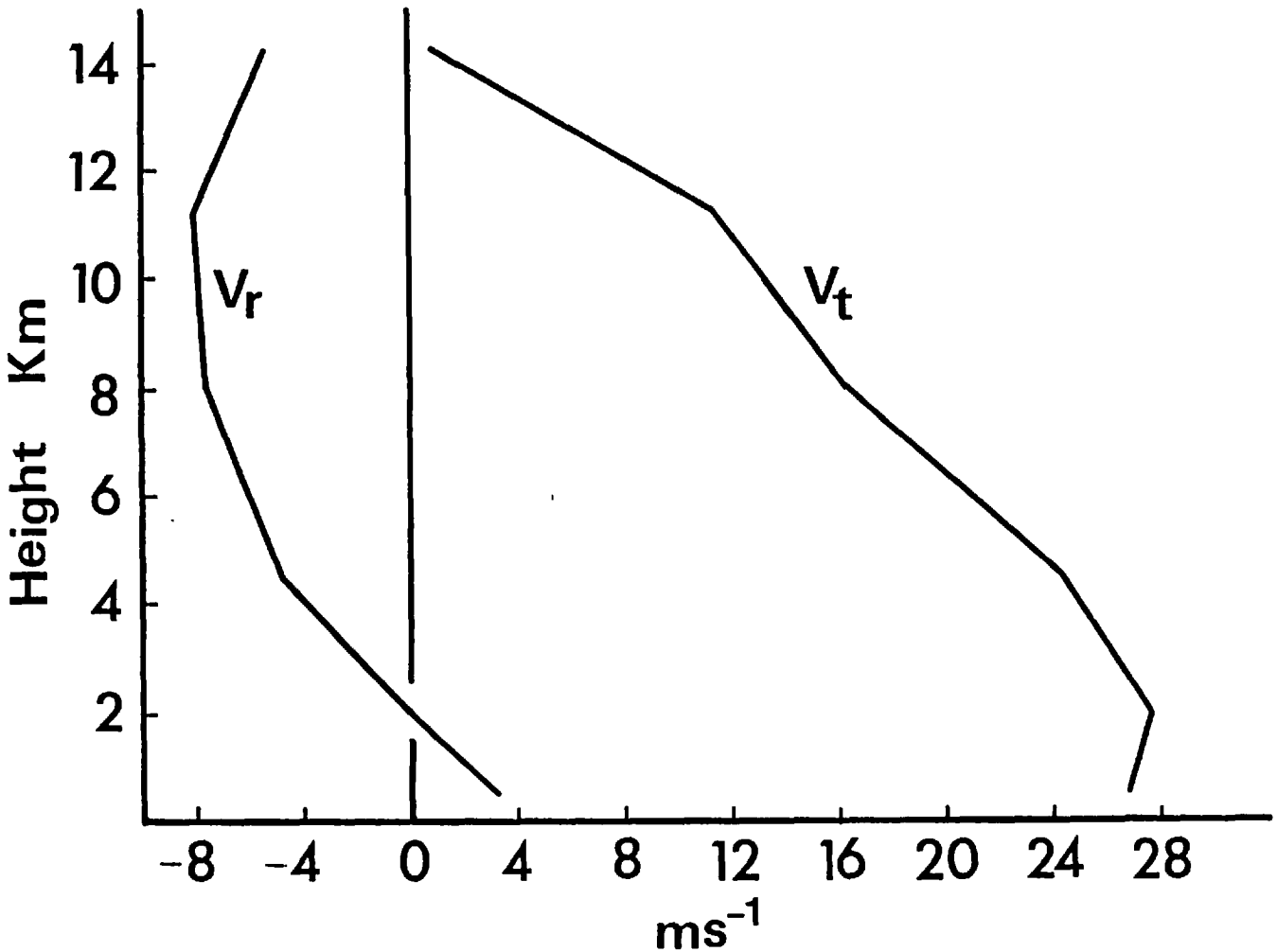

Fig.6.7 Wind profiles relative to the centre of the hurricane. V_r is the radial component and V_t is the tangential component. These profiles are at a distance of about 120 km from the eye.

information given by Miller (1958) who combined wind data from a number of hurricanes and obtained a composite picture of the hurricane circulation. If the speed of the convective elements forming a rainband is about 29 $m\,s^{-1}$ at a distance of 120 km, as Ligda's results show, then it can be inferred from the V_t-profile (Fig.6.7) that there is relative inflow at all levels at the front of the convective elements. On the other hand, the rainband as a whole may be moving outwards relative to the eye with a speed between 3 to 15 $m\,s^{-1}$, as was pointed out before. Thus the wind profile relative to the band may show inflow at all levels if the speed of the band is 8 $m\,s^{-1}$ or larger, or it may show inflow at low levels and outflow at upper levels if the speed of the band is smaller than 8 $m\,s^{-1}$ (see V_r-profile of Fig.6.7).

6.2.8 Measurements of meteorological variables within the bands

Gentry (1964) made observational studies of rainbands analysing data collected in longitudinal and normal traverses at several levels on different flights. For a specific rainband, however, information for only one level is given. Figs. 6.8 and 6.9 show data collected across a rainband of the intense Hurricane Daisy of 27 August, 1958. Data measured along (rather than across) a rainband in Hurricane Ella (1962) are presented in Fig.6.10. Based on the cases presented in Figs. 6.8, 6.9 and 6.10, plus many others not reproduced here (see Gentry, 1964), Gentry suggests the following conclusions:

(1) Rainbands in tropical storms (i.e. less than hurricane intensity) are likely to have a mean temperature colder than that of the ambient atmosphere, but will usually have some much warmer portions. This is especially true for the outer bands.

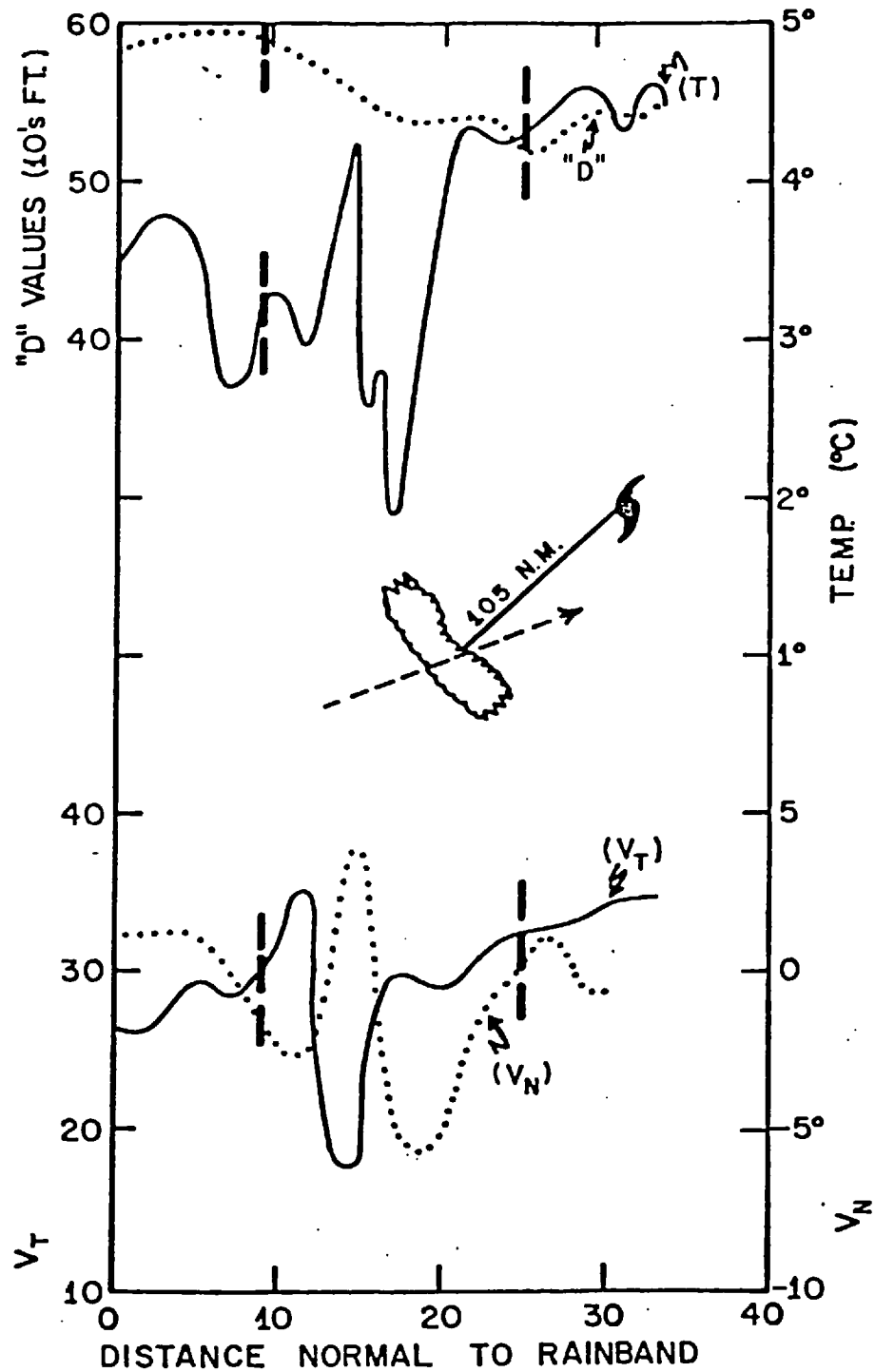

Fig.6.8 Temperatures, D-values and wind components (in knots) along a track normal to the rainband about 105 n mi southwest of the centre of Hurricane Daisy, August 27, 1958. Broken vertical lines on the profiles mark band boundaries. Flight elevation, 13,000 ft. (From Gentry, 1964)

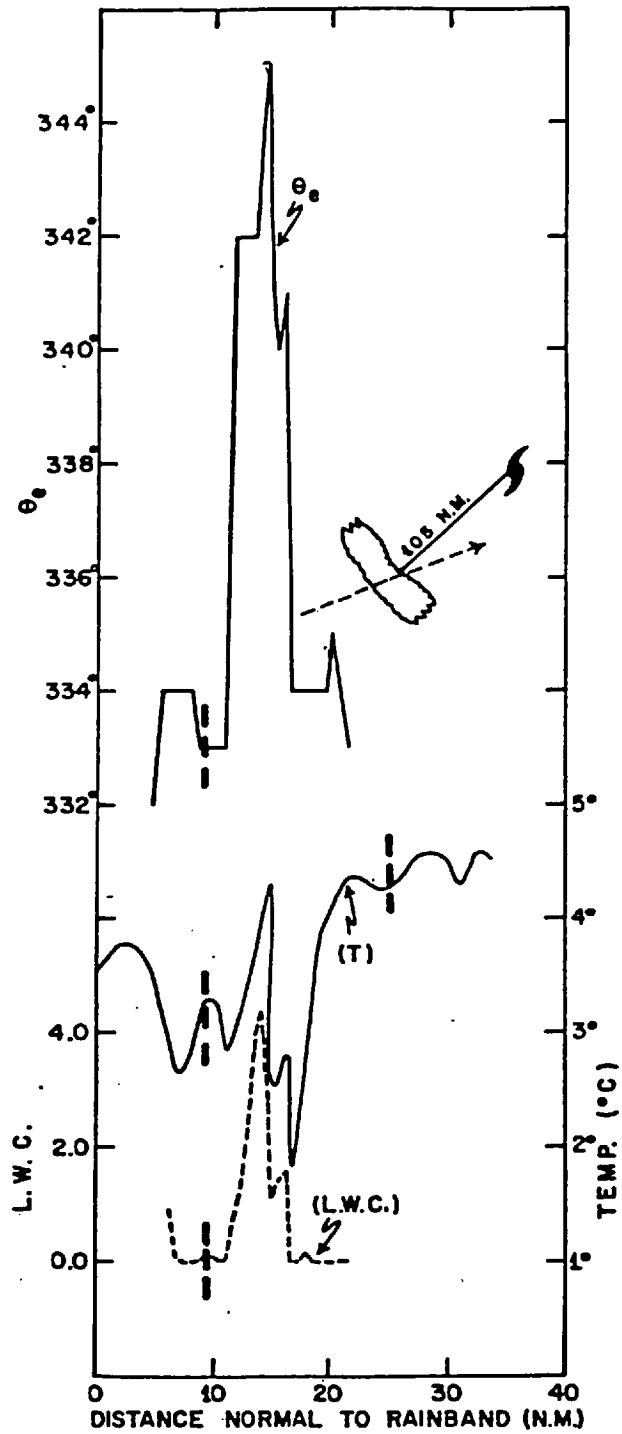

Fig.6.9 As for Fig.6.8, except data are equivalent potential temperature, liquid water content (g m^{-3}), and Temperature. (From Gentry, 1964)

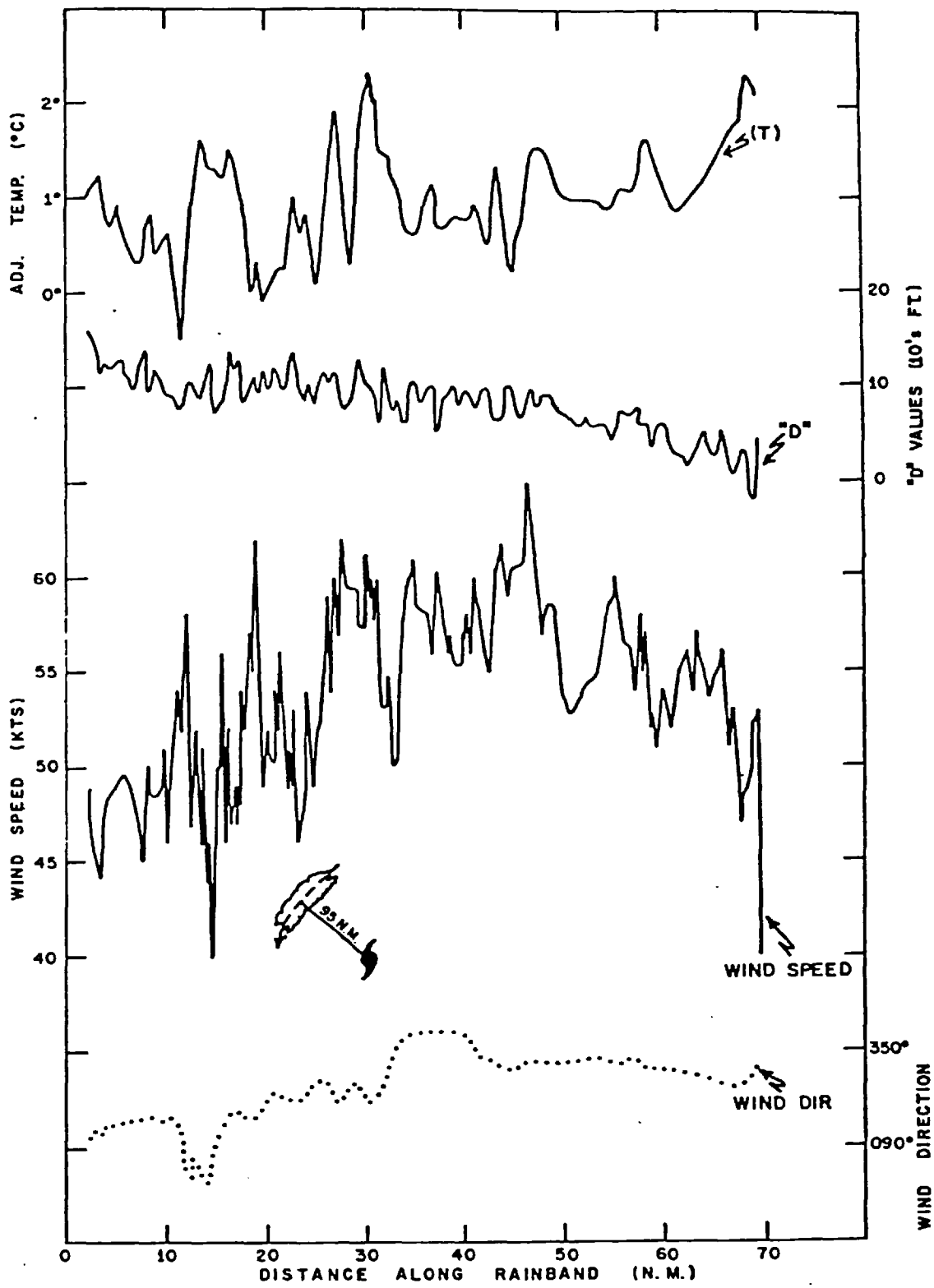

Fig.6.10 Temperatures, D-values and winds recorded on longitudinal traverse of a rainband about 95 n mi northwest of the centre of Hurricane Ella, October 17, 1962. Wind speeds are in knots. Flight elevation, 13,800 ft. (From Gentry, 1964)

(2) Rainbands in mature hurricanes are more likely to have higher mean temperatures than those in the ambient atmosphere, especially when the band is located near the eye wall.

(3) Gradients of temperature, wind direction and wind speed are much greater inside rainbands than in the areas between the bands.

(4) There is no strong correlation between location of the maximum (minimum) wind speed and the high or low pressure sides of bands (except in the eye wall).

(5) Temperature gradients within the bands are as much as 2.5°C per 2 n.mi (2.5°C per 3.7 km) and are frequently greater than 1.5°C per 10 n.mi (1.5°C per 18.5 km). The anomaly of the mean temperature in the bands varies directly with the intensity of the storm, directly with altitude (at least to above the 5000 m level), and inversely with radius. The later relationship, however, is not noticeable except for bands within about 50 n.mi (93 km) radius of the storm's centre.

(6) Winds along the bands vary greatly and apparently in association with microscale features of the band. Gradients in wind speed frequently exceed 10 kts per 5 n.mi (5 m s^{-1} per 9 km) and sometimes exceed 20 kts per 5 n.mi (10 m s^{-1} per 9 km). These gradients in wind speed are not as great as those along radii near the centre of the storm, but are far greater than previously indicated for variations along the bands.

(7) Exchange of air between various portions of the same band and between the various bands and their immediate environment takes place very rapidly both in the outer bands and in the walls of the eye. This is indicated by the large gradients of the component of the wind normal to the bands, both within the bands and in the air 1 to 5 n.mi (1.8 to 9.3 km) on either side of the

bands.

In some cases, the aircraft explorations do not show appreciable and systematic changes in meteorological variables, especially winds, at the boundaries of the rainbands. This may be due merely to the fact that the bands contain a chain of individual cumulonimbus and that changes of wind aloft will depend upon the position of the aircraft traverse with respect to the individual clouds. Therefore accounts of changes of the surface wind during the passage of such bands may be more informative than aircraft measurements.

In the next section the surface changes in some meteorological parameters observed during the passage of hurricane rainbands will be examined.

6.3 Surface Changes in Weather Elements Associated with the Passage of Tropical Cyclones

6.3.1 General sequence

The general sequence of surface changes in meteorological variables when a tropical cyclone approaches a station will be illustrated with Hurricane Cleo (1964) when it struck the greater Miami area. This hurricane remained small and concentrated most of the time, and destructive winds were confined to a small area near the eye.

Figure 6.11, constructed with hourly data, presents a sequence of the changes of surface weather elements at Miami International Airport. It can be seen that when this hurricane approached Miami the wind speed increased, the wind direction shifted gradually, the relative humidity increased, the temperature and pressure decreased, and the rainfall increased. The maximum wind speed in Fig.6.11 is about 32 $m\,s^{-1}$. However, it is necessary to point out that the plotted wind speeds are

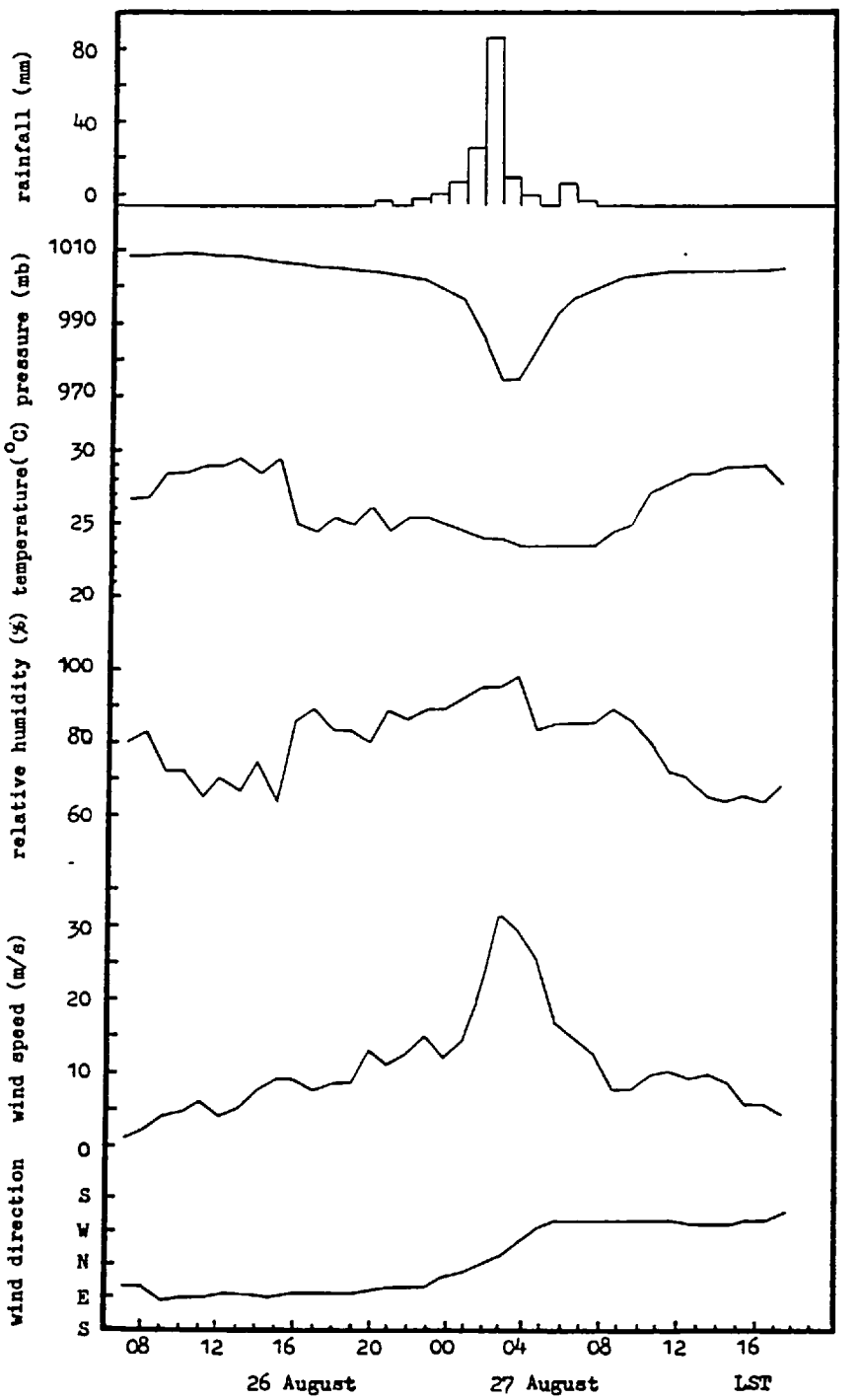

Fig.6.11 Sequence of surface changes in weather elements at Miami International Airport during the passage of Hurricane Cleo (1964).

average values for a period of about five minutes, and that the recorded winds show strong gusts with a maximum of about 44 m s^{-1}. In the period 0900 EST on 26 August to 0600 EST on 27 August, the wind backed gradually through 240°. The relative humidity varied from 65% at 1500 EST on 26 August to 100% at 0400 EST on 27 August. In the same period the temperature fell from 30°C to 24°C. The pressure decreased from 1012 mb at 1100 EST on 26 August to 977 mb at 0300 EST on 27 August. Precipitation was recorded in the period from 2000 EST on 26 August to 0800 EST on 27 August. The total amount of rainfall in this period was about 162 mm, and most of this fell between the 0200-0300 EST period, in which 93 mm were recorded.

6.3.2 Surface changes during the passage of rainbands

The surface changes in the weather elements during the passage of rainbands will be illustrated with Typhoon Babs (1956) when it struck Japan.

Figures 6.12 and 6.13, taken from a paper by Ushijima (1958), present surface data during the passage of outer rainbands of Typhoon Babs. The arrows in the top of the figures indicate the time during which the bands were observed to pass over the station. At Makurazaki (Fig.6.13) two outer bands passed the station during the period considered in the figure, the first at about 0645 LST and the second at about 1020 LST. With the approach of the first band there was a sharp increase in wind speed from less than 10 m s^{-1} to about 24 m s^{-1}. After the band had passed the station, the wind speed decreased to values lower than those before the passage of the band over the station. With the passage of the first rainband there was a shift in wind direction, a decrease in temperature, an increase in pressure, and rain fell (the rainfall trace indicates no precipitation before the band had passed the station). The increase in pressure, which is caused by the cooler air

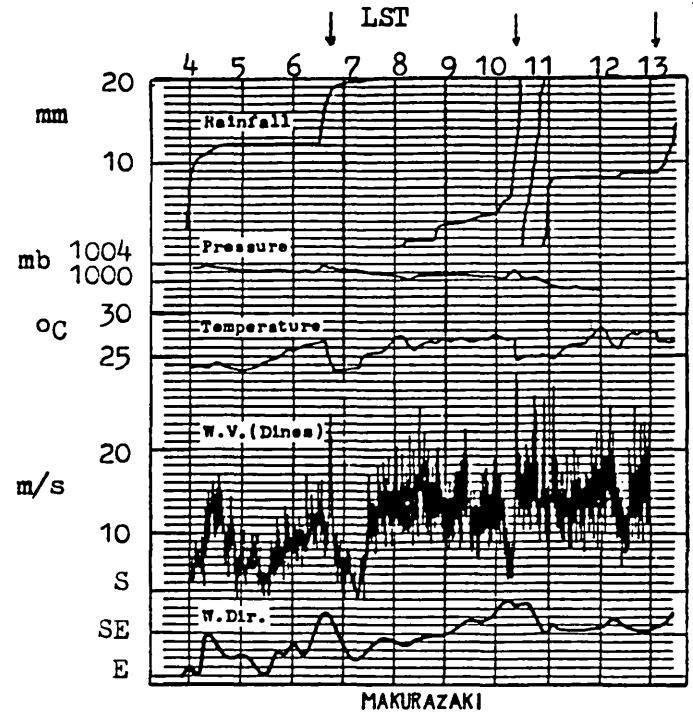

Fig.6.12 Surface changes in weather elements at Makurazaki during the passage of Typhoon Babs, 1956. Arrows show the arrival of the rainbands. (From Ushijima, 1958)

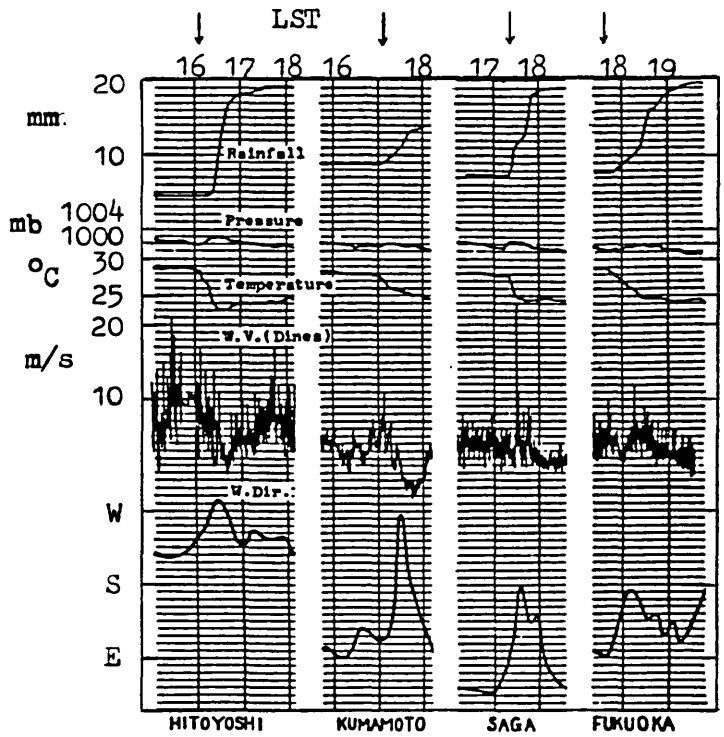

Fig.6.13 Surface changes in weather elements at several stations during the passage of Typhoon Babs, 1956. Arrows show the arrival of the rainbands. (From Ushijima, 1958)

in the downdraught, is preceded by a pressure dip of about 1 mb. With the passage of the second band (at approximately 1020 LST) the wind speed increased from very low values of about 5 m s^{-1} to 30 m s^{-1}. In this case, however, the wind speed decreased to values which were greater than those observed before the passage of the band. A small change in wind direction was observed, together with a decrease in temperature and an appreciable increase in pressure, which was again preceded by a pressure dip. An increase in rainfall intensity was also observed.

Figure 6.13 presents surface data concerning changes in weather elements at several stations during the passage of the outer band which, according to Ushijima, passed over Makurazaki at about 1020 LST. At all these stations the wind speed records show gusts associated with the passage of the band. At Hitoyoshi, Kumamoto and Fukuoka, the wind speed, once the gusts had taken place, decreased to values that are a little lower than those observed before the passage of the band. At Saga, however, the contrary occurred. A shift in wind direction is observed at all the stations, although in the case of Hitoyoshi it does not coincide exactly with the increase in wind speed. The temperature decreased at all the stations during the passage of the band, and an increase in pressure preceded by a pressure dip is also observed. At all the stations it started to rain with the passage of the band. At Hitoyoshi and Fukuoka, the passage of other bands is observed at about 1530 and 1730 LST respectively.

From the cases discussed above, as well as from others reported in the literature (e.g., Wexler, 1947; Ushijima, 1958; Tatehira, 1962; Sethu Raman, 1977), the following conclusions can be made in relation to the surface changes observed during the passage of hurricane rainbands over a site:

1. There is an increase in pressure produced by the downdraught, which is

preceded by a pressure dip of about 1 mb. The nature of this dip is unclear but it suggests the existence of mesolows in advance of hurricane rainbands. Mesoslows in advance of mid-latitude cumulonimbus cloud systems have been studied by Hoxit et al.(1976).

2. In general, the temperature falls and the relative humidity increases. However, in one case (Tatehira, 1962) no significant variation of temperature and relative humidity was observed. In another case (Ushijima, 1958) the temperature increased and the relative humidity decreased during the passage of the rainband.

3. During the passage of a rainband the rainfall intensity increases appreciably.

4. The wind speed increases sharply and large gusts are clearly observed in the wind strip charts. There is also an abrupt shift in wind direction.

In summary, the surface changes associated with the passage of hurricane rainbands are very similar to those observed during the passage of tropical squall lines (e.g. Fernandez, 1980b).

6.4 Tornadoes Associated with Hurricanes

It is not our intention to examine in detail the formation of tornadoes within hurricanes, but some aspects will be discussed.

Several cases of the occurrence of tornadoes associated with hurricanes have been reported (e.g., Malkin and Galway, 1953; Sadowski, 1962, 1966; Rudd, 1964; Pearson and Sadowski, 1965; Smith, 1965; Hill et al., 1966; Orton, 1970; Fujita et al., 1972; Novlan and Gray, 1974). An exceptional case was Hurricane Beulah

in 1967, in which 115 tornadoes were observed to occur (Orton, 1970). Most of the tornadoes have been observed to occur close to the time at which the storms cross land (Novlan and Gray, 1974) and most of them have spawned in the right front quadrants of the hurricanes (Smith, 1965; Fujita et al., 1972). The tornadoes are often associated with the strongest convective elements on the outer rainbands (Hill et al., 1966; Fujita et al., 1972). With a few exceptions the tornadoes associated with Hurricane Beulah (1967) occurred outside the area of hurricane force winds (Orton, 1970). Novlan and Gray (1974) have found that the most important difference between hurricanes which produce tornadoes and those which do not, are the values of wind shear between surface and 850 mb. This averages about 20 m s^{-1} for the tornado cases, but is much less in the cases which do not produce tornadoes. They also found that the differences in vertical stability are very small. Thus the dynamical aspects appear to dominate the thermodynamic aspects. Novlan and Gray have speculated that convective downdraughts may help to develop local areas of low-level horizontal wind shear which, from boundary layer frictional arguments, leads to intense small scale convergence, spin, and velocity concentration. This is supported by a detailed meso-analysis of one typhoon-tornado case in Japan which was made by Fujita et al. (1972). Their study revealed the existence of a mesocyclone and a mesojet in the immediate vicinity of the spawning ground of the tornado.

6.5 Theories of Band Formation

Several possible explanations about the origin of the spiral bands in tropical cyclones have been suggested in the literature. However, the physical mechanism or mechanisms which are responsible for the organisation of convective elements into spiral bands and the

outward propagation of these bands is still uncertain.

In this section a review of such explanations will be made.

6.5.1 Explanations inferred from observations

Fletcher (1945) suggested that the spiral bands were formed when lines of clouds observed frequently within the ITCZ are "coiled" into the centre of growing cyclones. According to Fletcher's theory only those hurricanes forming on the ITCZ will have spiral bands. This, of course, is not the case.

Wexler (1947) took into account the objection mentioned above to Fletcher's theory and extended his explanation. Wexler pointed out that if a circular vortex is introduced into a region of cloud streets originally oriented along the wind, as are frequently observed in tropical regions, then these streets or bands will spiral inward toward the centre. Their width and spacing will change, depending on the vertical wind and density gradients and the distribution and magnitude of the horizontal convergence associated with the vortex. Then, in this process, the prevailing bands are drawn into the hurricane circulation, which thereupon accentuates those bands of the proper wavelength and dissipates the remaining ones. This "resonance" effect, according to Wexler, causes the clouds comprising the "chosen" bands to grow into the cumulonimbus type.

Riehl (1951) simply suggested that the development of the spiral bands in hurricanes could be the result of internal gravity waves. Ligda (1955) supported the idea that there is a distinct difference between the outer and inner spiral bands. He considered that the inner spiral bands are essentially a friction gradient level phenomenon and the outer bands a squall-line type of disturbance. He

maintained that the spiral bands close to the eye are not caused by lines of thunderstorms or cumulonimbus clouds, but are a result of raindrop growth as the hydrometeors fall through lower cloud layers. These clouds, according to his theory, may be of the stratocumulus roll type. Concerning the cause of the outer spiral bands, Ligda suggests two possible reasons: first, these bands may be caused by a kind of microfrontal phenomenon, that is, they may occur at the boundary between low level air masses of different characteristics; second, the bands may be a type of squall-line phenomenon. Ligda favours the latter hypothesis, since it seems to agree better with occasional observations of tornadoes in the outer bands, and fits better with the general radar and surface observations. Kessler and Atlas (1956) simply proposed a banded structure of horizontal convergence.

Senn and Hiser (1959) reasoned that "the spiral bands form near the ring of maximum convergence close to the eye, as a result of some phenomena such as gravity waves, or the strong upthrust which occurs at the wall cloud, not by a uniform circular release of energy there which would create ever-widening circular bands of weather, but by energy which is probably released as it oscillates around the wall cloud which forms the eye. Such an oscillation might create one portion of a spiral band in a given quadrant at a given time and another section of the spiral at a later time in the next counter-clockwise quadrant. The result of this time differential in the continuous formation of the band would impart a spiral shape and establish its quadrants with respect to the storm center. This also accounts for irregularities in the shape of the eye, which is formed by spiral bands in the generative stages. Both the gravity wave and the hurricane's upper-level circular or outward wind field could then provide the mechanism for the outward propagation of the spirals which

usually remain in the same quadrant or quadrants in which they form".

Atlas et al.(1963) have reasoned, similarly to Ligda (1955), that the structure of the inner bands is the result of size distribution, trajectories, and thermodynamic interactions of falling hydrometeors. They built a three-dimensional model of a spiral band, utilising vertical radar cross-sections of echo intensity in Hurricane Esther (1961). They support the idea that with the exception of the outermost band(s) of convective elements (the pre-hurricane squall lines) and the wall cloud itself, the inner spiral bands of a hurricane are largely stratiform and have convective clouds only at their upwind ends. The authors suggest that the stratiform spirals are composed of plumes of precipitation released from convective generators at the head of the band. According to the authors, the generating clouds appear to propagate up-band, thus maintaining a virtually continuous plume for one or more hours, the typical band lifetimes. The net effect is echo motion along the band in both directions; the plume extends downwind while the source cloud propagates upwind. The outward radial component of propagation of the source clouds gives the band its outward velocity.

6.5.2 Explanations inferred from laboratory experiments

Laboratory experiments trying to simulate spiral bands have been attempted by Faller (1962) and Arakawa and Manabe (1963a, 1963b, 1966). Faller's thesis is that the spiral structure is a product of instability of a laminar Ekman boundary layer, the initial instability taking the form of spiral convective bands whose spacing is proportional to the depth of the boundary layer. Then he made a comparison of the forms of the basic laboratory experiments with that of hurricanes; comparison of the characteristics of the instability with the banded

structure of hurricanes, e.g. angles, spacings, etc., and analogy between the laminar flow of experimental models and the turbulent structure of the atmospheric boundary layer. The fact that hurricane bands are observed to move outward is a difference for which two possible explanations consistent with his thesis are suggested by Faller: (1) that the average band angle is greater than that of the stationary roll vortices and that they are advected outward by the normal component of flow; (2) that the additional energy source from the release of latent heat may couple with the original source of convective motion in the bands, so that the band shape is maintained but so that they tend to propagate outward.

Arakawa and Manabe (1963a, 1963b) found that in order to create a vortex type cloud it appears that the typhoon centre should have a precession motion and that the kernal (which consists of intense phenomena such as the atmospheric condensation occurring near the eye wall) should move with it. No physical explanation for the spiral bands is given.

6.5.3 Explanations based on the results of analytical and numerical studies

Tepper (1958) applied the model of the squall line he previously proposed (Tepper, 1950) to the hurricane radar band. His model is the model of the atmospheric gravity wave. As he pointed out, to produce an atmospheric gravity wave, two meteorological features are required: (1) a stratification of the ambient atmosphere, such that there exists a stable layer aloft, and (2) acceleration of the flow is required. He assumes, based on evidence of many soundings, that a stable layer exists aloft. Concerning the second condition, he prescribes that initially, at time $t = 0$ "something" happens to impress an inflow on the circulation. Solving the inviscid shallow

water equations with the method of characteristics, Tepper found a pattern of gravity waves propagating outward. He concludes that the fact that observations of squall lines and hurricane radar bands are similar, lends credence to the assumption that they may be produced by the same mechanism. Individual convective cells carried by the circulating winds will move relative to the radar band in a manner similar to that of individual convective cells relative to a squall line. His results indicate a propagation velocity of about 14 m s^{-1}.

Krishnamurti (1961, 1962) solved the primitive equations of atmospheric motion utilising the method of characteristics and imposing on such systems of equations the commonly observed geometry of the tangential wind field in hurricanes. He found that the computed vertical motion exhibits a spiral form, very similar to that which is observed in radar pictures of hurricanes.

Yamamoto (1963) treated "elastoid waves" and "elastoid-gravoid waves" for a horizontal circular vortex or a simple model of tropical cyclones. He found, introducing those types of waves, that dynamical possibilities for a banded structure and for a spiral shape of equal phase regions of upward motion exist in a case of a simple circular vortex of an incompressible homogeneous atmosphere.

Tang, Brooks and Watson (1964) extended the work of Yamamoto (1963) to a three dimensional baroclinic model. They obtained spiral bands in the vertical motion field for a thermally unstable atmosphere. Tang (1966) found that the thermal stability is the most important parameter affecting the lateral spacing and the crossing angle between the bands and concentric circles. The crossing angle and lateral spacing decrease as the atmosphere becomes more unstable.

Abdullah (1966) has explained the spiral structure of the rainbands as a manifestation of the Doppler shift. Since the inner part of the

hurricane has a high angular velocity compared with the outer part, a wave that is excited by a disturbance moving with the wind in the eye wall will be distorted into a spiral. Abdullah's main hypothesis is that the bands are associated with gravitational waves of finite amplitude propagating at the interface of a high-level inversion. An external source of disturbance is postulated in the form of a fresh surge of air at the exterior of the hurricane. He found that this mechanism leads to the formation of bands of the required shape. Then he suggests that the spiral bands of a hurricane are closely related to the squall lines of temperature latitudes. Working a numerical example, Abdullah found that a squall line appears first at the periphery of the eye, and it grows outward as it rotates cyclonically in the same sense as the basic flow. Once the squall line appears, it grows outward at a great rate. In his example, it takes less than 20 minutes to advance from the periphery of the eye to a point at the radius 100 km. This velocity (83 m s^{-1}) is very large compared with observational evidence.

Hlachova and Vitek (1967) solved the linearised ω-equation. In their solutions they found spiral bands of upward and downward motion.

MacDonald (1968) has presented some evidence for the existence of Rossby-like eddies in hurricanes. As pointed out by Willoughby (1977), MacDonald's idea is that the spiral rainbands may be vorticity waves that resemble Rossby waves but depend upon the radial gradient of relative vorticity in the hurricane, rather than on the meridional gradient of planetary vorticity.

Anthes, Rosenthal and Trout (1971), and Anthes, Trout and Rosenthal (1971) developed an asymmetric model which produced spiral bands of convection. Further, Anthes (1972) improved this model in order to describe the formation and maintenance of spiral bands in greater detail. The spiral bands in the model, with rainfall rates averaging about

2 cm/day, are approximately 90 km wide at large distances from the centre and somewhat wider close to the centre (approximately 100 km). These bands, formed near the centre, rotate cyclonically and propagate outward at a speed of about 12 m s^{-1}. Although the spiral bands in the model are internal gravity waves modified by latent heat release, the mechanism for their generation is unknown. The asymmetries in the outflow layer are shown to result from dynamic instability, with the source of eddy kinetic energy being the mean azimuthal flow. However, as pointed out by Diercks (1975), the physical relationship, if any, between inertial instability and spiral bands, is obscure and the simultaneous formation may be only coincidence.

Kurihara and Tuleya (1974) constructed a three-dimensional, 11-level, primitive equation model for a simulation of tropical cyclones. Their model produces spiral bands which behave like internal gravity waves, with a well defined pattern of low level convergence and surface pressure tendency. Once the band is formed in an area surrounding the centre, it propagates outward apparently without appreciable further supply of energy. The speed of propagation is approximately 100 km/h (28 m s^{-1}), and the widths approximately 100 km. In their study it was found that the surface pressure tendency is an appropriate quantity for detecting spiral bands in a tropical cyclone at the mature stage. However, these pressure tendency bands stretch much longer than the rainbands and many portions of the bands are without precipitation.

Mathur (1975) investigated the development of the propagating and stationary bands in a three-dimensional model of Hurricane Isbel (1964). Stationary and clockwise propagating bands developed in his model. The shape and the structure of these bands were different from those formed in the models by Anthes (1972) and Kurihara and Tuleya (1974). He concluded that development of the propagating bands in his model is related to the release of latent heat in the upper troposphere.

Then the propagating bands in the vertical motion fields in the middle and the upper troposphere form in the regions of strong heating in the upper troposphere and weak cooling in the middle troposphere. They dissipate when the cooling in the upper troposphere, due to vertical advection, exceeds the condensational heating. He thinks that their structure is similar to the outer bands observed in hurricanes; they move at an average speed of 8 to 12 m s^{-1}.

Diercks (1975) and Diercks and Anthes (1976b) used a linear model to study the formation of bands from internal gravity-inertia waves in a barotropic atmosphere. Their primary result is that rotation organises initial random perturbations into a spiral form in experiments with unstable static stability. With stable static stability, significant growth is not observed, but random perturbations are organised into a spiral pattern by rotation in the mean flow. These linear experiments also demonstrated that neither inertial instability nor latent heat release are necessary for the band formation in the linear model, that the Coriolis parameter is relatively unimportant in forming these bands, and that rotation is necessary before spiral bands form. In addition, bands formed without the effect of including surface friction. It was found that the band separation increases but the growth rate decreases in experiments in which adiabatic warming occurs with descent, and warming due to latent heat release occurs with ascending motion.

Diercks (1975) and Diercks and Anthes (1976a) have also used a three dimensional model (Anthes, 1972) to study the energy and angular momentum budgets of model rainbands. In the nonlinear model, spiral bands of upward motion formed continuously and propagated outward from the centre of the simulated hurricane. These bands were probably travelling gravity-inertia waves, consistent with the small differences in mean radial and tangential velocity components, temperature and humidity between the bands

and environment. Also, the nearly identical values of relative vorticity in the bands and environment support the conclusion that the model bands are gravity waves, modified slightly by rotation (the relative vorticity of a pure gravity wave is zero).

Kurihara (1976) investigated the linear development of the band structure in a tropical cyclone by solving an eigenvalue problem for perturbations of spiral shape. He showed that the spiral bands in three different modes may be intensified in an inner area of a tropical cyclone. However, only one of these modes (G-mode in Kurihara's terminology) has been observed in nature. Kurihara found that a spiral band which propagates outward can grow in the presence of the horizontal shear of the basic azimuthal flow. Without the basic circular vortex, this band is reduced to a neutral gravity-inertia wave with a particular vertical structure. The unstable spiral in this mode takes a pattern which extends clockwise from the centre of a storm in the northern hemisphere. An azimuthal wavenumber 2 and a radial scale (twice the band width) of 200 km, are preferred by this band. Kurihara also found that there exists practically no instability in the outer region of the storm in any kind of spiral band. He speculated that a band which grows in an inner area and propagates outward may become a neutral spiral while moving toward the outer region. Kurihara considered that some of the outer spiral bands observed in real tropical cyclones may be interpreted as this type of internal gravity-inertia wave. Thus the actual outer spiral bands, at least some of them, may be interpreted as the counterclockwise, outward-propagating, internal gravity-inertia waves which are intensified in an inner area by the radial shear of the azimuthal flow and possibly also by the effect of heating.

Jones (1977) improved the model proposed by Anthes, Rosenthal and Trout (1971) and Anthes (1972) for hurricane simulation, increasing significantly the domain size and refining the horizontal grid resolution.

This has been accomplished by a system of three nested grids, the inner two of which move with the hurricane centre. The grids are fully interacting with changes on finer grids feeding back to the coarser grids. In his experiments, there are two distinct band propagation rates and band widths. At the mid-troposphere level the bands typically propagate outward at about 60 m s^{-1} and have a wavelength of about 600 km. At the top of the boundary layer the typical band propagates outward at about 12 m s^{-1} and has a wavelength of about 120 km. Jones found that the occurrence of outward propagating spiral gravity wave bands is directly connected to barotropic instability near the eye-wall of the vortex. As pointed out by Jones, the mechanism for the generation of the spiral bands can be inferred from the relationship between the rotating azimuthal wave number two in the wind field (middle troposphere) and the region of origin of the spiral bands. The spiral bands are produced by the mutual adjustment of mass and momentum in the rotating elliptically-shaped asymmetry. Hence Jones concludes that the rotating asymmetry generates the spiral bands.

Fung (1977 a, b) has examined Rayleigh instability of the hurricane's boundary layer as the mechanism responsible for the organisation of the observed rainband pattern. She found that Rayleigh instability of the boundary layer produces spiral regions of upward and downward motion. The regions of upward motion provide a site for cloud formation, forming a spiral pattern which resembles the observed rainbands in a hurricane.

Willoughby (1977) has made an attempt to model spiral rainbands in hurricanes as inertia-buoyancy waves. The model is based on the non-hydrostatic equations describing in cylindrical coordinates linear perturbations on a barotropic vortex embedded in a uniformly stratified atmosphere. The system supports waves whose frequencies are confined to a passband between the local inertia frequency and the buoyancy frequency, and which obtain energy at the expense of the mean flow's

kinetic energy. Willoughby found that the very long radial wavelengths are not possible for outward-propagating waves because the magnitude of an inertia-buoyancy wave's frequency must lie between the buoyancy and local inertia values and also because of the role of the Doppler shift. On the other hand, for the shorter wavelengths in his model, the rate of energy supply is too slow to permit growth of outward propagating waves in the face of geometric spreading. In addition, a lower limit is imposed on the frequency of these waves because the large local inertial frequency in the eye wall must be less than the intrinsic frequency there. This means that the apparent frequency must assume higher values than are observed for spiral bands. So Willoughby (1977) concludes that *outward* propagating inertia buoyancy waves, excited near the storm's centre, do not seem to constitute a plausible model for hurricane rainbands. On the other hand, Willoughby (1978a) has found that *inward* propagating waves on a barotropic vortex are a plausible model for hurricane rainbands. In this context, inward propagation means that the energy is propagating inward from the storm's periphery. As pointed out by Willoughby, the intrinsic phase propagation is also inward, but because the waves are advected tangentially around the storm in the cyclonic sense, the phase lines appear to propagate outward at a fixed radius.

Willoughby (1978b) extended the model of rainbands on a barotropic vortex developed previously by him (Willoughby, 1977, 1978a) to simulate linear waves on a baroclinic mean vortex. Although the energetics is more complicated than in the case of barotropic vortex, the results support the model of rainbands as inward propagating inertia-buoyancy waves. The spiral bands may be excited with small amplitude perturbations at the storm's periphery by such processes as asymmetric frictional forces, flow over coastal topography, or shearing environmental steering currents. The role of the latter process as a mechanism for

the excitation of spiral bands, has been examined by Willoughby (1979). He found that inward propagating inertia-buoyancy waves are excited by imbalances between the Coriolis force due to the storm's motion and the pressure gradient force associated with a shearing environmental geostrophic wind. As the results are consistent with observations, Willoughby concludes that the interaction between the symmetric mean vortex and a shearing environmental steering current may be the cause of spiral bands in hurricanes.

6.6 Conclusion

In this chapter the main characteristics of spiral rainbands in hurricanes have been discussed. The outer rainbands or pre-hurricane squall lines appear to be similar in some aspects to tropical squall lines. Several explanations on the origin and organisation of hurricane rainbands have been examined. However, a convincing explanation of their origin is not yet available. Wave theory, as discussed by Willoughby, is an interesting possibility, but a comparison of the theory results with more observational data is essential. Although numerical models of hurricanes have been able to produce rainbands, some characteristics of the modelled bands appear not to agree with observations. For example, the modelled bands are much wider than the rainbands observed with radar.

An important aspect not considered here is the role of hurricane rainbands in the production of kinetic energy. The fact that much latent heat of condensation is released in the rainbands other than the eye wall, suggests that all the rainbands are important when considering the energy budget of the hurricane. Gentry (1964) found that the rainbands play an important role in the transformation of potential into kinetic energy, even though his data were insufficient

to make a complete kinetic energy budget. This topic should constitute an important aspect in further studies of hurricane rainbands.

REFERENCES

Abdullah, A.J., 1966 : The spiral bands of a hurricane: a possible dynamic explanation. J.Atmos.Sci., 23, 367-375.

Anthes, R.A., 1972 : The development of asymmetries in a three-dimensional numerical model of the tropical cyclone. Mon.Wea. Rev., 100, 461-476.

Anthes, R.A., 1974 : The dynamics and energetics of mature tropical cyclones. Rev.Geophys.Space Phys., 12, 495-522.

Anthes, R.A., S.L. Rosenthal and J.W. Trout, 1971 : Preliminary results from an asymmetric model of the tropical cyclone. Mon. Wea.Rev., 99, 744-758.

Anthes, R.A., J.W. Trout and S.L. Rosenthal, 1971 : Comparisons of tropical cyclone simulations with and wihout the assumption of circular symmetry. Mon.Wea.Rev., 99, 759-766.

Arakawa, A. and W. Schubert, 1974 : Interaction of a cumulus cloud ensemble with the large-scale environment. Part I. J.Atmos.Sci., 31, 674-701.

Arakawa, H. and D. Manabe, 1963a : Investigation of spiral rainbands and frontal structures in terms of shallow water waves. Pap.Meteor. Geophys., 14, 127-143.

Arakawa, H. and D. Manabe, 1963b : A model experiment on spiral rainbands - a dish pan experiment. Proc. of the Symposium on Tropical Meteorology, Rotorua, New Zealand, 5-13 November. New Zealand Meteorological Service, Wellington, 404-415.

Arakawa, H. and D. Manabe, 1966 : Some considerations on spiral cloud patterns in typhoonic area by means of experiments using travelling disturbing element through a shallow water tank. Geophys. Mag., 33, 89-98.

ASECNA, B.E., 1974 : Operation Pre-GATE ASECNA, 1-10 Août, 1973. Research Report, Agence pour la Sécurité de la Navigation Aérienne en Afrique et à Madagascar (ASECNA), Dakar, Senegal.

ASECNA, B.E., 1975 : Operation Pre-GATE ASECNA, 1-10 Août 1973, Compléments d'Analyse. Research Report, ASECNA, Dakar, Senegal.

Aspliden, C.I., Y. Tourre and J.B. Sabine, 1976 : Some climatological aspects of West African disturbance lines during GATE. Mon.Wea.Rev., 104, 1029-1035.

Atlas, D., K.R. Hardy, R. Wexler and R.J. Boucher, 1963 : On the origin of hurricane spiral bands. Geofísica Internacional, 3, 123-132.

Benjamin, T.B., 1968 : Gravity currents and related phenomena. J.Fluid Mech., 31, Part 2, 209-248.

Betts, A.K., 1974 : Further comments on "a comparison of the equivalent potential temperature and the static energy". J.Atmos.Sci., 31, 1713-1715.

Betts, A.K., 1976a : The thermodynamic transformation of the tropical subcloud layer by precipitation and downdrafts. J.Atmos.Sci., 33, 1008-1020.

Betts, A.K., 1976b : Modelling subcloud layer structure and interaction with a shallow cumulus layer. J.Atmos.Sci., 33, 2363-2382.

Betts, A.K., R.W. Grover and M.W. Moncrieff, 1976 : Structure and motion of tropical squall-lines over Venezuela. Quart.J.R.Met. Soc., 102, 395-404.

Betts, A.K. and R.D. Miller, 1975 : VIMHEX-1972 Rawinsonde Data. Research Report, Dept. of Atmospheric Science, Colorado State University, Ft.Collins.

Betts, A.K., and M.F. Silva Dias, 1979 : Unsaturated downdraft thermodynamics in cumulonimbus. J.Atmos.Sci., 36, 1061-1071.

Betts, A.K. and M.A. Stevens, 1974 : Rainfall and radar echo statistics : VIMHEX-1972. Research Report, Dept. of Atmospheric Science, Colorado State University, Ft.Collins.

Brown, J.M., 1979 : Mesoscale unsaturated downdrafts driven by rainfall evaporation: a numerical study. J.Atmos.Sci., 36, 313-338.

Browning, K.A., 1964 : Airflow and precipitation trajectories within severe local storms which travel to the right of the winds. J.Atmos.Sci., 21, 634-639.

Browning, K.A. and F.H. Ludlam, 1962 : Airflow in convective storms. Quart.J.R.Met.Soc., 88, 117-135.

Burpee, R.W., 1972 : The origin and structure of easterly waves in the lower troposphere of North Africa. J.Atmos.Sci., 29, 77-90.

Burpee, R.W., 1975 : Some features of synoptic-scale waves based on a compositing analysis of GATE data. Mon.Wea.Rev., 103, 921-925.

Burpee, R.W., 1977 : The influence of easterly waves on the patterns of precipitation in tropical Northern Africa. In Lectures on Forecasting of Tropical Weather, Including Tropical Cyclones, with Particular Relevance to Africa. WMO-No.492, W.M.O., Geneva, 41-71.

Carlson, T.N. and F.H. Ludlam, 1968 : Conditions for the occurrence of severe local storms. Tellus, 20, 203-226.

Charba, J., 1974 : Application of gravity current model to analysis of squall-line gust front. Mon.Wea.Rev., 102, 140-156.

Charney, J.G. and A. Eliassen, 1964 : On the growth of the hurricane depression. J.Atmos.Sci., 21, 68-75.

Chisholm, A.J. and J.H. Renick, 1972 : The kinematics of multicell and supercell Alberta hailstorms. Alberta Hail Studies, 1972, Research Council of Alberta Hail Studies Rep. No.72-2, 24-31.

Cruz, L.A. 1973 : Venezuelan rainstorms as seen by radar. J.Appl. Met., 12, 119-126.

Dhonneur, G., 1971 : Essai de synthèse sur les lignes de grains en Afrique Occidentale et Centrale. Publication No.20, ASECNA, Dakar.

Dhonneur, G., 1974 : Nouvelle approche des réalités météorologiques de l'Afrique Occidentale et Centrale. Doctoral Thesis, Chapitre IX: Les lignes de grains, Université de Dakar, Dakar.

Diercks, J.W., 1975 : Propagation and maintenance of spiral bands in linear and nonlinear models. Ph.D. Thesis, Pennsylvania State University, University Park, Pennsylvania.

Diercks, J.W. and R.A. Anthes, 1976a : Diagnostic studies of spiral rainbands in a nonlinear hurricane model. J.Atmos.Sci., 33, 959-975.

Diercks, J.W., 1976b : A study of spiral bands in a linear model of a cyclonic vortex. J.Atmos.Sci., 33, 1714-1729.

Eldridge, R.H., 1957 : A synoptic study of West African disturbance lines. Quart.J.R.Met.Soc., 83, 303-314.

Faller, A.J., 1962 : An experimental analogy to and proposed explanation of hurricane spiral bands. National Hurricane Research Project Report No.50, U.S. Weather Bureau, Washington, D.C. 307-313.

Fernandez, W., 1980a : Environmental conditions and structure of some types of convective mesosystems observed over Venezuela. Arch.Met.Geoph.Biokl., Ser.A (in the Press).

Fernandez, W., 1980b : Environmental conditions and structure of the West African and Eastern tropical Atlantic squall lines. Submitted for publication in Arch.Met.Geoph.Biokl., Ser.A.

Fernandez, W. and A.G. Thorpe, 1979 : An evaluation of theories of storm motion using observations of tropical convective systems. Mon.Wea.Rev., 107, 1306-1319.

Fletcher, R.D., 1945 : The general circulation of the tropical and equatorial atmosphere. J.Meteor., 8, 167-174.

Fortune, M.A., 1977 : The West African squall line: a satellite perspective of a tropical tempest. M.S. Thesis, University of Wisconsin, Madison, U.S.A.

Freeman, J.C., Jr., 1948 : An analogy between equatorial easterlies and supersonic gas flow. J.Meteor. 5, 138-146

Fritz, S., L.F. Hubert and A. Timchalk, 1966 : Some inferences from satellite pictures of tropical disturbances. Mon.Wea.Rev., 94, 231-236.

Fujita, T.T., K. Watanabe, K. Tsuchiya and M. Shimada, 1972 : Typhoon-associated tornadoes in Japan and new evidence of suction vortices in a tornado near Tokyo. J.Meteor.Soc. Japan, 50, 431-453.

Fung, I.Y., 1977a : The organization of spiral rainbands in a hurricane. Sc.D. Thesis, Massachusetts Institute of Technology, Cambridge, Mass.

Fung, I.Y., 1977b : The organization of spiral rainbands in a hurricane. Preprints 11th Tech.Conf. on Hurricanes and Tropical Meteorology, 13-16 Dec., Florida. Amer.Met.Soc., 40-43.

GARP-JOC, 1970 : The planning of GARP tropical experiments. GARP Publications Series No.4, World Meteorological Organization, Geneva.

Gentry, R.C., 1964 : A study of hurricane rainbands. National Hurricane Research Report No.69, U.S. Weather Bureau, Washington, D.C.

Gray, W.M., 1970 : Fundamental role of cumulus convection for kinetic energy transformation in the tropics and general circulation. Proc. of the Symposium on Tropical Meteorology, 2-11 June, Honolulu, Hawaii Institute of Geophysics, pp. DV, 1-8.

Gray, W.M., 1978 : Hurricanes: their formation, structure and likely role in the tropical circulation. In Meteorology over the Tropical Oceans (D.B. Shaw, Ed.), Royal Meteorological Society Bracknell, England, 155-218.

Green, J.S.A. and R.P. Pearce, 1962 : Cumulonimbus convection in shear. Tech.Note No.12, Dept. of Meteorology, Imperial College, London.

Grover, R.W., 1974 : Characteristics of tropical squall-lines over Venezuela. Atmospheric Science Report No.228, Dept. of Atmospheric Science, Colorado State University, Fort Collins, Colorado, 79 pp.

Hamilton, R.A. and J.W. Archbold, 1945 : Meteorology of Nigeria and adjacent territories. Quart.J.R.Met.Soc., 71, 231-262.

Hane, C.E., 1973 : The squall line thunderstorms : numerical experimentation. J.Atmos.Sci., 30, 1672-1690.

Henry, W.K., 1974 : The tropical rainstorm. Mon.Wea.Rev., 102, 717-725.

Hill, E.L., W.Malkin and W.A. Schulz, Jr., 1966 : Tornadoes associated with cyclones of tropical origin - practical features. J.Appl.Meteor., 5, 745-763.

Hlachova, P. and V. Vitek, 1967 ; Simple theoretical interpretation of the spiral structure of cloudiness in a tropical cyclone. Studia Geophysica et Geodaetica, 11, 311-316.

Hoxit, L.R., C.F. Chappell and J.M. Fritsch, 1976 : Formation of mesolows or pressure troughts in advance of cumulonimbus clouds. Mon.Wea.Rev., 104, 1419-1428.

Houze, R.A., 1975 : Squall lines observed in the vicinity of the Researcher during Phase III of GATE. Proc. 16th Radar Meteor. Conf., Houston, Amer.Met.Soc., 206-209.

Houze, R.A., 1976 : GATE radar observations of a tropical squall line. Proc. 17th Radar Meteor. Conf., Seattle, Amer.Met.Soc., 384-389.

Houze, R.A., 1977 : Structure and dynamics of a tropical squall line system. Mon.Wea.Rev., 105, 1540-1567.

Huschke, R.E., Ed., 1970: Glossary of Meteorology. Amer.Met.Soc., Boston, Mass., 638 pp.

Johnson, R.H., 1976 : The role of convective-scale precipitation downdrafts in cumulus and synoptic-scale interactions. J.Atmos.Sci., 33, 1890-1910.

Jones, R.W., 1977 : A nested grid for a three-dimensional model of a tropical cyclone. J.Atmos.Sci., 34, 1528-1533.

Jordan, C.L., 1963 : The accuracy of center positions of hurricanes as determined by the spiral overlay technique. Weather Radar, 10, 202-207.

Kessler, E. and D. Atlas, 1956 : Radar-synoptic analysis of Hurricane Edna, 1954. Geophys.Res. Paper No.50, Air Force Cambridge Research Center, Bedford, Mass.

Keulegan, G., 1958 : The motion of saline fronts in still water. Nat.Bur. of Standards Rep., U.S. Dept. of Commerce, Washington D.C., 29 pp.

Klemp, J.B. and R.B. Wilhelmson, 1978 : The simulation of three-dimensional convective storm dynamics. J.Atmos.Sci., 35, 1070-1096.

Krishnamurti, T.N., 1961 : On the vertical velocity field in a steady, symmetric hurricane. Tellus, 13, 171-180.

Krishnamurti, T.N., 1962 : Some numerical calculations of the vertical velocity field in hurricanes. Tellus, 14, 195-211.

Kurihara, Y., 1976 : On the development of spiral bands in a tropical cyclone. J.Atmos.Sci., 33, 940-958.

Kurihara, Y. and R.E. Tuleya, 1974 : Structure of a tropical cyclone developed in a three-dimensional numerical simulation model. J.Atmos.Sci., 31, 893-919.

LeRoux, M., 1976 : Processus de formation et d'evolution des lignes de grains de l'Afrique Tropicale Septentrionale. Recherches de Climatologie Tropical No.1, Dept.Geographie, Université de Dakar, Dakar.

Ligda, M.G.H., 1955 : Analysis of motion of small precipitation areas and bands in the Hurricane August 23-28, 1949. Technical Note No.3, Dept. of Meteorology, Massachusetts Institute of Technology, Cambridge, Mass.

Lilly, D.K., 1979 : The dynamical structure and evolution of thunderstorms and squall lines. Annual Review of Earth and Planetary Sciences, 7, 117-161.

Lindzen, R.S., 1974 : Wave-CISK in the tropics. J.Atmos.Sci., 31, 156-179.

Ludlam, F.H., 1963 : Severe local storms: A review. Meteor.Monographs, Vol.5, No.27, Amer.Met.Soc., pp.1-30.

Ludlam, F.H., 1976 : Aspects of cumulonimbus study. Bull.Amer. Met.Soc., 57, 774-779.

MacDonald, N.J., 1968 : The evidence for the existence of Rossby-like waves in the hurricane vortex. Tellus, 20, 138-150.

Madden, R.A. and F.E. Robitaille, 1970 : A comparison of the equivalent potential temperature and the static energy. J.Atmos.Sci., 27, 327-329.

Malkus. J.S., C. Ronne and M. Chaffee, 1961 : Cloud patterns in Hurricane Daisy. Tellus, 13, 8-30.

Mansfield, D.A., 1977 : Squall lines observed in GATE. Quart.J. R.Met.Soc., 103, 569-574.

Marwitz, J.D., 1972a : The structure and motion of severe hail-storms. Part.I : Supercell storms. J.Appl.Met. 11, 166-179.

Marwitz, J.D., 1972b : The structure and motion of severe hail-storms. Part II: Multicell storms. J.Appl.Met., 11, 180-188.

Mathur, M.B., 1975 : Development of banded structure in a numerically simulated hurricane. J.Atmos.Sci., 32, 512-522.

Malkin, W. and J.G. Galway, 1953 : Tornadoes associated with hurricanes - as illustrated by Franconia, Va., tornado, September 1, 1952. Mon.Wea.Rev., 81, 299-303.

Middleton, G.V., 1966 : Experiments on density and turbidity currents. Canadian J.Earth Sci., 3, 523-546.

Miller, B.I., 1958 : The three-dimensional wind structure around a tropical cyclone. National Hurricane Research Project Report No.15, U.S. Weather Bureau, Washington, D.C.

Miller, M.J. and A.K. Betts, 1977 : Travelling convective storms over Venezuela. Mon.Wea.Rev., 105, 833-848.

Miller, M.J. and R.P. Pearce, 1974 : A three-dimensional primitive equation model of cumulonimbus convection. Quart.J.R.Met.Soc., 100, 133-154.

Miller, R.C., 1967 : Notes on analysis and severe storm forecasting procedures of the Military Weather Warning Center. Air Weather Service Tech.Report 200.

Moncrieff, M.W., 1978 : The dynamical structure of two-dimensional steady convection in constant vertical shear. Quart.J.R.Met. Soc., 104, 543-567.

Moncrieff, M.W. 1979 : Dynamical interaction between tropical squall lines and the mesoscale environment. Unpublished manuscript presented at the Royal Meteorological Society Meeting on Cumulonimbus Downdraughts, London, November 21, 1979.

Moncrieff, M.W. and J.S.A. Green, 1972 : The propagation of steady convective overturning in shear. Quart.J.R.Met.Soc., 98, 336-352.

Moncrieff, M.W. and M.J. Miller, 1976 : The dynamics and simulation of tropical cumulonimbus and squall lines. Quart.J.R.Met.Soc., 102, 373-394.

Newton, C.W., 1950 : Structure and mechanism of the prefrontal squall line. J.Meteor., 7, 210-222.

Newton, C.W., 1963 : Dynamics of severe convective storms. Meteor. Monographs, Vol.5, No.27, Amer. Met.Soc., 33-58.

Newton, C.W. and H.R. Newton, 1959 : Dynamical interactions between large convective clouds and environment with vertical shear. J.Meteor., 16, 483-496.

Nitta, T., 1975 : Observational determination of cloud mass flux distributions. J.Atmos.Sci., 32, 73-91.

Novlan, D.J. and W.M. Gray. 1974 : Hurricane-spawned tornadoes. Mon.Wea.Rev., 102, 476-488.

Obasi, G.O.P., 1974 : The environmental structure of the atmosphere near West African disturbance lines. International Tropical Meteorology Meeting, Nairobi, Amer.Met.Soc., Boston, Part II, 62-66.

Ogura, Y. and H.R. Cho, 1973 : Diagnostic determination of cumulus cloud populations from observed large-scale variables. J.Atmos. Sci., 30, 1276-1286.

Ooyama, K., 1971 : A theory on parameterization of cumulus convection. J.Meteor.Soc. Japan, 49, 744-756.

Orton, R., 1970 : Tornadoes associated with Hurricane Beulah on September 19-23, 1967. Mon.Wea.Rev., 98, 541-547.

Pastushkov, R.S., 1975 : The effect of vertical wind shear on the evolution of convective clouds. Quart.J.R.Met.Soc., 101, 281-291.

Payne, S.W. and M.M. McGarry, 1977 : The relationship of satellite inferred convective activity to easterly waves over West Africa and the adjacent ocean during Phase III of GATE. Mon.Wea.Rev., 105, 413-420.

Pearson, A.D. and A.F. Sadowski, 1965 : Hurricane-induced tornadoes and their distribution. Mon.Wea.Rev., 93, 461-464.

Raymond, D.J., 1975 : A model for predicting the movement of continuously propagating convective storms. J.Atmos.Sci., 32, 1308-1317.

Raymond, D.J., 1976 : Wave-CISK and convective mesosystems. J.Atmos.Sci., 33, 2392-2398.

Riehl, H., 1951 : Aerology of tropical storms. Compendium of Meteorology, Amer.Met.Soc., Boston, Mass., 902-913.

Riehl, H., 1969 : Some aspects of cumulonimbus convection in relation to tropical weather systems. Bull.Amer.Met.Soc., 50, 587-595.

Riehl, H., 1973 : Controls of the Venezuelan rainy season. Bull.Amer.Met.Soc., 54, 9-12.

Riehl, H., 1977a : Venezuelan rain systems and the general circulation of the summer tropics I : rain systems. Mon. Wea.Rev., 105, 1402-1420.

Riehl, H., 1977b : Venezuelan rain systems and the general circulation of the summer tropics II : relations between low and high latitudes. Mon.Wea.Rev., 105, 1421-1433.

Riehl, H., L. Cruz, M. Mata and C. Muster, 1973 : Precipitation characteristics during the Venezuela rainy season. Quart. J.Roy.Met.Soc., 99, 746-757.

Riehl, H. and W. Lueckefedt, 1976 : Precipitation and thermodynamic structure of rain events in Venezuela. Mon.Wea.Rev., 104, 1162-1166.

Riehl, H. and J.S. Malkus, 1957 : On the heat balance and maintenance of circulation in the Trades. Quart.J.Roy.Met. Soc., 83, 21-29.

Riehl, H. and J.S. Malkus, 1958 : On the heat balance in the equatorial trough zone. Geophysica, 6, 503-537.

Riehl, H., D. Rossignol and W. Lückefedt, 1974 : On the structure and maintenance of West African squall lines. Institut für Meteorologie, Freie Universität Berlin, 29 pp.

Rudd, M.I., 1964 : Tornadoes during Hurricane Carla at Galveston. Mon.Wea.Rev., 92, 251-254.

Sadowski, A., 1962 : Tornadoes associated with Hurricane Carla, 1961. Mon.Wea.Rev., 90, 514-516.

Sadowski, A., 1966 : Tornadoes with hurricanes. Weatherwise, 71, 71-75.

Sanders, F. and R.J. Paine, 1975 : The structure and thermodynamics of an intense mesoscale convective storm in Oklahoma. J.Atmos.Sci., 32, 1563-1579.

Sanders, F. and K.A. Emanuel, 1977 : The momentum budget and temporal evolution of a mesoscale convective system. J.Atmos. Sci., 34, 322-330.

Schlesinger, R.E., 1978 : A three-dimensional model of an isolated thunderstorm : Part I. Comparative experiments for variable ambient wind shear. J.Atmos.Sci., 35, 690-713.

Senn, H.V. and H.W. Hiser, 1959 : On the origin of hurricane spiral rainbands. J.Meteor., 16, 419-426.

Senn, H.V., H.W. Hiser and R.C. Bourret, 1957 : Studies of hurricane spiral bands as observed on radar. National Hurricane Research Project Report No.12, U.S. Weather Bureau, Washington, D.C.

Sethu Raman, S., 1977 : Some micro-meteorological observations during the approach and passage of Hurricane Belle (1976). Preprints 11th Tech.Conf. on Hurricanes and Trop.Meteor., Florida, 13-16 December, Amer.Met.Soc., 554-557.

Sheets, R.C., 1968 : The structure of Hurricane Dora (1964). Technical Memorandum No.83, National Hurricane Research Laboratory, Miami, Florida.

Simpson, J.E., 1969 : A comparison between laboratory and atmospheric density currents. Quart.J.R.Met.Soc., 95, 758-765.

Simpson, J.E., 1972 : Effects of the lower boundary on the head of a gravity current. J.Fluid Mech., 53, Part 4, 759-768.

Sivaramakrisham, M.V. and M.V. Selvan, 1966 : On the use of spiral overlay techniques for estimating the center positions of tropical cyclones from satellite photographs taken over the Indian region. Proc. of the 12th Conference on Radar Meteorology, Norman, Oklahoma, Oct. 1966, American Meteorological Society, Boston, Mass. 440-446.

Smith, J.S., 1965 : The hurricane-tornado. Mon.Wea.Rev., 93, 453-459.

Takeda, T., 1971 : Numerical simulation of a precipitating convective cloud : the formation of a long-lasting cloud. J.Atmos.Sci., 28, 350-356.

Tam, H.Y., 1979 : Cumulonimbus convection and parameterization. Ph.D. Thesis, University of London, London, 178 pp.

Tang, W., 1966 : Meteorological variables critical to geometry of hurricane spiral bands. GCA Tech.Report No.66-17-G, Final Report, Contract No. Cwb-11191, GCA Corporation, Bedford, Mass.

Tang, W., E.M. Brooks and B.F. Watson, 1964 : Theoretical and observational studies of vortex cloud patterns. GCA Tech.Report No. 64-2-G, Final Report, Contract No. Cwb-10626, GCA Corporation, Bedord, Mass.

Tatehira, R., 1962 : A mesosynoptic and radar analysis of typhoon rainband. National Hurricane Research Report No.50, U.S.Weather Bureau, Washington, D.C., 115-126.

Tepper, M., 1950 : A proposed mechanism of squall lines: the pressure jump line. J.Meteor., 7, 21-29.

Tepper, M., 1958 : A theoretical model for hurricane radar bands. Proc. of the Seventh Weather Radar Conference, Miami Beach, Florida, Nov.17-20, Amer.Met.Soc., Boston, pp.K56-K65.

Thorpe, A.J. and M.J. Miller, 1978 : Numerical simulations showing the role of the downdraught in cumulonimbus motion and splitting. Quart.J.R.Met.Soc., 104, 873-893.

Tschirhart, G., 1958 : Les conditions aérologiques a l'avant des lignes de grains en Afrique Equatoriale. Météorologie Nationale, France, Service Météorologique de l'A.E.F., Monogr.No.11, 28 pp.

Ushijima, T., 1958 : Outer rain bands of typhoons. J.Meteor.Soc. Japan, 36, 1-10.

Watanabe, K., 1963 : The radar bands and typhoon structure. Proceedings of the Symposium on Tropical Meteorology, Rotorua, New Zealand, 484-491, New Zealand Meteorological Service, Wellington.

Wexler, H., 1947 : Structure of hurricanes as determined by radar. Annals of the New York Academy of Sciences, 48(8), 821-844.

Wilhelmson, R., 1974 : The life cycle of a thunderstorm in three dimensions. J.Atmos.Sci., 31, 1629-1651.

Willoughby, H.E., 1977 : Inertia-buoyancy waves in hurricanes. J.Atmos.Sci., 34, 1028-1039.

Willoughby, H.E., 1978a : A possible mechanism for the formation of hurricane rainbands. J.Atmos.Sci., 35, 838-848.

Willoughby, H.E., 1978b : The vertical structure of hurricane rainbands and their interaction with the mean vortex. J.Atmos. Sci., 35, 849-858.

Willoughby, H.E., 1979 : Excitation of spiral bands in hurricanes by interaction between the symmetric mean vortex and a shearing environmental steering current. J.Atmos.Sci., 36, 1226-1235.

Yamamoto, R., 1963 : A dynamical theory of spiral rainband in tropical cyclones. Tellus, 15, 155-161.

Yanai, M., S. Esbensen and J.H. Chu, 1973 : Determination of bulk properties of tropical cloud clusters from large-scale heat and moisture budgets. J.Atmos.Sci., 30, 611-627.

Zipser, E.J., 1969 : The role of organized unsaturated convective downdrafts in the structure and rapid decay of an equatorial disturbance. J.Appl.Met., 8, 799-814.

Zipser, E.J., 1977 : Mesoscale and convective-scale downdrafts as distinct components of squall-line structure. Mon.Wea.Rev., 105, 1568-1589.

ACKNOWLEDGEMENTS

I would like to thank Dr. M. W. Moncrieff, my supervisor, for his wise counsel and guidance throughout this research. My thanks are also due to Drs. A.J. Thorpe, D.A. Mansfield, M.J. Miller, J.S.A. Green and D.J. Raymond for their constructive comments and helpful suggestions. In addition, Dr. A.J. Thorpe collaborated with material and ideas in sections 6 and 7 of Chapter 5, resulting in a joint paper.

Drs. R.C. Sheets and H.E. Willoughby were most helpful during a visit made by the author to the National Hurricane and Experimental Meteorology Laboratory, Coral Gables, Florida. I am also very much indebted to the late Professor F.H. Ludlam for stimulating discussions and encouragement in the initial stages of this research.

Several organisations provided invaluable data. They are the Agence pour la Sécurité de la Navigation Aérienne en Afrique et a Madagascar (ASECNA), Météorologie Nationale de Mali, Colorado State University, Japan Meteorological Agency, Australian Bureau of Meteorology (Regional Office, W.A.), National Hurricane and Experimental Meteorology Laboratory (U.S.A.), National Climatic Center (U.S.A.) and the Royal Observatory (Hong Kong). Dr. K.J. Bignell kindly provided the sequence of satellite pictures shown in Fig.3.1.

I am most grateful to Mrs. Jean Ludlam for her careful typing of the manuscript, and for her continual support during my stay at Imperial College.

The work was supported by a Grant from the University of Costa Rica.